STUDY OF PILE CONFIGURATION FOR EFFICIENT STABILIZATION OF CLAYEY SLOPES USING THREE-DIMENSIONAL NUMERICAL ANALYSIS

by

Ragim Mamedov

B.S., Civil Engineering, Yıldız Technical University, 2021

Submitted to the Institute for Graduate Studies in
Science and Engineering in partial fulfillment of
the requirements for the degree of
Master of Science

Graduate Program in Civil Engineering
Boğaziçi University

2024

ACKNOWLEDGEMENTS

I would like to express my deepest gratitude to my advisor, Assistant Professor İrem Zeynep Yıldırım, for her invaluable guidance, support, and encouragement throughout the entire process of completing this thesis. Her expertise, patience, and dedication have been instrumental in shaping the direction of this research and enhancing its quality. I am also indebted to Emre Tekdemir, who provided invaluable assistance and support during analysis phases of this study. His diligent efforts and technical expertise significantly contributed to the success of this research endeavor.I am grateful to my family and friends for their unwavering encouragement and support throughout this academic journey.

Finally, I would like to acknowledge the financial support provided by Boğaziçi University Scientific Research Projects (BAP Project Code: 16961) for this study.

ABSTRACT

STUDY OF PILE CONFIGURATION FOR EFFICIENT STABILIZATION OF CLAYEY SLOPES USING THREE-DIMENSIONAL NUMERICAL ANALYSIS

This study investigated the short-term (undrained) behavior clayey slopes, stabilized with a group of piles, via three-dimensional (3D) finite element analysis. Deformations and stability conditions were investigated considering various soil strength parameters, pile head conditions, and pile spacing-to-diameter ratios, pile group position for slopes with and without surcharge loads. Both full models and slice models were used in this study. Slice models were utilized to evaluate the behavior of stabilized slopes under continuous load and those without surcharge load. Full models were specifically used in slope cases with applied local (finite length and width) loads. The main goal of this research work is to better understand the effects of pile configuration and pile head conditions on the stability of the pile-stabilized slopes to achieve efficient slope stabilization using pile groups. The aim is to gain design insight into the most optimal pile group configuration/configurations which yield higher factor of safety and lower pile head deformations, using the minimum number of piles and concrete volume. For this purpose, various efficiency factors that account for the number of piles were proposed and evaluated for the stability slopes stabilized with pile groups. The results showed that optimization has to be evaluated based on the required level of slope stabilization (the target factor of safety) and the feasibility of changing the location of the piles along the slope or installing more piles or installing a pile cap beam. For the case of locally-loaded slopes, when it is not possible to install more piles, the most efficient solution can be to install a pile group with a pile cap beam in the upper part of the slope. When it is not feasible to construct a pile cap beams due to space restrictions, increasing the rows of piles (installing two or three rows) in the upper part of a locally loaded slope yields a more efficient solution, with an effort to keep the total number of piles the same. This can be done by increasing the pile spacing over pile diameter ratio (S/D) while increasing the rows. The results also show that reducing the S/D ratio is the most economical solution for stabilizing natural slopes with weaker soils.

ÖZET

KİLLİ ŞEVLERİN EFEKTİF STABİLİZASYONU İÇİN KAZIK KONFİGÜRASYONUNUN ÜÇ BOYUTLU SAYISAL ANALİZLE İNCELENMESİ

Bu çalışmada, kazık gruplarıyla stabilize edilmiş killi şevlerin kısa süreli (drenajsız) davranışı üç boyutlu (3D) sonlu elemanlar analizi ile incelenmiştir. Deformasyonlar ve stabilite koşulları, çeşitli zemin mukavemeti parametreleri, kazık başı koşulları, kazık aralığı-kazık çapı oranları ve kazık grubu pozisyonları dikkate alınarak sürşarj yüklü ve yüksüz şevler için incelenmiştir. Bu çalışmada bütün modeler ve dilim modeller kullanılmıştır. Dilim modeller, sürekli yük altındaki ve yüksüz durumda kazıklarla stabilize edilmiş şevlerin davranışını incelemek için kullanılmıştır. Tam modeller özellikle yerel (sonlu uzunlukta ve genişlikte) yüklerin uygulandığı kazıklarla stabilize edilmiş şevler için kullanılmıştır. Bu araştırmanın temel amacı, kazık konfigürasyonunun (şev boyunca ve plan görünümündeki konumu) ve kazık başı koşullarının kazık gruplarıyla stabilize edilmiş şevlerin stabilitesi üzerindeki etkilerini, daha efektif bir stabilizasyon için daha iyi anlamaktır. Amaç, kazık sayısını ve beton hacmini minimuma indirerek daha yüksek güvenlik katsatısı ve daha düşük kazık başı deformasyonları sağlayan en uygun kazık grubu konfigürasyonu/konfigürasyonları ile ilgili öngörü edinmektir. Bu amaçla kazıklarla stabilize edilen şevler için kazık sayısını veya beton hacmini hesaba katan çeşitli verimlilik faktörleri önerilmiş ve değerlendirilmiştir. Sonuçlar, optimizasyonun, gerekli şev stabilizasyonu seviyesine (hedef güvenlik katsayısı) ve şev boyunca kazıkların konumunu değiştirmenin veya daha fazla kazık yerleştirmenin veya kazık başlık kirişi yerleştirmenin fizibilitesine göre değerlendirilmesi gerektiğini göstermektedir. Yerel yüklü şevlerde, daha fazla kazık kullanmanın mümkün olmadığı durumlarda, en etkili çözüm şev üst kısmında kazık başlık kirişli bir kazık grubunun kullanılması olabilir. Yer kısıtlamaları nedeniyle kazık başlık kirişleri inşa etmek mümkün olmadığında, yerel olarak yüklü bir şevin üst kısmındaki kazık sıralarını artırmak (iki veya üç sıra yerleştirerek), kazık sayısını arttırmadan daha verimli bir çözüm sağlar. Bu, kazık aralığının kazık çapına oranı (S/D) artırılarak sağlanabilir. Sonuçlar aynı zamanda nispeten zayıf zeminlere sahip yüksüz şevlerin stabilizasyonu için S/D oranının azaltılmasının en ekonomik çözüm olduğunu göstermektedir.

TABLE OF CONTENTS

ACKNOWLEDGEMENTS iii
ABSTRACT iv
ÖZET v
LIST OF FIGURES viii
LIST OF SYMBOLS xxi
LIST OF ACRONYMS / ABBREVIATONS xxiii
1. INTRODUCTION 1
1.1. General 1
1.2. Objectives 2
1.3. Scope 3
2. LITERATURE REVIEW 4
2.1. Slope stability and Slope Stability Analysis by Finite Element Method 4
2.2. Pile-Stabilized Slopes and Stability Analysis of Pile-Stabilized Slopes 6
3. RESEARCH METHODOLOGY 22
3.1. Plaxis 3D Overview 22
3.2. Material Modeling 23
3.2.1. Modeling of Soil 23
3.2.2. Modeling of Piles 30
3.2.3. Attributes of 3D Slope Models 31
3.2.4. Mesh Generation and Distribution in 3D Slope Stability Analysis 38
3.2.5. Slope Stability Analysis in Plaxis 3D: Staged Construction Steps 40
3.2.6. Selected Configurations for Paraetric Study 41
4. RESULTS OF THE NUMERICAL ANALYSIS 50
4.1. Effect of S/D 50
4.1.1. Factor of Safety 50
4.1.2. Pile Internal Forces 61
4.1.3. Displacements 66

4.2. Effect of Number of Rows 76
4.2.1. Factor of Safety 76
4.2.2. Internal Forces 83
4.2.3. Displacements 86
4.3. Effect of Pile Position 91
4.3.1. Factor of Safety of Pile-Stabilized Slopes 91
4.3.2. Internal Forces 96
4.3.3. Displacements 100
4.4. Pile Cap Beam Placement 110
4.5. Effectiveness of Pile Groups in Slope Stabilization 115
4.5.1. Slice Model Cases 115
4.5.2. Full Model Cases 116
5. CONCLUSIONS 128
REFERENCES 132

LIST OF FIGURES

Figure 2.1. The non-uniformly spaced pile arrangement to minimize cost in colluvial landslide (modified after Li *et al*., 2015). 12

Figure 2.2. Arch anti-slip pile-wall structures used to stabilize landslides (modified after Li *et al*., 2021)..... 16

Figure 2.3. Slope stabilizing pile configuration in polyline shape considering the landslide direction (modified after Dai *et al*., 2022)..... 19

Figure 2.4. Soil mass displacement directions for different pile configurations (modified after Shangguan *et al.*, 2023): a) parallel, b) staggered. 20

Figure 3.1. Determination of E_{50}^{ref} and E_{ur}^{ref} values from drained triaxial test results. 25

Figure 3.2. Determination of E_{oed}^{ref} value from oedometer test result. 25

Figure 3.3. Differences between MC model and HS model: (a) Total Stresses, (b) Unloading/Reloading Stiffness. 28

Figure 3.4. Geometry of 3D full model in the Plaxis 3D. 32

Figure 3.5. Geometry of the pile cap beam in Plaxis3D model. 32

Figure 3.6. Boundary conditions in Plaxis 3D model (Full and Slice Models). 33

Figure 3.7. Volume pile and interface. 33

Figure 3.8. Geometry of 3D slice models: (a) natural slope, (b) continuously loaded slope. 35

Figure 3.9. Slice models with various widths based on the pile configuration and loading condition. 36

Figure 3.10. Slice models with different number of piles in one slice. 37

Figure 3.11. Typical mesh distribution of pile-stabilized slopes in slice model..... 39

Figure 3.12. Typical mesh distribution of pile-stabilized locally loaded slopes in full model. 40

Figure 3.13. Staged construction steps for pile-stabilized loaded slope cases..... 41

Figure 3.14. Staged construction steps for pile-stabilized natural slope cases. 41

Figure 3.15. Plaxis 3D example of the analyzed pile-stabilized slopes using slice model. 43

Figure 3.16. 3D geometry of the analyzed locally loaded pile-stabilized slopes. 43

Figure 3.17. Plan view of pile group configurations: Case 1 through Case 16. 45

Figure 3.18. Plan view of pile group configurations: Case 17 through Case 36. 46

Figure 3.19. Plan-view of SD3_PN13_RN2_36_M in Plaxis 3D (free pile head condition)..... 48

Figure 3.20. Plan-view of SD3_PN13_RN2_36_M_HPC in Plaxis 3D (constrained pile head condition). 48

Figure 4.1. S/D ratio versus FS_{0_PS} (slice model cases, S_u=40 kPa). 51

Figure 4.2. S/D ratio versus FS_{0_PS} (%) increase with respect to largest S/D ratio (S/D=4) (slice model cases, S_u=40 kPa). 53

Figure 4.3. S/D ratio versus FS_{0_PS} (slice model cases, S_u=30 kPa). 54

Figure 4.4. S/D ratio versus FS_{0_PS} (%) increase with respect to largest S/D ratio (S/D=4) (slice model cases, S_u=30 kPa). 55

Figure 4.5. S/D ratio versus FS_{CL_PS} (slice model cases, S_u=40 kPa). 57

Figure 4.6. S/D ratio versus FS_{CP_PS} (%) increase with respect to largest S/D ratio (S/D=4) (slice model cases, S_u=40 kPa). 58

Figure 4.7. S/D ratio versus FS_{LPS} (full model cases, S_u=40 kPa, single row configurations, free pile head condition). 60

Figure 4.8. S/D ratio versus FS_{LPS} (full model cases, S_u=40 kPa, single row configurations constrained pile head condition). 61

Figure 4.9. S/D ratio versus maximum pile bending moment values of continuously loaded pile-stabilized slope (slice model cases, S_u=40 kPa). 62

Figure 4.10. S/D ratio versus maximum pile shear force values of continuously loaded pile-stabilized slope (slice model cases, S_u=40 kPa). 63

Figure 4.11. S/D ratio versus maximum pile bending moment values of locally loaded pile-stabilized slope (full model cases, S_u=40 kPa, single row configuration free pile head condition). 64

Figure 4.12. S/D ratio versus maximum pile shear force values of locally loaded pile-stabilized slope (full model cases, S_u=40 kPa, single row configurations, free pile head condition). 65

Figure 4.13. Bending moment diagram of central piles in single row configurations in locally loaded pile-stabilized slopes (full model cases, S_u=40 kPa, free pile head condition). 66

Figure 4.14. S/D ratio versus maximum U_{PH} values of continuously loaded pile-stabilized slope (slice model cases, S_u=40 kPa). 68

Figure 4.15. S/D ratio versus maximum U_{SC} values of continuously loaded pile-stabilized slope (slice model cases, S_u=40 kPa). 68

Figure 4.16. S/D ratio versus maximum U_{ST} values of continuously loaded pile-stabilized slope (slice model cases, S_u=40 kPa). 69

Figure 4.17. S/D ratio versus maximum U_{PH} of locally loaded pile-stabilized slope (full model cases, S_u=40 kPa, single row configurations, free pile head condition). 71

Figure 4.18. S/D ratio versus maximum U_{SC} values of locally loaded pile-stabilized slope (full model cases, S_u=40 kPa, single row configurations, free pile head condition). 71

Figure 4.19. S/D ratio versus maximum U_{ST} values of locally loaded pile-stabilized slope (full model cases, S_u=40 kPa, single row configurations, free pile head condition). 72

Figure 4.20. Pile location versus U_{PH} of locally loaded pile-stabilized slope (full model cases, S_u=40 kPa, single row configurations, free pile head condition): (a) crest , (b) middle , (c) toe. 73

Figure 4.21. Pile location versus U_{PH} of locally loaded pile-stabilized slope (full model cases, S_u=40 kPa, single row configurations, constrained pile head condition): (a) crest , (b) middle , (c) toe. 74

Figure 4.22. Effect of S/D ratio on critical surface, incremental displacements (full model cases, S_u=40 kPa, single row configurations)..... 75

Figure 4.23. Number of rows versus FS_{0_PS} (slice model cases, S_u=40 kPa). 77

Figure 4.24. Number of rows versus *FS* (%) increase with respect to natural unstabilized slope (slice model cases, S_u=40 kPa). 78

Figure 4.25. Number of rows versus FS_{0_PS} (slice model cases, S_u=30 kPa). 79

Figure 4.26. Number of rows versus *FS* (%) increase with respect to natural unstabilized slope, S_u=30 kPa. 80

Figure 4.27. Number of rows versus FS_{CL_PS} (slice model cases, S_u=40 kPa). 81

Figure 4.28. Number of rows versus *FS* (%) increase with respect to continuously loaded unstabilized slope (slice model cases, S_u=40 kPa). 82

Figure 4.29. Number of rows versus maximum pile bending moment values of continuously loaded pile-stabilized slope (slice model cases, S_u=40 kPa). ... 84

Figure 4.30. Number of rows versus maximum pile shear force values of continuously loaded pile-stabilized slope (slice model cases, S_u=40 kPa). 85

Figure 4.31. Number of rows versus maximum U_{PH} values of continuously loaded pile-stabilized slope (slice model cases, S_u=40 kPa). 87

Figure 4.32. Number of rows versus maximum U_{SC} values of continuously loaded pile-stabilized slope (slice model cases, S_u=40 kPa). 88

Figure 4.33. Number of rows versus maximum U_{ST} values of continuously loaded pile-stabilized slope (slice model cases, S_u=40 kPa). 88

Figure 4.34. Pile location versus U_{PH} of locally loaded pile-stabilized slope (full model cases, S_u=40 kPa, S/D=3, free pile head condition). 89

Figure 4.35. Effect of number of rows on critical surface of locally loaded pile-stabilized slope on incremental displacements (full model cases, S_u=40 kPa, S/D=3, free pile head condition). 90

Figure 4.36. Pile position versus FS_{0_PS} and FS_{CL_PS} (slice models cases, S_u=40 kPa). 92

Figure 4.37. Pile position versus FS_{LPS} (full models cases, S_u=40 kPa, single and double row configurations, free pile head condition)..... 94

Figure 4.38. Pile position versus FS_{LPS} (full models cases, S_u=40 kPa, single and double row configurations, constrained pile head condition). 95

Figure 4.39. Pile position versus maximum pile bending moment values of locally loaded pile-stabilized slope (full model cases, S_u=40 kPa, single row configurations, free pile head condition). 97

Figure 4.40. Pile position versus maximum pile bending moment values of locally loaded pile-stabilized slope (full model cases, S_u=40 kPa, single row configurations, constrained pile head condition)..... 98

Figure 4.41. Pile position versus maximum pile shear force values of locally loaded pile-stabilized slope (full model cases, S_u=40 kPa, single row configurations, free pile head condition). 98

Figure 4.42. Pile position versus maximum pile shear force values of locally loaded pile-stabilized slope (full model cases, S_u=40 kPa, single row configurations, constrained pile head condition). 99

Figure 4.43. Pile bending moment diagram versus pile length for different pile positions (full model cases, S_u=40 kPa, free pile head condition). 100

Figure 4.44. Pile position versus maximum U_{PH} of locally loaded pile-stabilized slope (full model cases, S_u=40 kPa, single row configurations, free pile head condition). 102

Figure 4.45. Pile position versus maximum U_{PH} of locally loaded pile-stabilized slope (full model cases, S_u=40 kPa, single row configuration, constrained pile head condition). 102

Figure 4.46. Pile position versus maximum U_{SC} of locally loaded pile-stabilized slope (full model cases, S_u=40 kPa, single row configurations, free pile head condition). 103

Figure 4.47. Pile position versus maximum U_{SC} of locally loaded pile-stabilized slope (full model cases, S_u=40 kPa, single row configurations, constrained pile head condition). 104

Figure 4.48. Pile position versus maximum U_{ST} of locally loaded pile-stabilized slope (full model cases, S_u=40 kPa, single row configurations, free pile head condition). 105

Figure 4.49. Pile position versus maximum U_{ST} of locally loaded pile-stabilized slope (full model cases, S_u=40 kPa, single row configurations, constrained pile head condition). 105

Figure 4.50. Pile location versus U_{PH} of locally loaded pile-stabilized slope (full model cases, S_u=40 kPa, single row configurations, free pile head condition) : (a) S/D=2 , (b) S/D=3, (c) S/D=4..... 107

Figure 4.51. Pile location versus UP_H of locally loaded pile-stabilized slope (full model cases, S_u=40 kPa, single row configurations, constrained pile head condition) : (a) S/D=2 , (b) S/D=3, (c) S/D=4..... 108

Figure 4.52. Effect of pile group position on the critical surface of locally loaded pile-stabilized slope, incremental displacements (full model cases, S_u=40 kPa single row configurations, free pile head condition). 109

Figure 4.53. Pile bending moment diagram versus pile length for locally loaded pile-stabilized slope case (full model cases, S_u=40 kPa, single row configurations)..... 113

Figure 4.54. Pile location versus U_{PH} of locally loaded pile-stabilized slope (full model cases, S_u=40 kPa, single row configurations): (a) crest, (b) middle, (c) toe. . 114

Figure 4.55. Number of piles versus FS_{0_PS} 116

Figure 4.56. Pile configuration case number versus FS_{LPS}. 117

Figure 4.57. Total number of piles in pile group versus FS_{LPS}. 118

Figure 4.58. Plan views of configurations: (a) Cases 26 and 27, (b) Cases 28 and 34..... 119

Figure 4.59. Plan views of configurations: (a) Cases 8 and 10, (b) Cases 11 and 12. 120

Figure 4.60. Plan views of configurations: (a) Cases 5 and 6, (b) Case 7. 121

Figure 4.61. Pile configuration case number versus E1..... 122

Figure 4.62. FS_{LPS} versus E2 coefficient. 124

Figure 4.63. Total volume of concrete used versus FS_{LPS}. 125

Figure 4.64. Plan view of configurations: (a) Cases 21 and 22, (b) Cases 23 and 32, (c) Cases 32 and 33. 126

Figure 4.65. Pile configuration case number versus E3..... 127

LIST OF TABLES

Table 3.1. The parameters required for HS and HSS soil models (modified after Brinkgreve *et al*., 2021). 24

Table 3.2. Suggested ranges of m values (modified after von Soos *et al*., 1991). 26

Table 3.3. Soil properties utilized in the parametric study. 30

Table 3.4. Pile material properties (adopted from Gerolymos *et al.*, 2014). 31

Table 3.5. Comparison of the results of the analysis performed using single row and double row slice models. 37

Table 3.6. Predifined values of r_e (modified after Brinkgreve *et al*., 2021). 38

Table 3.7. Coarseness factor distribution. 39

Table 3.8. Slice model cases analyzed in the parametric study. 44

Table 3.9. Full model cases analyzed in the parametric study. 49

Table 4.1. Results of the safety analyses performed on the of natural pile-stabilized slopes (slice model cases, S_u=40 kPa). 51

Table 4.2. Results of safety analyses performed on the natural pile-stabilized slope (slice model cases, S_u=30 kPa). 54

Table 4.3. Results of the safety analyses performed on the continuously loaded pile-stabilized (slice model cases, S_u=40 kPa). 56

Table 4.4. Results of the safety analyses performed on locally loaded pile-stabilized slope (full model cases, S_u=40 kPa, single row configurations). 60

Table 4.5. Maximum pile internal forces of continuously loaded pile-stabilized slopes (slice models, S_u=40 kPa). 62

Table 4.6. Maximum pile internal forces of locally loaded pile-stabilized slopes (full model cases, S_u=40 kPa, single row configuration free pile head condition)... 64

Table 4.7. Displacements values of continuously loaded pile-stabilized slopes (slice model cases, S_u=40 kPa). 67

Table 4.8. Displacements values of locally loaded pile-stabilized slopes (full model, S_u=40 kPa, single row configurations, free pile head condition)..... 69

Table 4.9. Results of the study analyses performed on natural pile-stabilized slope (slice model cases, S_u=40 kPa). 76

Table 4.10. Results of the safety analyses performed on natural pile-stabilized slope (slice model cases, S_u=30 kPa). 79

Table 4.11. Results of the safety analyses performed on continuously loaded pile-stabilized slope (slice model case, S_u=40 kPa). 81

Table 4.12. Results of the safety analyses performed on locally loaded pile-stabilized slope (full model cases, S_u=40 kPa, S/D=3, free pile head condition). 83

Table 4.13. Maximum pile internal forces of continuously loaded pile-stabilized slope (slice models, S_u=40 kPa). 84

Table 4.14. Maximum pile internal forces of locally loaded pile-stabilized slope (full model cases, S_u=40 kPa, S/D=3, free pile head condition). 86

Table 4.15 Maximum displacement values of continuously loaded pile-stabilized slopes (slice model cases, S_u=40 kPa). 87

Table 4.16. Maximum displacements values of locally loaded pile-stabilized slopes (full model cases, S_u=40 kPa, S/D=3, free pile head condition). 89

Table 4.17. Results of the analyses performed on natural and continuously loaded pile-stabilized slopes (slice models cases, S_u=40 kPa). 92

Table 4.18. Results of the analyses performed on locally loaded pile-stabilized slopes (full model cases, S_u=40 kPa). 93

Table 4.19. Maximum pile internal force values of locally loaded pile-stabilized slopes (full model cases, S_u=40 kPa). 96

Table 4.20. Maximum displacement values of locally loaded pile-stabilized slopes (full model cases, S_u=40 kPa) 101

Table 4.21. Maximum pile bending moment and pile head displacements of locally loaded pile-stabilized slopes. 111

Table 4.22. Results of the analyses performed on locally loaded pile-stabilized slopes (full model cases, S_u=40 kPa). 112

Table 4.23. Results of the safety analysis performed on natural pile-stabilized slopes (slice model cases, S_u=40 kPa). 115

LIST OF SYMBOLS

c	Cohesion
D	Pile diameter
E	Young's modulus
E_{50}^{ref}	Secant stiffness in standard drained triaxial test
E_{oed}^{ref}	Tangent stiffness for primary oedometer loading
E_{ur}^{ref}	Unloading/ reloading stiffness
FS	Factor of safety
FS_{0_PS}	Factor of safety of pile-stabilized natural slope
FS_{LPS}	Factor of safety of pile-stabilized locally loaded slope
FS_{CL_PS}	Factor of safety of pile-stabilized cont. loaded slope number
G_0^{ref}	Reference shear modulus at very small strains
L_d	Diagonal length
l_e	Target element size
m	Power for stress level dependency of stiffness
r_e	Relative element size factor
R_f	Failure ratio
R_{inter}	Interface strength reduction factor
S	Spacing
S_u	Interface strength reduction factor
U_{PH}	Pile head displacement
U_{SC}	Slope crest displacement
U_{ST}	Slope toe displacement
v	Poisson ratio
v_{ur}	Poisson's ratio for unloading – reloading

σ_t	Tension cut-off stress
γ	Unit weight
$\gamma_{0.7}$	Threshold shear strain
ψ	Dilatancy angle
ϕ	Friction angle

LIST OF ACRONYMS / ABBREVIATONS

2D	Two-dimensional
3D	Three-dimensional
FD	Finite Difference
FDM	Finite Difference Method
FE	Finite Element
FEM	Finite Element Method
HS	Hardening Soil Model
HSS	Hardening Soil Model with Small Strain Stiffness
HPC	Horizontal Pile Cap
VPC	Vertical Pile Cap
PN	Number of piles
RN	Number of rows

1. INTRODUCTION

1.1. General

In geotechnical engineering, maintaining the stability of slopes is crucial, especially in regions susceptible to natural calamities like landslides. Dealing with concerns related to slope stability requires the implementation of stabilization methods. Among these methods, the use of piles emerges as a notable strategy, providing significant reinforcement to address and mitigate slope instability.

The efficacy of pile stabilization hinges upon several key factors including pile spacing, pile group position along the slope, number of rows in the pile group, and the placement of the pile cap beam. These factors collectively influence the overall performance and effectiveness of the slope-stabilized slope. A comprehensive investigation of these factors requires advanced computational methods. In this thesis, Finite Element Method (FEM) was utilized for simulating and analyzing the behavior of slopes stabilized using a group of piles. Both full and slice modeling approaches were employed in 3D simulations to capture the coupled stability (pile stability and slope stability) of the pile-stabilized slope. Full models were specifically utilized for the cases of a localized surcharge load. This approach enables appropriate modeling of the locally loaded pile-stabilized slope scenarios, facilitating a thorough examination of the system's response under varying pile configurations. Conversely, using the slice models offers practical solutions for natural slopes (without the surcharge loads) and also for continuously loaded (*i.e.*, infinite surcharge loads) slopes. The use of these diverse modeling approaches, allowed a thorough evaluation of the performance of slopes stabilized with a group of piles for two different loading scenarios.

The pile-slope systems analyzed in this study were limited to clayey slopes stabilized using piles that are socketed in sand. This condition was selected to reflect one of the most common geotechnical scenarios encountered in practice that is suitable for pile stabilization. In the safety analysis phase of both slice and full models, the undrained strength parameters were implemented to evaluate the slope stability under loading conditions. Another important aspect of this study was that the piles were modeled using elastoplastic parameters, as such the failure of the pile could be simulated. This also allowed the detection of the critical failure mode for the pile-stabilized slope system. Performance indicators for stabilization such as the factor of safety, internal pile forces, pile head displacements, as well as displacements at the slope crest and toe, were carefully recorded and evaluated. Additionally, a distinct feature of this scientific study is that it sheds light on the behavior of pile group configurations that have not been previously investigated. The main novelty of this study is the study of continuously and locally loaded slopes with the use of various pile configurations with varying number of rows, pile spacing, pile location along the slope and pile head conditions, not only considering a line placement but with varying plan-view locations of pile that also create non-rectangular pile groups (*e.g.*, circular pile groups with a center pile).

1.2. Objectives

The primary objective of this study is to better understand the effects of pile group configuration and pile head condition on the stability of slopes stabilized with a group of piles, considering stabilization efficiency (through factors of safety and deformation values) and cost-effectiveness for each pile group configuration. Cost-effectiveness was evaluated by considering the number of piles used for each case analyzed. Efficiency factors were proposed and evaluated to understand the effectiveness of stabilization. By examining factors such as pile spacing, number of rows of the pile group, pile group position along the slope, and pile head condition, this research aims to provide valuable insights for engineers and designers in selecting the most suitable pile group configurations, shedding light on efficient design practices for slope

stabilization projects. For the pile-stabilized slope cases, in the full model cases, various scenarios were investigated using a 3D Finite Element (FE) analysis for pile-stabilized slopes. These scenarios included three different S/D ratios (2 to 4), pile groups arranged in configurations with one, two, or three rows, and two pile head conditions (free and constrained). Additionally, in the cases analyzed the pile groups were positioned at three different locations along the slope: crest, middle, and toe. The effectiveness of a few non-rectangular pile group configurations was also investigated. For the slice models, the analysis considered eight S/D ratios ranging from 1.33 to 4, along with pile groups arranged in configurations of one, two, or three rows. The pile heads were considered free in all cases, and the pile groups were positioned at the crest, middle, and toe of the slope. During the analysis, factors such as the factor of safety, internal forces within the piles, displacements at the pile heads were recorded. These findings were then utilized to assess and compare the performance of various configurations of pile-stabilized slopes. In essence, this study seeks to contribute to the advancement of geotechnical engineering practice by offering insights into the interaction between the slope and the pile group configurations.

1.3. Scope

This thesis is organized into five main chapters. Chapter 1 provides a brief overview of the thesis topic, outlining the study's objectives and scope. Chapter 2 introduces fundamental concepts and traditional methods of for slope stability analysis and provides a review of previous studies on different pile configurations used in slope stabilization. Chapter 3 details the methodology employed in the study using the 3D FE software. Chapter 4 presents and discusses the main results and major findings of the numerical analyses. Chapter 5 summarizes the results and provides the final conclusions.

2. LITERATURE REVIEW

This chapter presents a literature review on various aspects of slope stability, paying particular attention to pile groups used in slope stabilization. At the beginning of this chapter, an overview of slope stability and fundamental concepts are provided, and the factors influencing slope failures are discussed. Previous studies performed using finite element method (FEM) are presented next. Various parameters of the pile group configuration, such as the position of the pile group along the slope, the pile spacing over pile diameter ratio (S/D), and the number of rows in the pile group, all play crucial roles in the overall stability of the slopes stabilized with piles. This chapter provides a comprehensive overview of the existing research on pile-stabilized slopes, with special emphasis on the influence of the configuration of the pile group.

2.1. Slope stability and Slope Stability Analysis by Finite Element Method

Slopes can be grouped into two: natural slopes and artificial slopes. Natural slopes are formed by by natural processes such as erosion, precipitation, and tectonic movements, and artificial slopes are created by man during the construction of various structures such as roads, railways, dams and quarries.

There are many reasons for the failure of natural slopes and artificial slopes. According to Abramson et al. (1996), there are two main reasons for slope failures, one of them is the increase of shear stress and the second one is the reduction of the shear strength of slope soil. Factors that cause the increase of shear stress in slopes include applying of surcharge loads, erosion, natural soil movements like settlement, overloading resulting from rains or snow, increased lateral stresses, or earthquakes. Conversely, a reduction of shear strength may occur due to degradation of soil properties, physicochemical effects and increased pore pressure.

According to Terzaghi (1950), slope failures can be caused by two types factors: external factors and internal factors. Externally, changes in slope geometry, can significantly impact its stability. Loading at the slope crest, and conversely unloading at the slope toe and changes in water levels, are among those external factors. Internally, weathering over time weakens rock and soil, and can cause reductions in shear strength. Seepage can also alter the effective stresses and cause failures.

With the initiation of affordable personal computing, the FEM has gained prominence in slope stability analysis, surpassing traditional limit equilibrium methods by eliminating the need for pre-assumed failure surface shapes. FE methods's flexibility allows it to handle complex slope configurations and soil deposits in both two-dimensions (2D) and three dimensions (3D). With the use of FEM stresses and strains can be computed accurately, critical failure mechanisms beyond simple geometrical shapes can be attained. Both FEM and finite difference (FD) methods are gaining popularity in the analysis of pile-stabilized slope. Both of these methods use the strength reduction technique to calculate the factor of safety (*FS*).

Griffiths and Lane (1999) highlighted the limits of limit equilibrium methods for slope stability analysis, recommending the FE method as a more accurate alternative. Duncan (1996) stated that FEM has great potential over traditional methods for the realistic analysis of field conditions, and highlighted the tendency of FEM to predict larger deformations than those observed in actual field conditions. Rabie (2013) highlighted the advantages of the analysis using FEM over the analysis performed using limit equilibrium methods in the estimation of the *FS* of slopes by making a comparison of the two methods for slopes under the effect of rainfall. The results of the limit equilibrium analyses generally indicated lower *FS* values for both saturated and unsaturated slopes. FEM can provide a more accurate and reliable assessment of slope stability under varying moisture conditions which are simplified or overlooked in the limit equilibrium method.

2.2. Pile-Stabilized Slopes and Stability Analysis of Pile-Stabilized Slopes

The use of piles has become a reliable and effective method, especially for the stabilization of landslides. The pile stabilization can increase the stability of slopes that are prone to collapse due to various factors such as weak soil layers or external load. The main mechanisms by which piles stabilize slopes are shear reinforcement, the arching effect and increased resistance to lateral displacement (Hu *et al*., 2021). Piles act as rigid inclusions within the soil, enhancing the shear strength of the slope and thereby reducing the potential for shear failure. The presence of piles causes an arching effect in the soil, causing redistribution of the loads and reducing the load on weaker soil layers (Lai *et al*., 2018). In addition, the piles provide increased resistance to lateral movements of the soil, helping to maintain the integrity of the slope. Successful implementation of piles for slope stabilization in numerous projects over the past decades underlines its reliability. The effectiveness of stabilization of slopes with piles is influenced by many factors. Previous studies on pile-stabilized slopes have extensively analyzed the impact of pile placement on slope stability. Researchers have investigated various aspects such as the optimal positioning of piles within the slope (Jesmani *et al.*, 2015; Mezazigh *et al.*, 1998) the S/D ratio (Pan *et al.*, 2017; Aliah *et al.*, 2016; Ellis *et al.*, 2010), pile head conditions (Chae *et al*., 2004; Yang *et al*., 2011), rows of piles (Ito *et al.*, 1982) and the influence of pile diameter (Liang and Yamin, 2010) and length (El Sawwaf, 2008). These studies have employed both numerical simulations and field experiments (Smethurst and Powrie, 2007) to assess how different configurations affect the overall stability of slopes. For instance, some research has focused on the placement of piles in the middle (Abdelaziz *et al.,* 2015) or lower parts of slopes (Ausilio *et al.,* 2000). These studies demonstrate that strategic positioning can significantly enhance the *FS* and mitigate the risk of landslides. Additionally, studies have explored the interaction between piles and soil, highlighting how piles can redistribute stress and provide additional resistance to soil movements.

Cai and Ugai (2000) presented a comprehensive analysis of the stability of slopes reinforced with piles using 3D strength reduction technique coupled with the 3D FEM. In this study, a detailed comparison with the simplified Bishop's method was conducted. Noticeable discrepancies in the *FS* predictions were revealed, especially for piles with a hinged head. The influence of important parameters such as the S/D ratio, the location of the piles themselves, as well as the pile head condition for slope stability have been carefully studied and analyzed. The study highlighted the disadvantage of flexible piles and advocated for fixed-head conditions. Restrained head conditions (hinged or fixed) were recommended to increase the *FS*. According to the results of the analysis, the piles positioned in the middle of the slope yield the highest *FS*. Additionally, based on limit equilibrium analysis using Bishop's method, the pile position along the slope that leads to the highest *FS* was found to be the crest of the slope, which contradicted the results of the analysis performed using FEM.

Won *et al.* (2005) introduced a coupled analysis approach using FLAC 3D and presents findings from both analytical and numerical studies. Key findings of this study includes: the identified coupled effect between piles and soil and the coupled method's ability to dynamically adjust the critical slip surface based on pile-soil interaction. The analysis demonstrated that fixed head conditions provide higher stability due to better resistance to lateral soil movement. The importance of pile group position was analyzed, and the results of the analyses showed that highest stability was achieved when piles were installed in the middle of slope. The middle position allowed the piles to intercept the slip surface more effectively.

Chandrasekaran *et al.* (2009) presented the results of static lateral load tests conducted on model groups of piles (1x2, 2x2, 1x4 and 3x3) embedded in soft clay. This study used piles with a length-to-diameter ratio of 15, 30 and 40, and S/D ratios from 3 to 9. The study focused on the influence of pile-group interaction. Results of this study showed that the lateral capacity of piles in a 3x3 group with S/D=3 is approximately 40% less than that of a single pile. This reduction occurred due to pile-soil-pile interaction, which caused overlapping stress zones around the piles and a subsequent decrease in passive resistance. Additionally, group interaction resulted in a 20% increase in the maximum bending moment in the piles of the groups with S/D=3 compared

to a single pile. This is attributed to soil softening caused by the interaction between piles. It was found that group efficiency values of pile groups significantly depend on the S/D ratio, reducing notably at S/D=5 or below. Experiments have demonstrated that lower S/D ratios result in overlapping stress zones, thus reducing efficiency. Efficiency increased with larger S/D ratios and fewer piles, emphasizing the critical influence of S/D ratio. The row position of piles in the group also affected the variation in bending moments, with leading row piles experiencing higher moments. Measurements indicated that leading row piles share more load and carry higher moments, while middle row piles experienced the lower moments due to greater interaction and reduced soil resistance.

Kourkoulis *et.al.* (2011) conducted a comprehensive study to determine the optimal S/D ratio for effective soil arching and cost-efficient slope stabilization. They examined the critical S/D ratio necessary to induce sufficient soil arching by evaluating the ratio of soil displacement between piles to pile head displacement, which should ideally range between 1 and 2. Their parametric analysis revealed that at a very dense configuration with S/D=2, strong arching was guaranteed but was not cost-effective, while in the case of a sparse configuration with S/D=7, no arching developed, rendering it ineffective. They observed that S/D=5 caused piles to behave almost as isolated units, allowing soil to flow between them without significant arching effects, thus being ineffective for stabilization. Conversely, S/D=4 was identified as the largest S/D ratio that still generated sufficient soil arching, requiring fewer piles and ensuring cost-effectiveness while retaining soil between the piles. They also analyzed equivalent pile configurations with single row of piles, two pile-frames, and also a staggered pile frames, which maintain the same number of piles per unit width. The results showed that single piles might be inadequate for stabilizing deep landslides, whereas pile groups, particularly two-pile frames and staggered pile frames configurations, significantly enhanced the load-carrying capacity by distributing the load through both bending and axial forces. Staggered pile frames were especially effective in mitigating the pile shadow effect, thereby improving the overall performance of the pile group configurations in slope stabilization.

Li *et al.* (2011) investigated the pile positioning in slope stabilization using numerical analysis with FLAC 2D. The resuls highlighted the significant influence of soil-pile interaction on slope stability, identifying three failure mechanisms based on pile location. When piles were near the toe, failure occurred above the pile top; when piles are near the crest, failure occurred below the pile; and when piles are in the middle, the failure passed through the row of piles. The results of the analysis showed that the middle pile group location gave the highest *FS* value while the S/D ratio affected stability in different ways depending on the location of the pile group. In particular, a lower S/D ratio increased stability when the piles are in the middle of the slope, but had little effect at the toe or crest of the slope. The middle position allowed the piles to support both the upper and lower parts of the slope, providing a balanced stabilizing effect.

Li *et al.* (2012) discussed the challenge of determining the optimal position of piles to reinforce and stabilize slopes. It employs a combination of limit slope stability analysis and the plastic state theory to calculate the limit lateral loads on piles. This study examined various considerations such as the most effective and safety-maximizing positions for piles within the slope. The conclusions drawn include: (1) if the maximum force provided by the piles is sufficiently large, the most effective positions are near the slope toe where the stabilizing force requirement is minimized, and the stabilizing force needed to increase the *FS* is the lowest. This means that less force is required to achieve the same level of stability compared to other positions; (2) for sufficiently long piles, the position yielding the maximum *FS* was determined in the upper to middle part of the slope where the force supply was the greatest. This force is dependent on the depth of the soil layer between the sliding surface and the ground surface. Near the toe, this depth is small, meaning the piles provide less stabilizing force. Therefore, they need to be placed higher up where this depth is larger.

Kahyaoglu *et al.* (2012) experimentally investigated the effect of the S/D ratio and pile head condition on the distribution of moment and lateral pressure of the soil along the piles stabilizing the slope. This study utilized an experimental setup to simulate a slice from an infinitely long row of piles in an inclined sand bed, comprising a test box with rigid steel plates (1200 mm length, 480 mm width, 500 mm depth) and aluminum piles (750 mm length, 20 mm

diameter). Strain gauges, displacement transducers and pressure sensors were used to measure the bending moments and soil pressures. This study indicated that decreasing S/D ratio enhanced load transfer due to the soil arching mechanism between piles. This load transfer increased rapidly with soil displacement but stabilized thereafter. Free head piles experienced bending moments approximately twice as high as fixed head piles. The authors recommended to use restrained head conditions achieved by connecting pile heads with buried beams fixed by tie-rods or tension anchors to mitigate the large bending moments in free head piles. In cases wherefixed head conditions are not feasible, decreasing S/D ratio was advised to improve stability. The soil arching mechanism was more pronounced in fixed head piles, which resisted sliding and reduced surficial soil displacements, whereas free head piles showed pile head movement exceeding soil movement.

Dagget *et al.* (2014) examined the effectiveness of pile reinforcement in increasing the stability of failing slopes by investigating the behavior of slope displacement with and without piles. Using the FEM-based software ABAQUS, these researchers analyzed the effect of the S/D ratio and their configuration on slope stability using a 2D horizontal slice model. To study the effects of S/D ratio, models with S/D ratios of 4, 6, 8, and 10 were analyzed. It was found that S/D=4 demonstrated the best performance, characterized by the smallest displacements and the highest load transfer efficiency. With an increase in S/D ratio, the influence of the piles on the stability of the slope diminished that allowed the soil to flow more easily through the gaps between piles. Regarding pile configuration, models with single, double and staggered rows were investigated. Staggered rows were found to be the most effective, resulting in the smallest displacements and efficient load transfer. In contrast, double rows exhibited higher displacements and less effective load transfer.

Ho *et.al* (2014) demonstrated the disadvantages of using 2D slope models compared with using 3D slope models. The study addressed the limitations of 2D FE models by incorporating the complexities of soil flow between piles, soil arching effects, and 3D stress distributions. The study investigated the impact of various factors on the effectiveness of piles in slope stabilization. Piles were strategically placed at the toe, middle, and crest of the slope, with the

middle of the slope identified as the optimal location, providing the highest *FS*. Piles at the toe and crest offered minimal improvement, with *FS* values of 1.39, similar to those obtained for the natural slope prior to stabilization. In order to evaluate the optimal pile length, pile lengths starting from 20 m to 38 m were analyzed, corresponding to a pile length to slope height ratio (L/H) of 0.5 to 0.95 for a 40 m high slope. The *FS* increased significantly up to L/H = 0.70, indicating this as the optimal pile length; beyond this ratio, the *FS* plateaued, showing no further stability improvement. Furthermore, fixed-head piles outperformed free head piles, offering higher *FS* values due to restrictions on rotations and displacements at the pile head, enhancing the overall performance of the pile group.

Li *et al.* (2015) presented an analytical approach to optimize the arrangement of stabilizing piles for colluvial landslides by utilizing a half-simplified flattened ellipsoid model (*see* Figure 2.1) to capture the 3D nature of the sliding mass in colluvial landslides. This model reflects the natural variation in sliding mass thickness and driving force intensity across different sections of a landslide. The model assumes that the sliding mass has a maximum depth at the central part of the landslide, that decreases towards the boundaries of the landslide. The spatial geometry of the sliding mass was represented using elliptic equations for cross-sectional and longitudinal profiles. The driving force intensity varies spatially, being highest near the major slip profile and decreasing towards the boundaries. Given that the driving force is highest in the central part of the landslide, the model suggests that pile spacing should be closer in this region and it should increase steadily towards the boundaries where the driving force is lower. By applying the non-uniformly spaced arrangement principle to the Erliban landslide, the authors demonstrated that the spatially varying driving force could be effectively managed with fewer stabilizing piles. In the case study of the Erliban landslide, the optimal non-uniformly spaced arrangement required fewer piles than the conventional uniformly spaced arrangement. Specifically, 25 piles were required instead of 31, resulting in a 19.4% reduction in pile spacing. The reduction in the number of piles directly translated to lower construction costs.

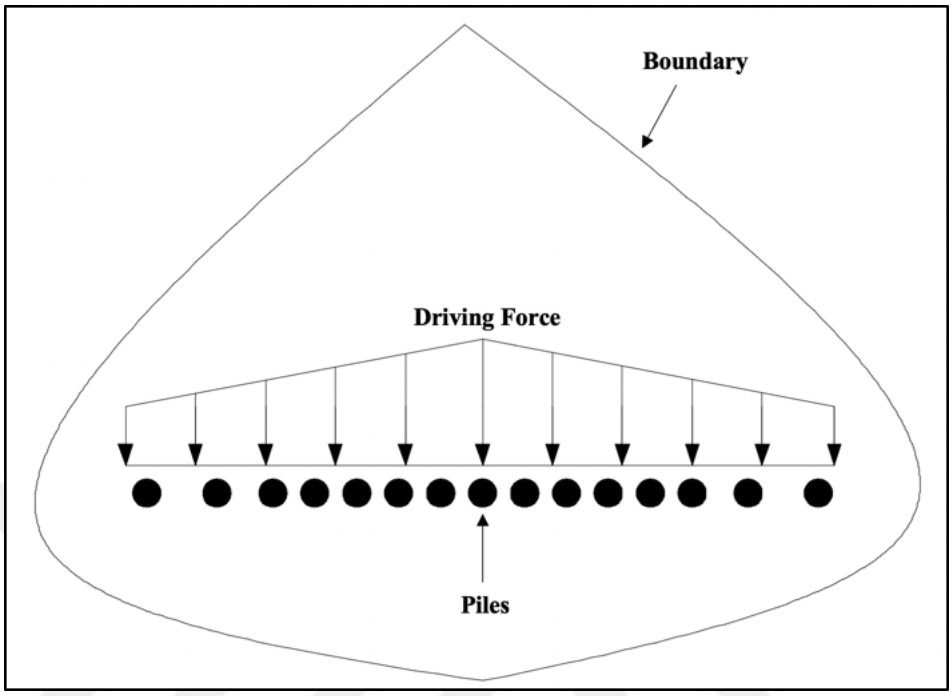


Figure 2.1. The non-uniformly spaced pile arrangement to minimize cost in colluvial landslide (modified after Li *et al*., 2015).

Gao *et al.* (2015) investigated the stability of slopes reinforced with a single row of piles, extending the traditional 2D analysis to a 3D one. The study utilized a 3D rotational failure mechanism to analyze slopes, highlighting the importance of end effects that are often overlooked in 2D stability assessments. These end effects are particularly significant for slopes with narrow widths, providing additional resistance to slope failure by limiting the extent of the failure surface. Results of this study showed that this additional resistance contributes to the overall stability of the slope, making the 3D analysis more suitable for designing slopes reinforced with piles compared to traditional 2D methods. The study also explored the impact of the S/D ratio on the *FS*, revealing that smaller S/D ratios significantly increased *FS* due to the enhanced group effect of closely spaced piles. When the S/D ratio is less than 2.5, the increase in *FS* was notable, as the piles worked more effectively as a group. Conversely, as the S/D ratio increased, the piles start to act more individually, reducing their collective stabilizing effect. Furthermore, the study identified the most effective location for piles as being between the middle and the crest of the slope. This positioning maximized the stabilizing effect by

providing resistance where the potential slip surface is most vulnerable, with parametric studies showing that the *FS* is highest when piles are placed between the middle and crest of the slope.

He *et al*. (2016) investigated the soil arching in pile-stabilized slopes. The researchers developed a FE model using Plaxis software and applied the orthogonal testing method to determine the significance and optimal combination of factors affecting soil arching. For single row of piles, the most important factor was the S/D ratio. In contrast, for double rows of piles, the most important factors were the S/D ratio and the distance between the rows. The study showed that staggered pile designs are more effective than parallel ones. Staggered piles bear more stress and thus are better at controlling slides than those of parallel pile configurations. This was attributed to the staggered design allowing the back row to support more load.

Li *et al*. (2019) found the solution of the problem of stabilizing large and complex slopes using piles by a simplified analytical model. This study revealed the disadvantage of using single row piles and recommended the use of double row piles for such slopes. The study presents an analytical model combining the kinematic approach of limit analysis with the strength reduction method to determine the optimal location of pile groups in various conditions. The study investigated the optimal position for multi-row stabilizing piles. and suggested that the optimum location for double row piles is in the middle to lower part of the slope.

Wei *et al.* (2019) studied the behavior of slopes reinforced with a single row of piles and focused on both the development of the critical sliding surface and optimum position of piles. Results of these analyses revealed that as the S/D ratio decreases, the critical sliding surface gets shallow, the surface divides into two parts and with increasing the S/D ratio the sliding surface gradually forms a separate single surface and the sliding surface gets significantly deeper. This behavior is attributed to the shear strain mobilization around the piles. When piles are closely spaced, the soil movement between them is restricted, creating two separate slip surfaces. As the spacing increases, the soil has more freedom to move, merging the slip surfaces into one. It means that the presence of piles tends to shift the mechanism of slope failure, which results in a decrease in the critical sliding surface as compared to slopes with no reinforcement. Notably,

the study challenges conventional analyses based on maximum shear force. In fact, the study claims that maximum shear strain directly determines the actual critical sliding surface. This paper states that the location of maximum shear force within the pile would not coincide with the actual critical slip surface, so shear strain should be considered while analyzing slope stability. The study also provided a strategy of optimal pile position offering that it should be located somewhere between the midpoint of the slope and the midpoint of critical slip surface. The purpose of such placement is to minimize the use of materials and the cost of construction and maximizing the efficiency of slope reinforcement. It also recognized the influence of soil type on optimal pile positioning, noting variations between sandy and clayey soils. In particular, to balance the resistance against soil movement a middle location is recommended for sandy slopes due to fact that sandy slopes tend to have shallow slip surfaces due to low cohesion. In the case of clayey slopes, a deeper slip surface is observed In this case the optimal pile position is slightly towards the crest of the slope to provide adequate resistance to the deeper slip surfaces.

Wang *et al.* (2020) investigated the effectiveness of a novel anti-sliding structural system comprising arched micropile groups in enhancing the stability of the Tizicao high-position landslide in the Wenchuan seismic area of China. Using FD coupled with the strength reduction technique, the research evaluated the landslide stability improvements achieved by micro pile groups and groups in combination with prestressed anchor cables. The embedded micropile groups alone were found to improve the stability of the landslide better than when combined with prestressed anchor cables. Multirow arc-shaped arrangement of micro pile groups demonstrated a substantial arching effect, effectively impeding landslide movement, the load from the sliding mass shared in two main parts. The micropiles took a part of the load directly. The soil arching effect behind the micropiles took a significant portion of the load. More than 80% of the total load was handled by the soil arching effect.

Benmebarek *et al.* (2021) investigated the efficacy of pile configurations to enhance the stability of cohesive slopes through numerical analyses performed using Plaxis 2D and 3D. The study first examined unstabilized slope stability through both 2D and 3D analyses, which

yielded similar *FS*, thereby validating the numerical models. The optimal pile location was identified as the middle of the slope, providing the highest *FS* due to balanced distribution of stabilizing forces. Comparative analyses consistently showed higher *FS* values for mid-slope pile placements in both 2D and 3D analyses. Additionally, pile head conditions played a significant role; fixed and hinged heads improved *FS* substantially compared to non-rotated and free heads, with free head piles allowing more movement and contributing less to stabilization. For fixed-head piles, the optimal length was found to be at about half the slope height. S/D ratio analysis revealed that in 3D models, *FS* declined sharply when the S/D ratio exceeded 4. Notably, at S/D=8, a significant *FS* reduction occurred, indicating diminished arching effectiveness, and at S/D=12, *FS* values approached to those of unstabilized slopes, confirming the loss of soil arching effect. S/D=4 was identified as the critical S/D ratio for effective soil arching. The study highlighted the superiority of 3D analyses over 2D analyses in capturing the impact of S/D ratio, as 2D analysis failed to accurately reflect the reduction in *FS* for S/D ratios greater than 4.

Li *et al.* (2021) presented a comprehensive analysis of new systems named as arched anti-slip pile-wall structures (*see* Figure 2.2) designed to solve problems related to unreasonable force and large deformation taking place in traditional anti-slip structures, specially developed for the loess landslide control project in Northern Shanxi Province. The results showed that the arched anti-slip pile-wall system offered noticeable advantages over traditional structures. By establishing a rigid connection between the piles and the cap beam, the system forms a rigid structure with a sliding soil mass, effectively distributing the bending moments created by the landslide thrust and minimizing stresses and deformations throughout the system. This resulted in an improvement in overall stiffness and bending moment capacity, lowering the possibility of the structural failure of an individual pile owing to excess load. Comparative analysis shows that the system of arched anti-slip pile-wall structures was significantly superior to traditional structures, providing a reduction in the displacement of the pile head by about 60% and the total bending moment by 6%. Additionally, modified versions of the system, namely the anchorage arch anti-slide pile-wall structure system and pull-rod arch anti-slide pile-wall structure system further enhanced structural robustness by controlling cap beam deformation and coordinating

stress distribution among piles. It is noteworthy that the system of anti-slip pile-wall structures with a pull-rod turns out to be the most effective solution, demonstrating excellent efficiency in landslide risk management with 95% structural reliability.

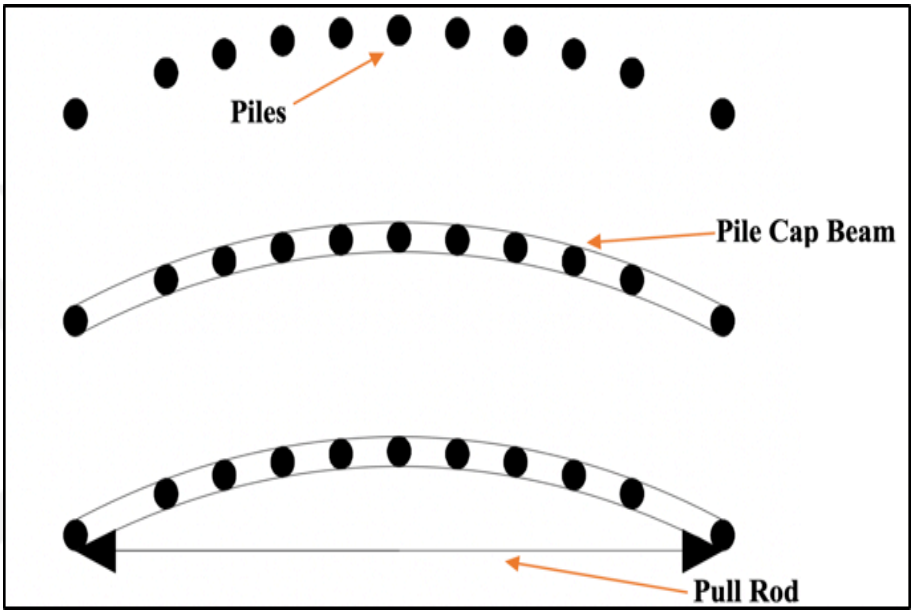


Figure 2.2. Arch anti-slip pile-wall structures used to stabilize landslides (modified after Li *et al*., 2021).

Xie *et al.* (2021) investigated the interaction between load-caused landslides and double-row anti-slide piles. Through model tests, it explored the influence of S/D ratio and row spacing variations on pile-soil interaction, revealing three distinct stages of during slope failure evolution.: initial deformation, soil arch stability, and soil arch deformation. Results indicated that, an optimal row spacing of 3-5 times pile diameter and S/D=4 establish an effective slope stabilization, higher S/D ratio increased soil flow around piles, significantly impacting landslide displacement control whereas smaller S/D ratio (S/D=3) resulted in shielding effects that reduced the efficiency of the system. Additionally, results showed that increasing row spacing weakens the reinforcement effect between front piles and rear piles. Notably, excessively high row spacing and S/D ratio eliminate the soil arching stability stage during slope failure evolution.

Lei *et al.* (2021) discussed the critical problem of slope failure and the effectiveness of stabilizing piles in preventing such phenomena. Through numerical simulation using the FD method, the study examined factors such as failure mode, load distribution, bending moment distribution and *FS*. It concluded that failure mode of single row and double row piles differ, with the latter demonstrating more complex behavior broken down into five different scenarios. Single row piles are most effective in the lower to middle part of the slope, where they intercept the deep sliding surfaces. Double row piles perform best when the second row is at the toe and the first row in the lower middle part of the slope. This configuration maximized the *FS* by providing resistance to both shallow and deep sliding surfaces.

Fayed *et al.* (2021) investigated the effect of pile installation on slope stability using a 3D FE model validated by a large-scale experimental model. The study employed Plaxis 3D coupled with the shear strength reduction technique to analyze the impact of various factors, including pile position along the slope, pile length, diameter, and S/D ratio. The main findings indicated that the optimal pile position was from the middle to the upper part of the slope. The effect of the S/D ratio on the safety was minimal when the piles were placed near the crest or toe of the slope. Additionally, vertical piles were found to increase slope stability more effectively than the inclined ones. Regarding the pile diameter, it was found that increasing the diameter beyond 0.5m offered negligible improvement in the *FS*, indicating that larger diameters did not significantly enhance soil-pile interaction.

Wang *et.al.* (2022), analyzed the influence of pile configurations on the stabilization of slopes along the Chengdu–Lanzhou Railway. This study was conducted using the MIDAS GTS NX program, which is a FEM based software. The study investigated the impact of various factors on the effectiveness of piles in slope stabilization. Using piles with a diameter of 1.5 meters, the research explored nine different S/D ratio values ranging from 1.33 to 6.67 meters. The results demonstrated a clear trend: as S/D ratio increased, the reinforcement effect diminished, with the *FS* dropping from 1.795 to 1.367 with an increase in S/D ratio from 1/33 to 6.67. The arrangement of piles also played a crucial role. The staggered configuration was more effective than a parallel one, especially for larger S/D ratios, as it provides more even pile

internal force distribution and hence, superior support. Additionally, the study varied the horizontal distance between piles and the slope toe, from 7.5 meters to 13.5 meters. The optimal position of the piles was identified at 11.5 meters from the slope toe, where the *FS* reached a peak value of 1.701. Pile positions with either closer to or farther from the toe compared with this optimal distance resulted in reduced *FS*, underscoring the significance of precise pile placement for maximum slope stability.

Dai *et al.* (2022) investigated various pile configurations, with special emphasis on the Davangjiang landslide site. Authors compared the effects of straight line and polyline layouts of piles on landslide stabilization using numerical methods. The straight line layout of piles proved to be more effective in preventing landslide movements, ensuring the structural safety of the piles compared to the polyline layout (*see* Figure 2.3). This effectiveness is attributed to the uniform distribution of pile head displacement, smaller plastic zones, and even internal force distribution, all contributing to a more stable performance in stabilizing landslides. In contrast, the polyline layout posed greater risks to the structural integrity of the piles and is less effective in landslide stabilization, as indicated by larger displacement zones, more extensive plastic failure areas, and higher, non-uniform internal forces. Furthermore, the soil arching effect was more favorable under the straight line arrangement, as the uniform soil arching effect leads to better distribution of stresses and forces, reducing the risk of localized failures and enhancing overall stability. Conversely, the polyline arrangement resulted in uneven soil arching, increased stress concentrations, and higher risks of structural damage.

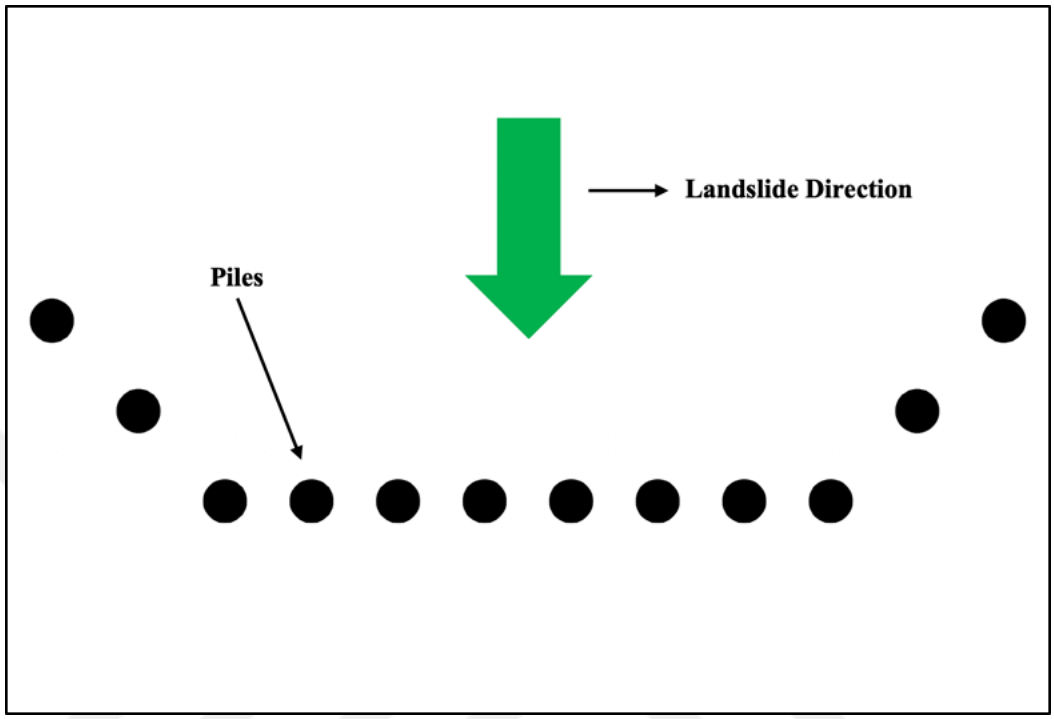


Figure 2.3. Slope stabilizing pile configuration in polyline shape considering the landslide direction (modified after Dai *et al*., 2022).

Shangguan *et al.* (2023) investigated the effect of soil arching in piles that stabilize landslides, paying special attention to the Xinyang landslide in Jilin Province. In this study a FD based software, FLAC-3D, was used for numerical analysis to study the effect of the configuration of piles, placed in a double row fashion. The results showed that in a parallel arrangement, soil arches are formed between two adjacent piles in the same row. Conversely, a staggered arrangement generated more complex stress patterns, in which soil arching start occuriong between the adjacent piles located in different rows; in other words between piles from front row and rear row. Figure 2.4 shows a simple schematic of the soil displacement tendency and hence, the soil arching locations for both parallel and staggered pile group arrangements. Regarding displacement, the parallel pile row arrangement showed larger displacements in the spaces between piles, with relatively smaller displacements around the piles. In contrast, the staggered arrangement effectively restricted soil movement, resulting in less overall soil displacement compared to the parallel arrangement. These observations showed

that the staggered arrangement proves to be more effective in generating soil arches and minimizing soil displacement, demonstrating its advantage in stabilizing slopes.

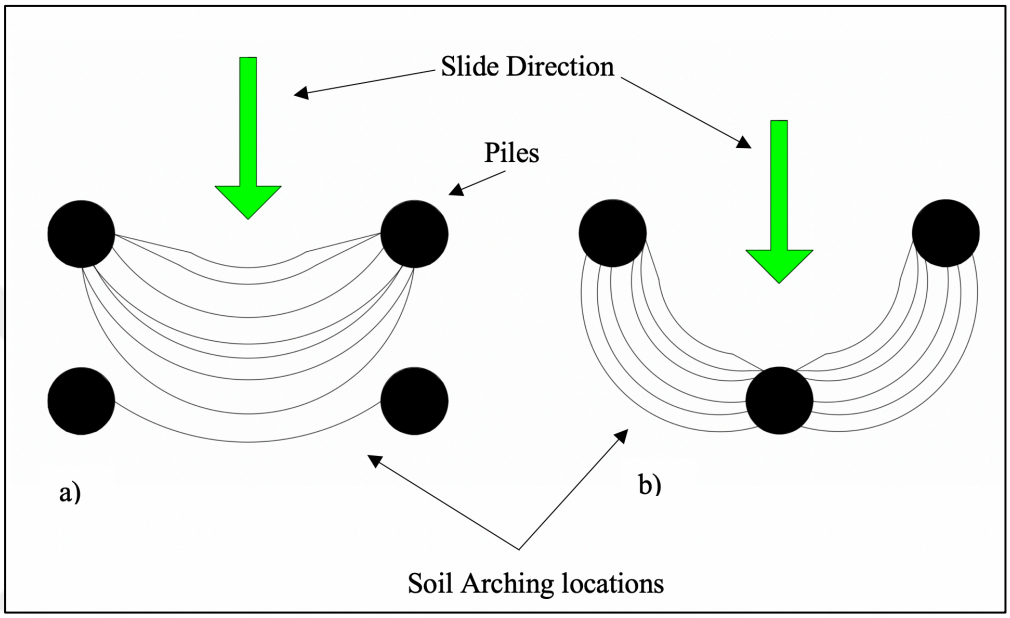


Figure 2.4. Soil mass displacement directions for different pile configurations (modified after Shangguan *et al.*,2023): a) parallel, b) staggered.

Herda *et al.* (2023) evaluated the usefulness of multiple rows of minipiles to improve slope stability, particularly in cases when single row piles are insufficient for complex slope conditions. Through consolidated undrained triaxial (CIU) tests on reconstituted saturated residual soil samples, the study explained the behavior of shear strength by noting an increase in the friction angle of the soil with relative density, while soil cohesion remains relatively constant. Using a simplified method of pile-slope analysis, the study evaluated the response of stabilized slopes with minipiles, examined factors such as the number of rows of piles, the position of the piles and geometry of the slope. The study confirms that using multiple rows of minipiles significantly increases the stability of residual soil slopes compared to a single row. More rows of minipiles increase slope stability, resulting in smaller net forces on piles, optimizing pile design. The study found that piles placed near the slope toe provided the highest increase in *FS*. Stability decreased as piles are placed further from the slope toe. Minipiles near

the slope toe were more effective in enhancing stability. The slope toe was critical for stabilization because it is where the driving forces of the sliding mass are most effectively counteracted. Piles at the toe acted as a barrier, preventing the soil mass from moving downward.

While extensive research has been conducted on the optimal positioning, spacing, and diameter of piles for stabilizing slopes, there remains a significant gap in the literature regarding the combined parametric effects of pile group position, spacing, number of rows, and pile head condition. Most studies tend to focus on individual factors in isolation, providing valuable but limited insights into slope stabilization techniques. However, the complex interaction between these parameters is crucial for a comprehensive understanding of slope stabilization using pile groups. Additionally, in the majority of the studies performed to date, the piles in the pile groups were assumed elastic, and the structural failure of the piles were not taken into account leading to unreasonably high *FS* values. A parametric investigation that considers the combined effects of these variables and the critical failure mechanism of the pile-slope system considering piles can also fail structurally, can provide insights into more effective and efficient stabilization strategies. Such an investigation would provide a more integrated approach, enhancing the design and implementation of pile groups for slope stabilization, ensuring greater safety and cost-effectiveness in geotechnical engineering practice and shed light to future research in this topic.

3. RESEARCH METHODOLOGY

Pile-stabilized slope cases investigateed in this study were modeled and analyzed by the geotechnical software that utilize 3D FE method. The methodology of this research study, including the details of the 3D FE software, material modeling, attributes of 3D models, analysis stages, and the case selection approach are presented in this chapter.

3.1. Plaxis 3D Overview

In recent years, there has been an increase in geotechnical software that performs three-dimensional slope stability analyses using both FE and Finite Difference (FD) methods, such as Plaxis 3D, Flac 3D and GTS NX. In this study, pile-stabilized slope models were simulated in the 3D FE software Plaxis 3D which is widely used in geotechnical engineering practice. The name Plaxis is derived from the words plastic and axisymmetry. Plaxis 3D works in two user interfaces: the input and output interface. The Input interface is mainly used for defining the 3D model and the details of the analysis. At the beginning of the input interface, project properties are requested from the user. Input interface includes introduction of soil properties, determining the structures, generation of mesh, determining water levels, and defining stages of construction.

3.2. Material Modeling

3.2.1. Modeling of Soil

FEM is a numerical method widely used in engineering. It allows engineers to solve complex problems by dividing a domain into smaller, simpler elements, where equations are formulated and solved locally. Within the framework of this method, displacements are determined using the specified stress-strain relationships and solutions of the corresponding differential equations. Selecting the appropriate material model in Plaxis 3D is crucial for obtaining accurate and reliable results (Obrzud and Truty, 2018) . The accuracy of FEM analyses heavily depends on the choice of constitutive models that describe how materials respond to various loading conditions. Therefore, selecting the material model carefully is an important step in conducting FE analyses. Plaxis 3D offers many well-known soil constitutive models widely used in geotechnical analysis. Among them, are simple linear elastic models, Mohr-Coulomb (MC) models, hardening soil (HS) models, hardening soil models with a small strain stiffness (HSS), NGI-ADP models.

The linear elastic model assumes elastic material behavior and is suitable for initial analyses of small strains where the stress-strain relationship remains linear throughout deformation. MC model is widely used to describe material failure using a linear failure envelope defined by cohesion and friction angle parameters. HS model is an advanced geotechnical model that incorporates soil stiffness variations with stress levels.The HSS model enhances the HS model by incorporating increased stiffness at small strains, thereby improving accuracy in simulating soil behavior. The NGI-ADP model, developed by the Norwegian Geotechnical Institute, incorporates anisotropic, dynamic, and plastic behaviors, making it suitable for advanced analyses involving anisotropic soils and dynamic loading conditions.

The HS and HSS models are constitutive soil models that utilize hardening plasticity principles, to provide more accurate predictions of soil response under various loading conditions. Particularly suitable for soft or clayey soils, they exhibit an advantageous feature where the yield surface can expand with plastic strains (Brinkgreve *et al*., 2021). All of the input parameters required for HS and HSS models are provided in Table *3.1*. The formulations of the major parameters and their selection are explained in the following sections.

In HS models, three distinct stiffness parameters are incorporated to accurately capture the stress-dependent stiffness behaviors of soils: tangent stiffness for primary oedometer loading (E_{oed}^{ref}), secant stiffness in a standard drained triaxial test (E_{50}^{ref}), and unloading/reloading stiffness (E_{ur}^{ref}). In a standard drained triaxial test, the secant stiffness is defined as the stiffness at 50% of the maximum deviatoric stress, at a reference stress level. In Plaxis 3D, the default reference stress level (p^{ref}) value for stiffness parameters is 100 kPa. For practical geotechnical engineering applications, it's recommended to set E_{50}^{ref} equal to E_{ur}^{ref} and E_{ur}^{ref} equal to 3 times E_{50}^{ref} and this is the default setting used in Plaxis 3D (Brinkgreve *et al*., 2021).

Table 3.1. The parameters required for HS and HSS soil models (modified after Brinkgreve *et al*., 2021).

Model		Parameter	Symbol	Unit	
HS Model	**HSS Model**	Effective cohesion	c'	kPa	Failure parameters as in Mohr-Coulomb model
		Effective friction angle	φ'	Degree	
		Dilatancy angle	ψ	Degree	
		Tension cut-off	σ_t	kPa	
		Secant stiffness in standard drained triaxial test	E_{50}^{ref}	kPa	Basic parameters for soil stiffness
		Tangent stiffness for primary oedometer loading	E_{oed}^{ref}	kPa	
		Unloading/Loading stiffness	E_{ur}^{ref}	kPa	
		Power for the stress-level dependency of stiffness	m	-	
		Poisson ratio for unloading-reloading	v_{ur}	-	Advanced parameters
		Failure ratio	R_f	-	
		Reference stress for stiffness	p^{ref}	kPa	
		Reference shear modulus at very small strains	G_0^{ref}	kPa	
		Threshold shear strain	$y_{0.7}$	-	

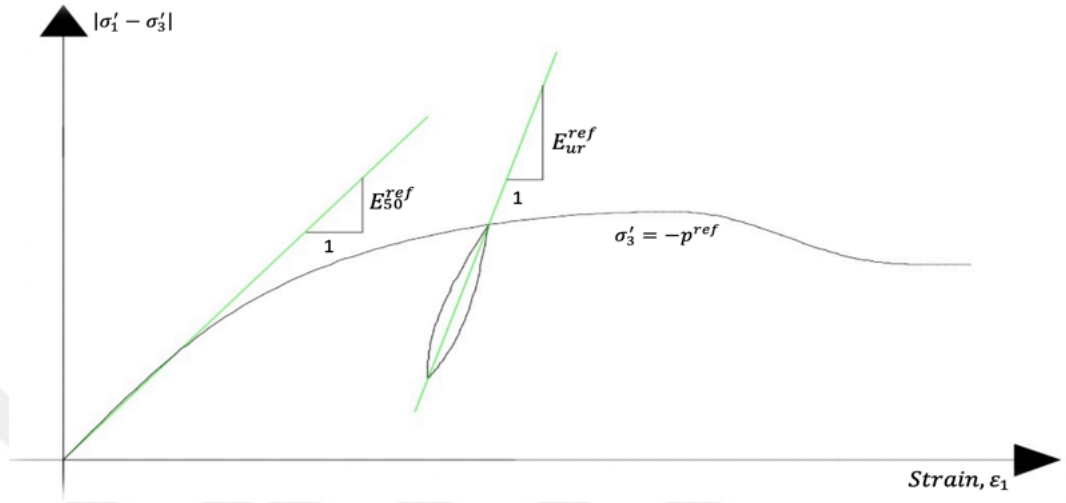


Figure 3.1. Determination of E_{50}^{ref} and E_{ur}^{ref} values from drained triaxial test results.

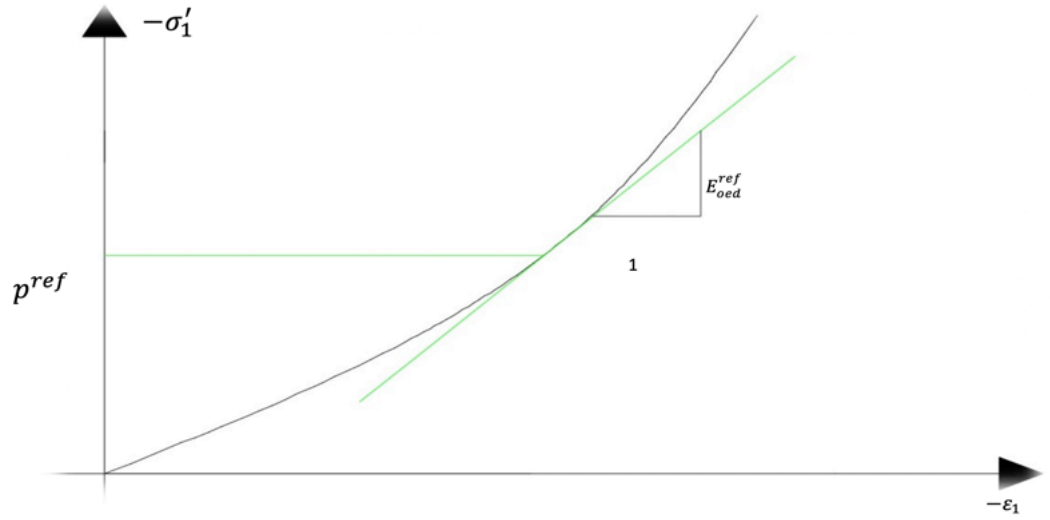


Figure 3.2. Determination of E_{oed}^{ref} value from oedometer test result.

In the HS models, stress dependency of soil stiffness for oedometer conditions is expressed as

$$E_{oed} = E_{oed}^{ref} \left(\frac{\sigma}{p^{ref}} \right)^{m}, \tag{3.1}$$

where the parameter denoted as *m* governs the stress-dependent stiffness of soil. In natural soil, the exponent *m* varies between 0.3 and 1. For clays this parameter equals to 1, while for silts and sands it varies from 0.5 to 1 (Obrzud and Truty, 2010). Suggested range of values for *m* are shown in Table 3.2.

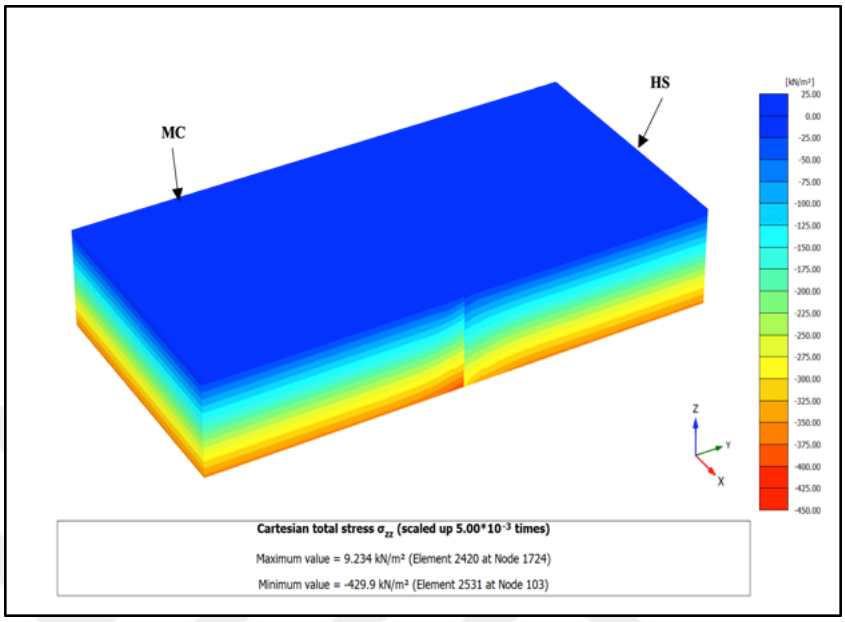
Table 3.2. Suggested ranges of *m* values (modified after von Soos *et al*., 1991).

Soil Type	***m***
Gravel, poorly graded	0.4-0.6
Gravel: sandy, well graded	0.5-0.7
Gravel: silty or clayey, well graded, not crushed	0.5-0.7
Gravel-sand-clay mixture, crushed	0.7-0.9
Sand: fine, uniform	0.6-0.75
Sand: coarse, uniform	0.55-0.7
Sand: well-graded and gravelly sand	0.55-0.7
Sand: with fines, not crushed	0.65-0.8
Sand: with fines, crushed	0.75-0.9
Silt: low plasticity	0.6-0.8
Silt: medium and high plasticity	0.7-0.9
Clay: low plasticity	0.9-1
Clay: medium plasticity	0.95-1
Clay: high plasticity	1
Silt or clay: organic	0.85-1
Peat	1
Mud	0.9-1

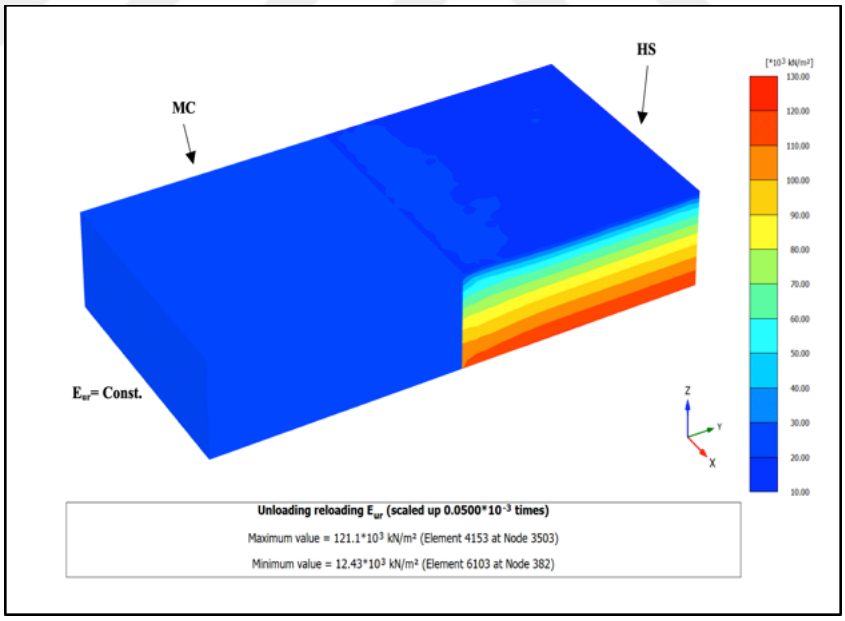
Another parameter utilized in simulating the plastic yielding of soils is failure ratio (R_f), which is the ratio of the ultimate deviatoric stress, and the asymptotic value of the shear strength defined with respect to MC failure criterion. If R_f =1, the failure criterion is satisfied and perfectly plastic yielding occurs. R_f in Plaxis is given as 0.9 for the standard default value (Brinkgreve *et al*., 2021).

The HS model assumes the elastic behavior of the soil during unloading and reloading. However, the ability of the soil to undergo elastic deformation and fully recover after applied deformation is limited by a narrow range, as strain amplitude increases, soil stiffness decreases in a nonlinear manner. The non-linear dependency of soil stiffness on very small strain amplitudes must be accurately considered. The HS model with small-strain stiffness, in addition to all the features of the standard HS model, provides the capability to address this aspect (Brinkgreve *et al*., 2021). A modified version of the HS, the HSS model considers the enhanced stiffness of soils under small strain conditions, at such low levels of strain, soils usually exhibit a higher level of rigidity than under engineering deformation conditions (Obrzud and Truty, 2010).

Main characteristic of the HS model is its consideration of the stress dependency of soil stiffness. In order to better explain the differences between MC and HS model as well as stress-dependent stiffness behavior of HS model, a simple 3D Plaxis model is created. Figure 3.3a presents the total vertical stress distribution of the same model using both MC and HS soil constitutive models, side by side for comparison purposes. Figure 3.3b depicts the variation in unloading/reloading stiffness (E_{ur}) values for the soils modeled with MC and HS constitutive models. The results shown in Figure 3.3b highights the stress dependency of soil stiffness, a key feature of the HS model. Similar dependency is valid for HSS model.



(a)



(b)

Figure 3.3. Differences between MC model and HS model: (a) Total Stresses, (b) Unloading/Reloading Stiffness.

The HSS model has two additional parameters: the initial small-strain shear modulus (G_0^{ref}) and the shear strain level at which the secant shear modulus decreases to approximately 70% of the initial small-strain shear modulus ($y_{0.7}$). Most importantly these parameters are influenced by the material's actual state of stress and void ratio (Brinkgreve *et al*., 2021). The initial value of the small-strain shear modulus can also be calculated as

$$G_0^{ref} = \frac{E_0^{ref}}{2(1+v_{ur})}, \tag{3.2}$$

by using to small strain Young's modulus (E_0^{ref}) and Poisson ratio (v_{ur}) for unloading-reloading which is suggested as 0.2 by default in Plaxis 3D. The Second parameter, $y_{0.7}$ value can be expressed as

$$y_{0.7} = \frac{1}{9\times G_0}\left[[2c'(1+\cos(2\varphi')] - \sigma_1'(1+K_0)\sin(2\varphi')\right], \tag{3.3}$$

where G_0 is the shear modulus at small strain level, c' is cohesion, K_0 is the earth pressure coefficient at rest (initial stress state) and σ_1' is the effective vertical stress. The HSS model is a recommended constitutive model, especially useful for modeling over-consolidated clays and sands. Most soil types can be effectively modeled using the HSS model, which incorporates two distinct hardening mechanisms. The shear mechanism addresses plastic straining primarily caused by shearing, a behavior typically observed in granular soils and overconsolidated cohesive soils. Shear hardening captures irreversible strains resulting from primary deviatoric loading, while compression hardening models irreversible plastic strains due to primary compression in both oedometer and isotropic loading scenarios (Brinkgreve *et al.*, 2021). Satisfactory results are also achieved for scenarios involving normally consolidated clays under undrained loading conditions. The HSS model successfully integrates both shear and compression hardening. For slope stability analyses, the HSS model is advocated as one of the premier choices for assessing deformations (Brinkgreve *et al.*, 2021). In the study, both clays and sands were modeled using the HSS model in Plaxis 3D, which offers two drainage options: 'Undrained A', utilizing effective stress parameters and deriving undrained shear strength (S_u) as an output based on generated pore pressures, and 'Undrained B', requiring explicit undrained

strength parameters where S_u is an input, suited for scenarios in which effective strength parameters are unavailable (Brinkgreve *et al.*, 2021). A summary of the material properties used in this study is provided in Table 3.3.

Table 3.3. Soil properties utilized in the parametric study.

Soil	**Drainage Condition**	γ (kN/m^3)	S_u (kPa)	c' (kPa)	ϕ' (^{o})	E_{50}^{ref} (kN/m^2)	E_{oed}^{ref} (kN/m^2)	E_{ur}^{ref} (kN/m^2)	ψ (^{o})
Clays	Undrained B	16	30-40	-	-	8000-9500	8000-9500	24000-28500	0
Dense Sand	Drained	18	-	1	42	70000	70000	210000	12

3.2.2. Modeling of Piles

In this study, volume piles with interface elements were used to accurately represent the behavior of piles undergoing lateral movement of the soil. This choice was due to the recognition of the volume pile option as the most suitable and accurate for such modeling in Plaxis 3D (Brinkgreve *et al.*, 2021). The piles were assumed as drilled shafts and an elastoplastic approach was adopted to model reinforced concrete to simulate plastic deformations of the pile and the potential failure in the coupled pile-slope system. In the elastoplastic pile material modeling approach, the parameters of the Mohr-Coulomb (MC) constitutive model were assigned to reinforced concrete elements. The piles were designed using a macroscopic reinforced concrete material approach proposed by Gerolymos *et al.* (2014). Macroscopic material approach considers the details of the reinforcement and the volumes of concrete as uniform element. This approach is relatively simple and straightforward. This approach boasts simplicity and immediate applicability to bending moment-based failure within the studied pile-slope scenario. The validity of this approach was demonstrated by Tekdemir (2023). Table 3.4 presents a summary of the material properties which corresponds to C30 concrete, used in this study.

Table 3.4. Pile material properties (adopted from Gerolymos *et al.*, 2014).

E (GPa)	**c (kPa)**	$\boldsymbol{\phi(^o)}$	$\boldsymbol{\sigma_t}$ **(kPa)**
30	15262	0	7534

3.2.3. Attributes of 3D Slope Models

The slopes were modeled using two different methods: one approach involved a full model, and the other approach utilized slice modeling. As mentioned in the first part of this study, full models are very useful for studying the behavior of pile groups under applied local surcharge loads. The width of the full model was 150 meters, the length was 100 meters, and the height is 35 meters. The surcharge load was modeled with dimensions of 12 meters in the X direction and 24 meters in the Y direction. This load was placed in the middle of the slope, one meter from the crest of the slope. The magnitude of surcharge load is 100 kPa. Example of the full model with geometrical parameters is shown in Figure 3.4.. In models with a constrained pile head, a pile cap beam was installed with a cross-section of two by two meters and a length of 39 meters in all cases. Pile cap beam dimensions is shown in Figure 3.5. Boundary conditions preset in Plaxis 3D were employed. A graphical representation of boundary conditions are presented in Figure 3.6..

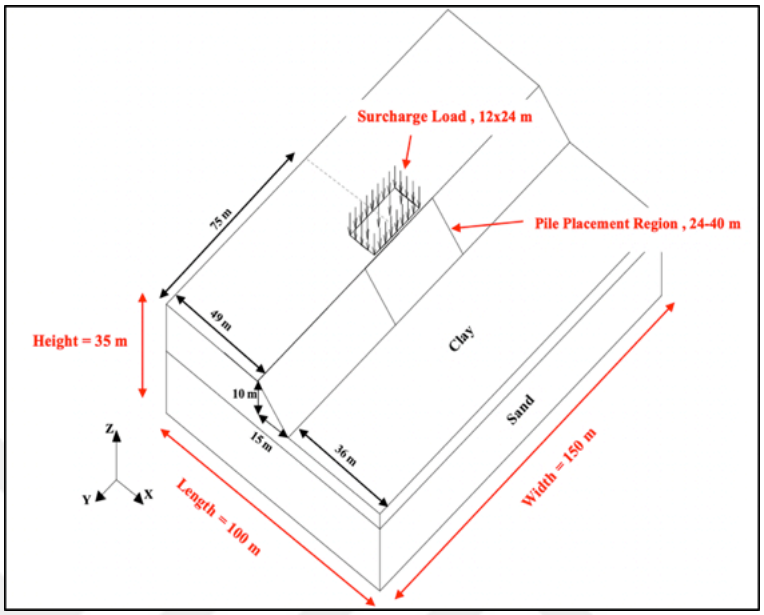


Figure 3.4. Geometry of 3D full model in the Plaxis 3D.

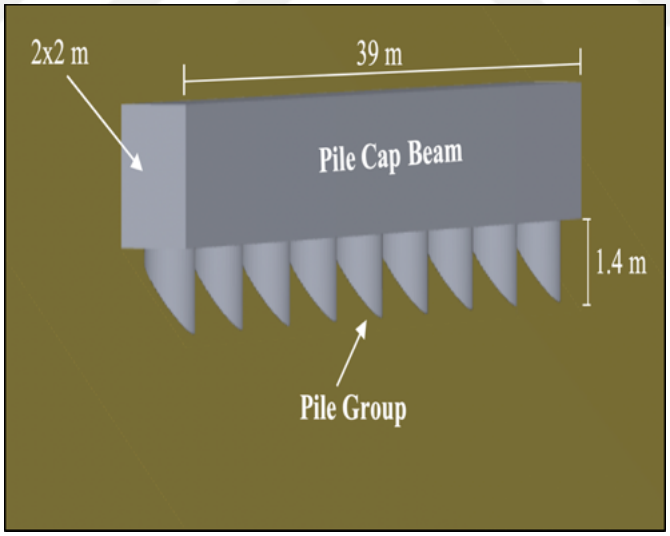


Figure 3.5. Geometry of the pile cap beam in Plaxis3D model.

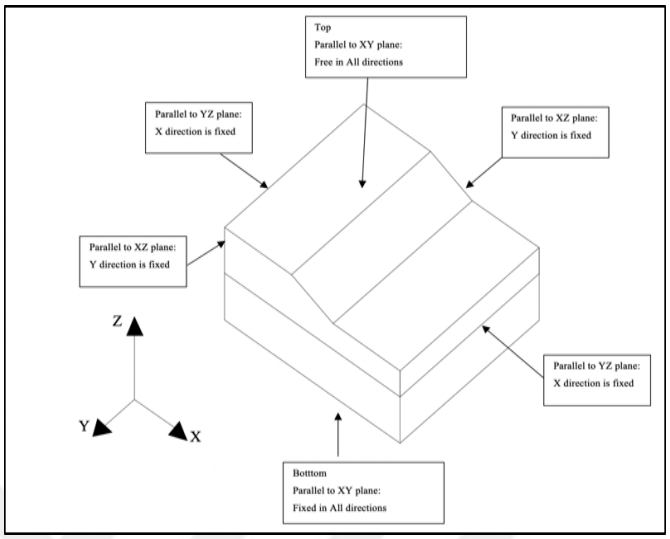


Figure 3.6. Boundary conditions in Plaxis 3D model (Full and Slice Models).

In this study piles with a diameter of 1.5 meter were installed in the middle of the slope, opposite the load application zone. Piles were simulated using volume elements accompanied by interfaces. The interaction between a structure and soil can be simulated by applying interface elements, as without an interface, the piles and the soil are tied together. These interfaces were positioned around the pile and at its base to facilitate the creation of gaps between the volume piles and the surrounding soil. A view of the pile and its interfaces, taken from Plaxis 3D, are presented in Figure 3.7.

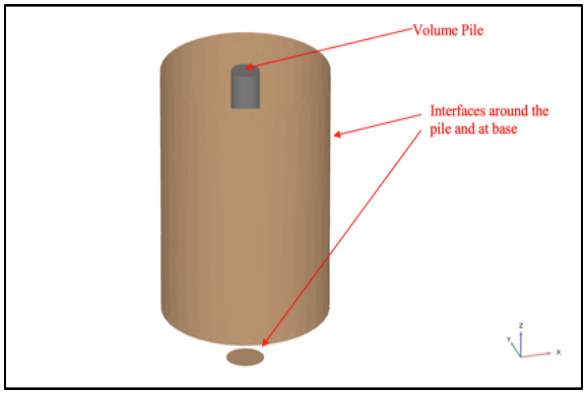
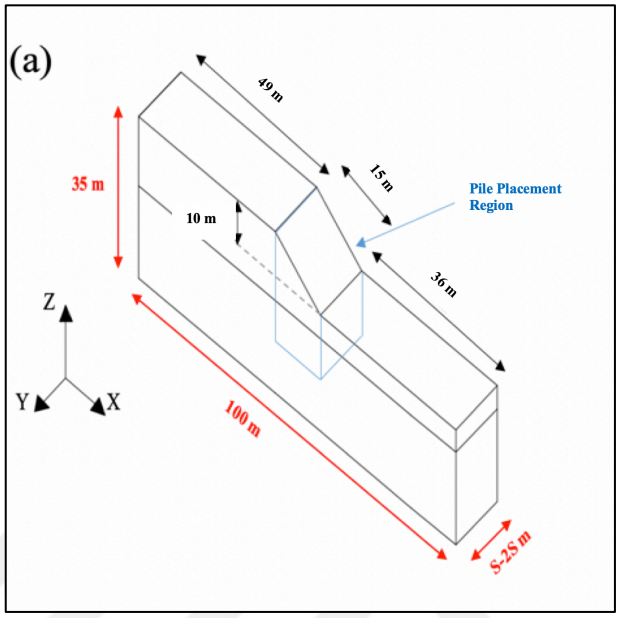


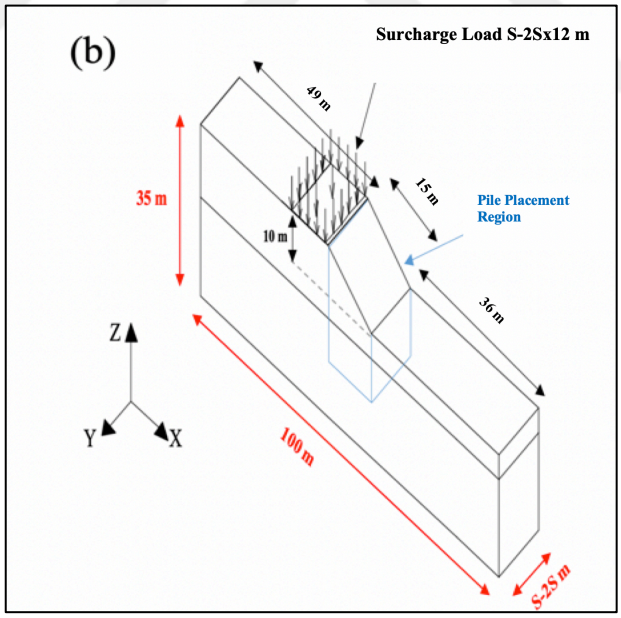
Figure 3.7. Volume pile and interface.

Interfaces are composed of 12-node elements. Interface elements consist of pairs of nodes that are compatible with the 6-node triangular side of a soil element. The main interface parameter is the strength reduction factor (R_{inter}), which plays a vital role in managing the transmission of stresses between soil and structural elements. The determination of R_{inter} values was based on skin friction coefficients between the soils and the construction materials, at the same time change of the skin friction is the function of grain distribution of soils, moisture content, normal load and type of construction material (Potyondy and Eng, 1961).

The interface strength reduction factor (R_{inter}) can be set using two options, rigid and manual, where the rigid option is used when the interface should not have reduced strength with respect to the surrounding soil, resulting in $R_{inter} = 1$. In the manual option, the value of R_{inter} must be entered manually. Suitable values for R_{inter} for the cases of the interaction between various types of soils and structures in the contact with the soil can be found in literature. For example, according to Ter-Martirosyan *et al.* (2019) R_{inter} values varied in the range between 0.52 and 0.71 for fine sands. Kolybin *et al.* (2016) includes a table displaying the values of the strength reduction factor, which vary based on the type of soil, moisture content, and the material of the structure. The values varied in the range of 0 to 0.67. In this study, for interaction between soil and concrete surfaces, R_{inter} values were assigned as 0.6 for clay layers and 0.9 for dense sand layers. The dimensions of the slice models are shown in Figure 3.8. The length and height of the models are the same compared to the full models. The main distinguishing feature between the full model and the slice model is the width.



(a)



(b)

Figure 3.8. Geometry of 3D slice models: (a) natural slope, (b) continuously loaded slope.

In slice modeling of a pile-slope system, the width of each slice is an important parameter that can affect the accuracy and computational efficiency of the analysis. The width of the slice should be determined based on the geometry of the slope, the spacing of the piles, and the

desired level of detail in the analysis. The width of each slice is often related to the spacing between the piles. For example, if piles are spaced at regular intervals, the slice width can be set equal to the pile spacing. This ensures that each slice contains one pile, which simplifies the analysis of the interaction between the pile and the soil. The slice width should be chosen to ensure numerical stability and convergence of the analysis. Extremely narrow slices may lead to numerical difficulties, while very wide slices may oversimplify the problem. In practice, the slice width is often selected through a combination of engineering judgment and iterative testing to ensure a good representation of the pile-slope system. In this study, three different methods were utilized for selecting slice widths. The staggered pile configuration, natural slope, and continuously loaded slope models required different width parameters due to both geometrical and numerical reasons.

As can be seen in Figure 3.9, the first two slices are modeled to analyze the identical problem, differing only in that the first uses a slice model with one pile, while the later uses a slice model with two piles. The width of the slice directly depends on the distance between the piles and the number of piles. The third slice model was prepared to study the effect of staggering.

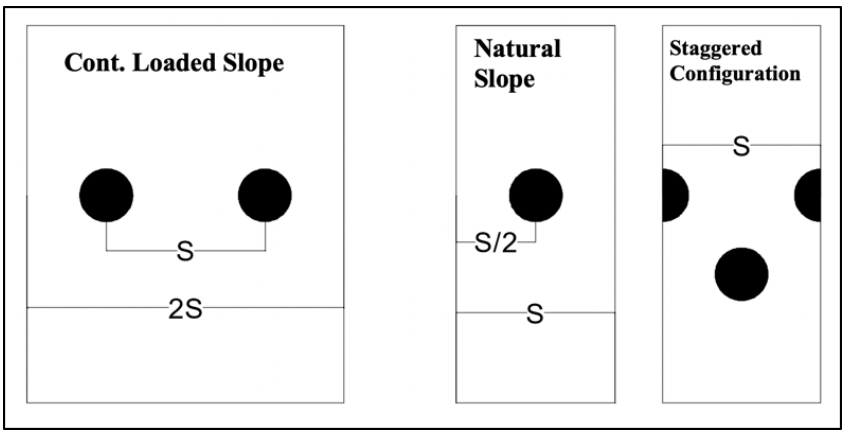


Figure 3.9. Slice models with various widths based on the pile configuration and loading condition.

In the case of a natural slope case, a slice model with one pile was utilized. However, in the cases with continuous loading, a slice model with two piles were used. To ensure the similarity or equality of the results of the analyses conducted, in other words to eliminate the effect of slice selection on the results, initially analyses was carried out using both of these two slide models and the results were compared with each other. The models prepared for this comparsion purposes were presented in Figure 3.10. The results of these analyses are presented below in Table 3.5.

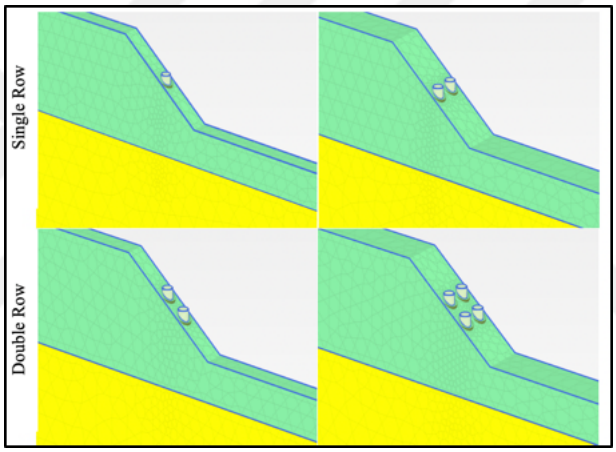


Figure 3.10. Slice models with different number of piles in one slice.

Table 3.5. Comparison of the results of the analysis performed using single row and double row slice models.

Case	FS_{0_PS} Model Type		% Difference
	One Pile	Two Piles	
Single row	2.02	2.02	0
Double rows	2.215	2.217	0.1

3.2.4. Mesh Generation and Distribution in 3D Slope Stability Analysis

When the geometry of the model is fully defined, it must be devided it into elements for finite element calculations. This process, known as meshing, is performed in the mesh mode. The distribution and density of mesh elements significantly impact the outputs of Finite Element analysis; in Plaxis 3D, generation of mesh begins with calculating the model's diagonal length (L_d) and selecting a unitless relative element size factor (r_e) to determine mesh refinement, ranging from very coarse to very fine (Brinkgreve *et al*., 2021).

Table 3.6. Predifined values of r_e (modified after Brinkgreve *et al*., 2021).

Element distribution	**r_e**
Very coarse	2.0
Coarse	1.5
Medium	1.0
Fine	0.7
Very Fine	0.5

Then, the target element size (l_e), specific to each model's geometry, is used to calculate the size of each element by applying selected coarseness factors. Using a coarser mesh in slope stability calculations may oversimplify geometry and soil behavior, potentially yielding overly optimistic safety factor assessments, while a finer mesh offers more detailed stress distribution data, enhancing accuracy in factor of safety calculations. In areas with large stress concentrations or deformation, a finer finite element mesh is desirable, especially near edges, corners, or structural objects, while other parts may not require such detail. Table 3.7 shows coarsness factor destribution in 3D slope models, both for slice and full models. The valididty of this destribution was demonstrated by Tekdemir (2023). Typical mesh distribution of pile-stabilized slopes in slice model and the full model are presented in Figure 3.11. and Figure 3.12, respectively.

Table 3.7. Coarseness factor distribution.

Element	Coarseness Factors	General Mesh Density
Piles and Pile Cap Beam	0.05	Fine
Interfaces	0.05	
Soil Volume Around Piles	0.25	
Other Volumes	0.65 and 1	

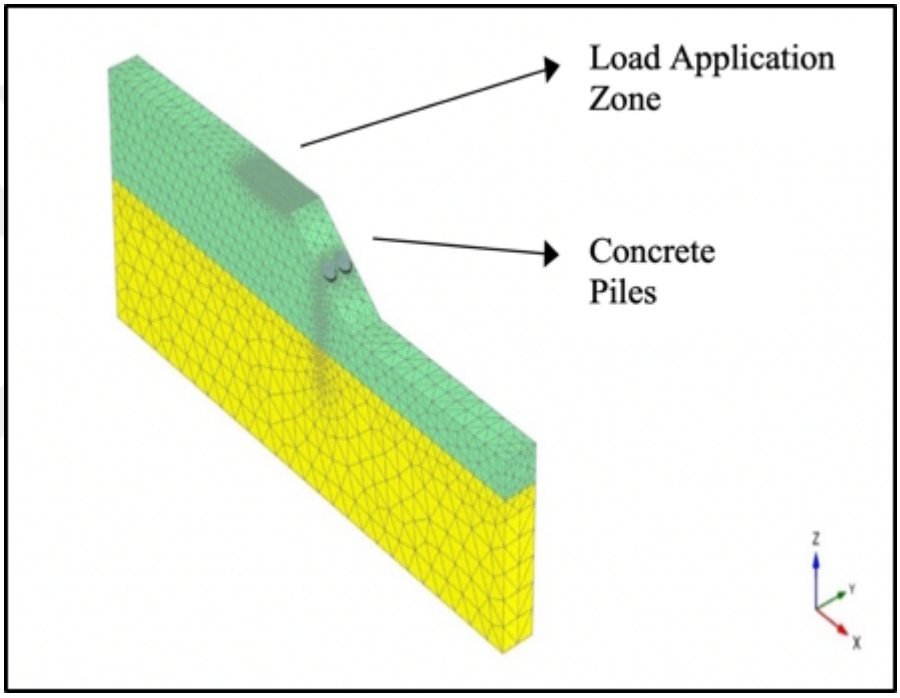


Figure 3.11. Typical mesh distribution of pile-stabilized slopes in slice model.

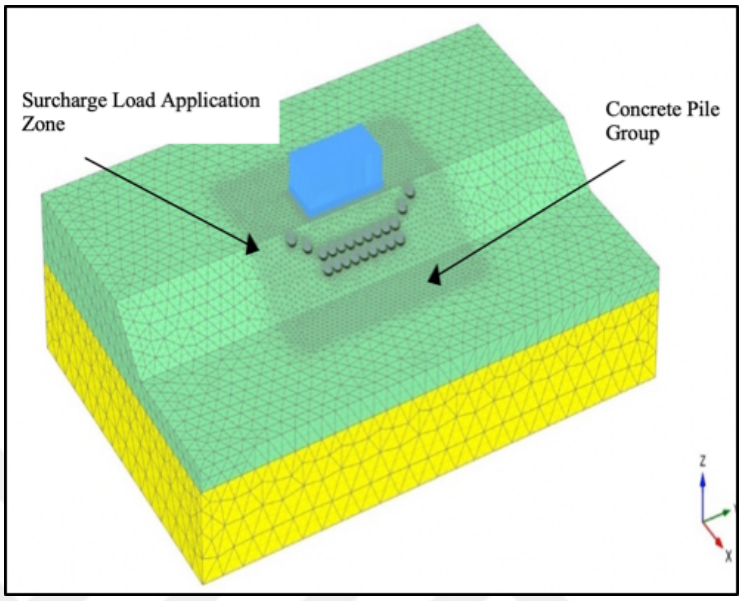


Figure 3.12. Typical mesh distribution of pile-stabilized locally loaded slopes in full model.

3.2.5. Slope Stability Analysis in Plaxis 3D: Staged Construction Steps

In Plaxis 3D, slope stability analysis involves several steps simulated as plastic deformation phases, followed by a conclusive safety phase where the overall factor of safety of the slope is determined using the strength reduction method. The initial phase, termed the first deformation phase, computes the stresses and pore pressures. In slope cases, the gravity loading option is employed to establish force equilibrium by considering the weight of the modeled geometry. Subsequently, displacements calculated during this initial phase are reset to zero. Phase two, the plastic nil phase, remains unchanged from the initial model and serves solely to stabilize any out-of-balance forces. In phase three, volume piles and interface elements are activated. Due to limitations in simulating pile installation in 3D using FEM, volume piles are assumed to be constructed as 'wished-in place piles'. Displacements calculated in this phase are preserved. Additionally, for cases involving pile-stabilized loaded slopes, an extra deformation step is included, activating the surcharge load, before entering the safety phase. In the case of pile-stabilized slopes, the ultimate phase is the safety phase. Here, both tan(φ') and c' or S_u values are systematically reduced until failure, yielding the factor of safety value. The staged

construction steps, in Plaxis 3D models of pile-stabilized natural slopes and loaded slope cases are illustrated in Figure 3.13. and Figure 3.14.

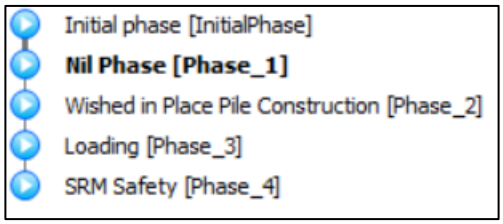


Figure 3.13. Staged construction steps for pile-stabilized loaded slope cases.

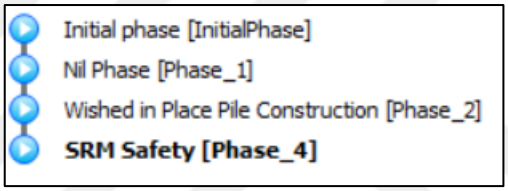


Figure 3.14. Staged construction steps for pile-stabilized natural slope cases.

3.2.6. Selected Configurations for Paraetric Study

Since the main goal of this study is to determine the most effective configurations for stabilizing slopes, the first step towards this was the division of the configuration into its constituent parts. As the configuration itself consists of the S/D ratio, the number of rows, as well as the position of this configuration, it can be concluded that the effectiveness of the configuration directly depends on these factors. It should be noted that each component of the configuration makes its unique contribution to slope stabilization. An additional factor is the installation of a pile cap beam on the pile group. The pile cap beam affects the shape of the pile deformation under loads. In addition to the previous reasons for choosing these configurations, it can also be mentioned that the selected parameters of the configuration were chosen in such a way that when assessing the effect of one parameter, the other parameters remained unchanged, allowing to assess the sole effect of the single parameter on slope stabilization. For example, when identifying the effect of the S/D ratio, other components such as the number of

rows, the position of the group itself, and the presence of a pile cap beam remains constants in this evaluation. The same procedure was used to determine the effect of other parameters. Due to the meticulous methodology employed in the selection of parameters for each configuration, the study provides an opportunity to accurately assess the impact of each parameter on the overall effectiveness of slope stabilization. This contributes to the identification of the most cost-efficient solutions for practical applications. In this study, slice models were used to assess the effectiveness of configurations in continuously loaded slopes and natural slopes. The typical slice model analyzed in Plaxis 3D is shown in Figure 3.15. The cases (both staggered and non-staggered) analyzed usng the slice models are summarized in Table 3.8.

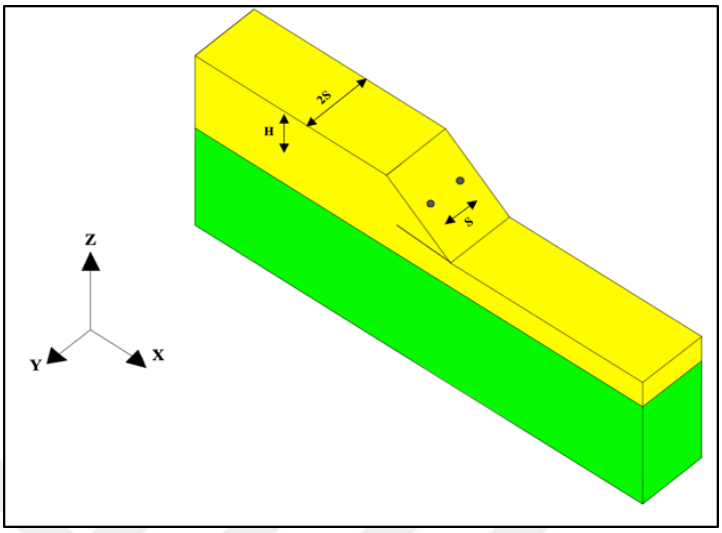


Figure 3.15. Plaxis 3D example of the analyzed pile-stabilized slopes using slice model.

As previously stated, full models were used for the locally loaded slope cases. An example of these cases as shown in Figure 3.16.

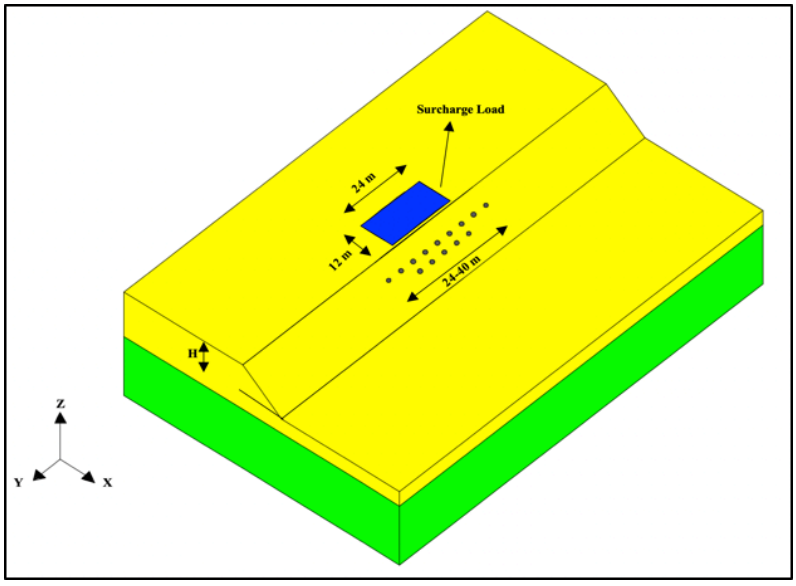


Figure 3.16. 3D geometry of the analyzed locally loaded pile-stabilized slopes.

Table 3.8. Slice model cases analyzed in the parametric study.

Case No	Number of rows/Staggered	Load condition	S_u (kPa)	Model	Pile position	S/D
37	Single Row	No Load	40	Slice	Middle	1.33
38	Single Row	No Load	40	Slice	Middle	1.67
39	Single Row	No Load	40	Slice	Middle	2.00
40	Single Row	No Load	40	Slice	Middle	2.67
41	Single Row	No Load	40	Slice	Middle	3.33
42	Single Row	No Load	40	Slice	Middle	4.00
43	Double Row	No Load	40	Slice	Middle	2.00
44	Double Row	No Load	40	Slice	Middle	2.67
45	Double Row	No Load	40	Slice	Middle	3.33
46	Double Row	No Load	40	Slice	Middle	4.00
47	Triple Row	No Load	40	Slice	Middle	2.00
48	Triple Row	No Load	40	Slice	Middle	2.67
49	Triple Row	No Load	40	Slice	Middle	3.33
50	Triple Row	No Load	40	Slice	Middle	4.00
57	Single Row	Continuous Load	40	Slice	Middle	1.33
58	Single Row	Continuous Load	40	Slice	Middle	1.67
59	Single Row	Continuous Load	40	Slice	Middle	2.00
60	Single Row	Continuous Load	40	Slice	Middle	2.67
61	Single Row	Continuous Load	40	Slice	Middle	3.33
62	Single Row	Continuous Load	40	Slice	Middle	4.00
63	Double Row	Continuous Load	40	Slice	Middle	2.00
64	Double Row	Continuous Load	40	Slice	Middle	2.67
65	Double Row	Continuous Load	40	Slice	Middle	3.33
66	Double Row	Continuous Load	40	Slice	Middle	4.00
67	Triple Row	Continuous Load	40	Slice	Middle	2.00
68	Triple Row	Continuous Load	40	Slice	Middle	2.67
69	Triple Row	Continuous Load	40	Slice	Middle	3.33
70	Triple Row	Continuous Load	40	Slice	Middle	4.00
77	Single Row	No Load	30	Slice	Middle	2.00
78	Single Row	No Load	30	Slice	Middle	3.00
79	Single Row	No Load	30	Slice	Middle	3.50
80	Single Row	No Load	30	Slice	Middle	4.00
81	Double Row	No Load	30	Slice	Middle	2.00
82	Double Row	No Load	30	Slice	Middle	3.00
83	Double Row	No Load	30	Slice	Middle	3.50
84	Double Row	No Load	30	Slice	Middle	4.00
85	Triple Row	No Load	30	Slice	Middle	2.00
86	Triple Row	No Load	30	Slice	Middle	3.00
87	Triple Row	No Load	30	Slice	Middle	3.50
88	Triple Row	No Load	30	Slice	Middle	4.00
89	Staggered	No Load	40	Slice	Middle	2.67
90	Staggered	No Load	40	Slice	Middle	3.33
91	Staggered	No Load	40	Slice	Middle	4.00

Various pile configurations were investigated using Plaxis 3D. A total of 36 cases were analyzed using Plaxis 3D. Plan view of pile group configurations: Case 1 through Case 16 and Case 17 through Case 36 are shown in Figure 3.17 and Figure 3.18, respectively. These configurations were mainly identified to study the effects of various parameters on the stability of slopes stabilized with a group of piles. The investigation was not limited to only rectangular pile groups, efficiency of other configurations, such as circular groups with piles with a center pile were also investigated.

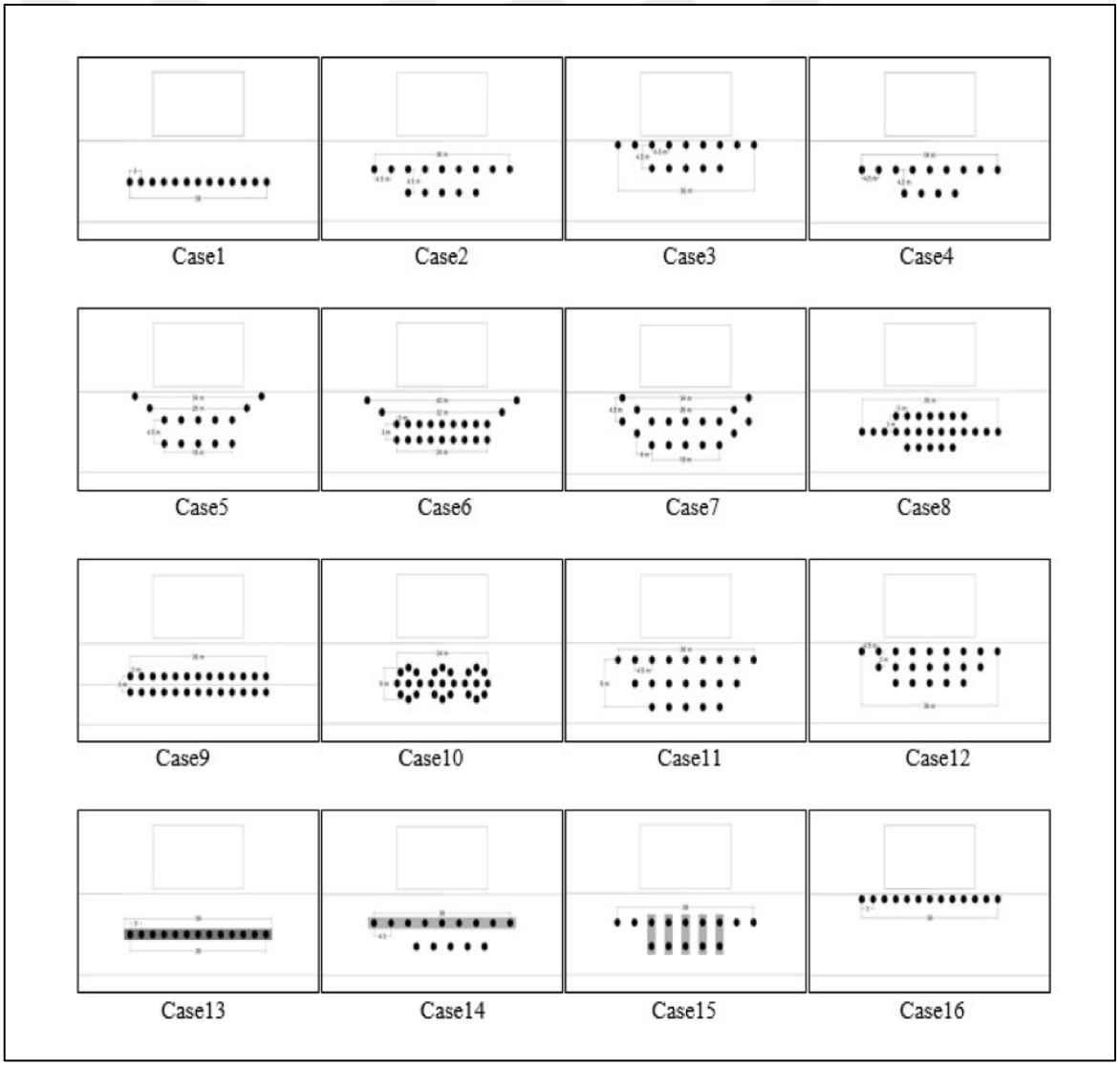


Figure 3.17. Plan view of pile group configurations: Case 1 through Case 16.

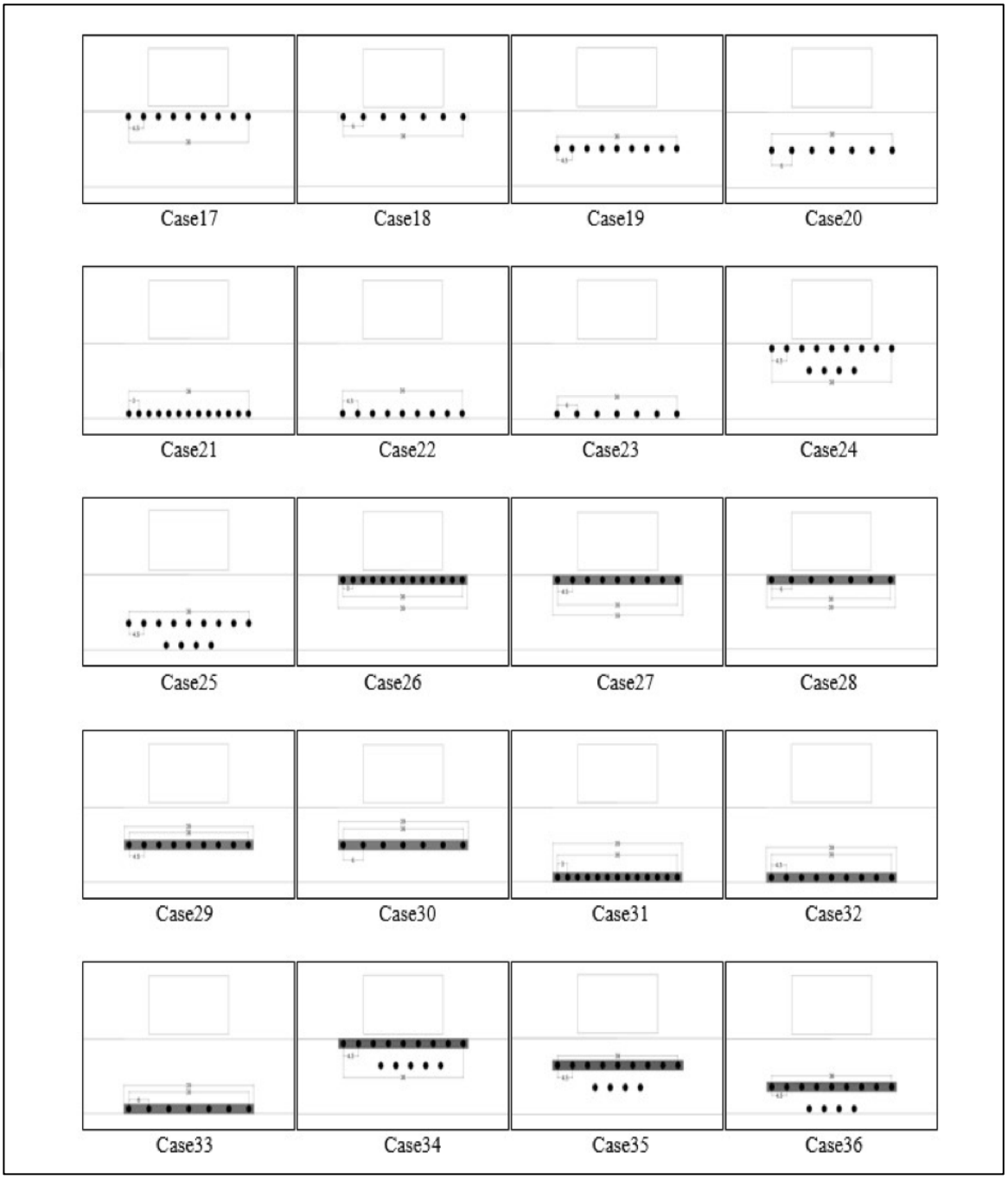


Figure 3.18. Plan view of pile group configurations: Case 17 through Case 36.

After all configurations were determined, it was necessary to name these configurations using abbreviations. The main goal in using a unique name with abbreviations for each pile configuration was to ensure that, the detailes of the pile group configuration would be

understood by the reader quickly. The abbreviations were selected to include the S/D ratio, the number of piles in the group, the number of rows in this group of piles, the length of the slope section reinforced with piles, the location of the pile group along the slope, and the condition of the pile heads. SD indicated the S/D ratio in this configuration, PN the number of piles, and RN the number of rows. Figure 3.19 and Figure 3.20 depict two different configurations, together with their names, with free and constrained pile head conditions, respectively. Three options were used to indicate the condition of the pile heads. In the case of constrained pile head conditions, two separate abbreviations were used indicate the orientation of the pile cap in the plan view. The abbreviations HPC was used for a horizontal pile cap, that is for a pile cap placed parallel to the slope width. The abbreviation VPC was used for vertical pile cap used to indicate a pile cap placed perpendicular to the slope width. In the case of free pile head condition, no abbreviation was used at the end of the description indicating the absence of a pile cap. Accordingly, the case name: SD3_PN13_RN2_36_M, refers to piles spaced at 3D, a total of 13 piles, two pile rows, a reinforcement length of 36 m, with piles placed in the middle of the slope height and without the presence of a pile cap. Similarly, SD3_PN13_RN2_36_M_HPC refers to piles spaced at 3D, a total of 13 piles, two pile rows, a reinforcement length of 36 m, with piles placed in the middle of the slope height and with the presence of a pile cap on the pile row closest to the slope crest and placed parallel to the slope width. Details of all pile group configuration cases analyzed are presented in Table 3.9.

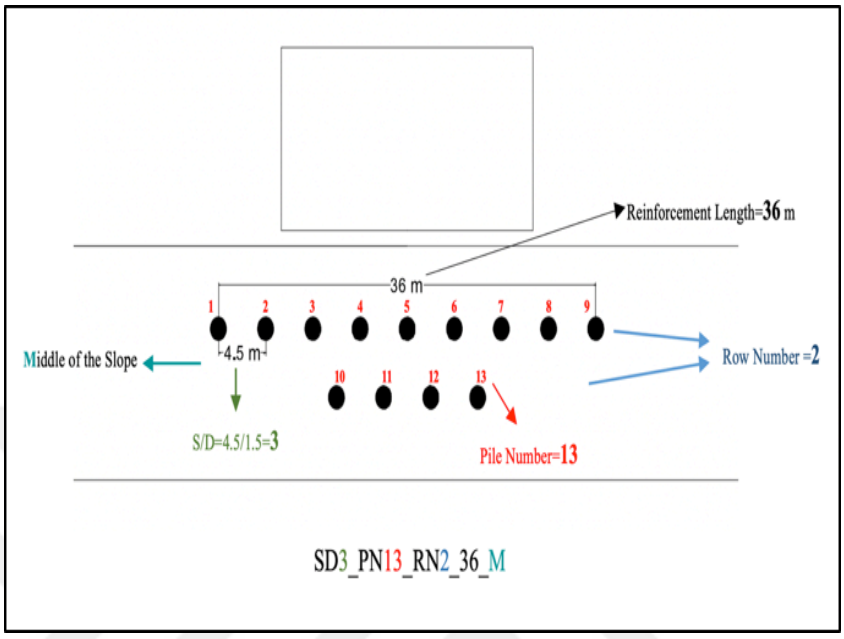


Figure 3.19. Plan-view of SD3_PN13_RN2_36_M in Plaxis 3D (free pile head condition).

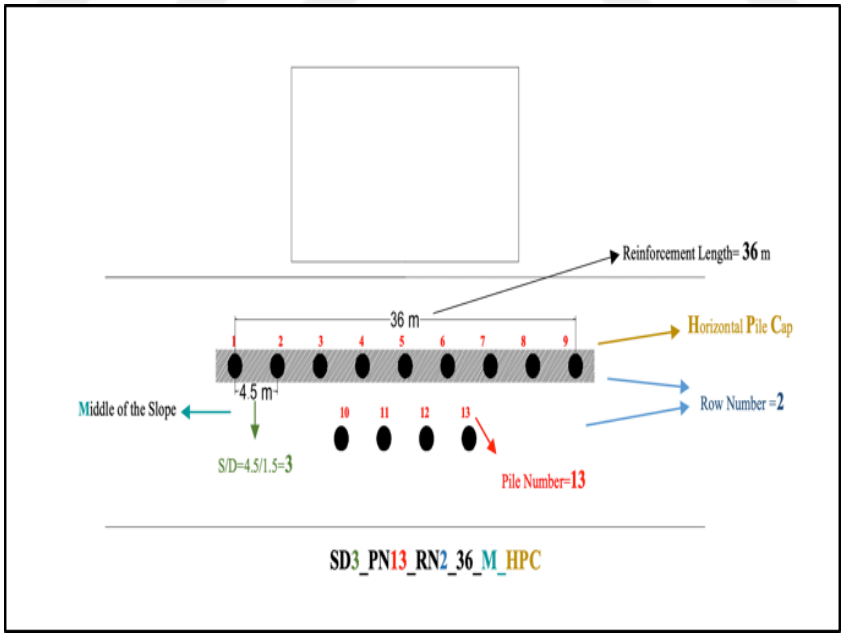


Figure 3.20. Plan-view of SD3_PN13_RN2_36_M_HPC in Plaxis 3D (constrained pile head condition).

Table 3.9. Full model cases analyzed in the parametric study.

Case No	Case Name	Load Condition	S_u (kPa)	Model	Pile Position	S/D	Number of rows
1	S/D2_PN13_RN1_36_M	Local Load	40	Full	Middle	2	1
2	S/D3_PN14_RN2_36_M	Local Load	40	Full	Middle	3	2
3	S/D3_PN14_RN2_36_C	Local Load	40	Full	Crest	3	2
4	S/D3_PN13_RN2_36_M	Local Load	40	Full	Middle	3	2
5	S/D3_PN14_RN2_34_M	Local Load	40	Full	Middle	3	2
6	S/D2_PN22_RN2_40_M	Local Load	40	Full	Middle	2	2
7	S/D3_PN18_RN2_34_M	Local Load	40	Full	Middle	3	2
8	S/D2_PN25_RN3_36_M	Local Load	40	Full	Middle	2	3
9	S/D2_PN26_RN2_36_M	Local Load	40	Full	Middle	2	2
10	S/D2_PN27_RN3_24_M	Local Load	40	Full	Middle	2	3
11	S/D3_PN21_RN3_36_M	Local Load	40	Full	Middle	3	3
12	S/D3_PN21_RN3_36_C	Local Load	40	Full	Crest	3	3
13	S/D2_PN13_RN1_36_M_HPC	Local Load	40	Full	Middle	2	1
14	S/D3_PN14_RN2_36_M_HPC	Local Load	40	Full	Middle	3	2
15	S/D3_PN14_RN2_36_M_VPC	Local Load	40	Full	Middle	3	2
16	S/D2_PN13_RN1_36_C	Local Load	40	Full	Crest	2	1
17	S/D3_PN9_RN1_36_C	Local Load	40	Full	Crest	3	1
18	S/D4_PN7_RN1_36_C	Local Load	40	Full	Crest	4	1
19	S/D3_PN9_RN1_36_M	Local Load	40	Full	Middle	3	1
20	S/D4_PN7_RN1_36_M	Local Load	40	Full	Middle	4	1
21	S/D2_PN13_RN1_36_T	Local Load	40	Full	Toe	2	1
22	S/D3_PN9_RN1_36_T	Local Load	40	Full	Toe	3	1
23	S/D4_PN7_RN1_36_T	Local Load	40	Full	Toe	4	1
24	S/D3_PN13_RN2_36_C	Local Load	40	Full	Crest	3	2
25	S/D3_PN13_RN2_36_T	Local Load	40	Full	Toe	3	2
26	S/D2_PN13_RN1_36_C_HPC	Local Load	40	Full	Crest	2	1
27	S/D3_PN9_RN1_36_C_HPC	Local Load	40	Full	Crest	3	1
28	S/D4_PN7_RN1_36_C_HPC	Local Load	40	Full	Crest	4	1
29	S/D3_PN9_RN1_36_M_HPC	Local Load	40	Full	Middle	3	1
30	S/D4_PN7_RN1_36_M_HPC	Local Load	40	Full	Middle	4	1
31	S/D2_PN13_RN1_36_T_HPC	Local Load	40	Full	Toe	2	1
32	S/D3_PN9_RN1_36_T_HPC	Local Load	40	Full	Toe	3	1
33	S/D4_PN7_RN1_36_T_HPC	Local Load	40	Full	Toe	4	1
34	S/D3_PN13_RN2_36_C_HPC	Local Load	40	Full	Crest	3	2
35	S/D3_PN13_RN2_36_M_HPC	Local Load	40	Full	Middle	3	2
36	S/D3_PN13_RN2_36_T_HPC	Local Load	40	Full	Toe	3	2

4. RESULTS OF THE NUMERICAL ANALYSIS

A series of numerical analysis was performed to investigate the behavior of slopes stabilized with pile groups. The factor of safety (*FS*), internal pile forces (shear force and momemts along the pile) and displacements at pile head, slope toe and slope crest were derived at the end of each analysis performed. The effects of various parameters on the results of the FE analyses are presented in the following sections.

4.1. Effect of S/D

This section presents the influence of the pile spacing to pile diameter ratio (S/D) on the *FS*, internal pile forces, and slope deformations. Full and slice models were used to study the influence of S/D ratio for various loading conditions on the slope. Slice models were used to consider considering continuous loading and natural slope (no surcharge load) cases. The full models were used for local loading cases. Two different clayey soils with S_u=30 kPa and S_u=40 kPa were considered in slice model cases and two pile head conditions in full models (*i.e.*, free and constrained head) were investigated in full models.

4.1.1. Factor of Safety

The FS_{0_PS} values obtained from the analysis of the natural pile-stabilized slopes considering various S/D ratio and number of rows are presented in Table 4.1 for a clayey slope soil with S_u=40 kPa. Figure 4.1 presents S/D ratio versus the factor of safety of the natural pile-stabilized slope (FS_{0_PS}) with S_u=40 kPa. A clear inverse relationship between S/D ratio and FS_{0_PS} exists. As expected, reducing S/D ratio has a positive effect on slope stabilization, in essence FS_{0_PS} increases.

Table 4.1. Results of the safety analyses performed on the of natural pile-stabilized slopes (slice model cases, S_u=40 kPa).

Case No	Number of rows	Load Condition	S_u (kPa)	Model	Pile Position	S/D	FS_{0_PS}
39	Single Row	No Load	40	Slice	Middle	2.00	2.02
40	Single Row	No Load	40	Slice	Middle	2.67	1.97
41	Single Row	No Load	40	Slice	Middle	3.33	1.91
42	Single Row	No Load	40	Slice	Middle	4.00	1.83
43	Double Row	No Load	40	Slice	Middle	2.00	2.22
44	Double Row	No Load	40	Slice	Middle	2.67	2.17
45	Double Row	No Load	40	Slice	Middle	3.33	2.10
46	Double Row	No Load	40	Slice	Middle	4.00	2.04
47	Triple Row	No Load	40	Slice	Middle	2.00	2.36
48	Triple Row	No Load	40	Slice	Middle	2.67	2.31
49	Triple Row	No Load	40	Slice	Middle	3.33	2.25
50	Triple Row	No Load	40	Slice	Middle	4.00	2.18

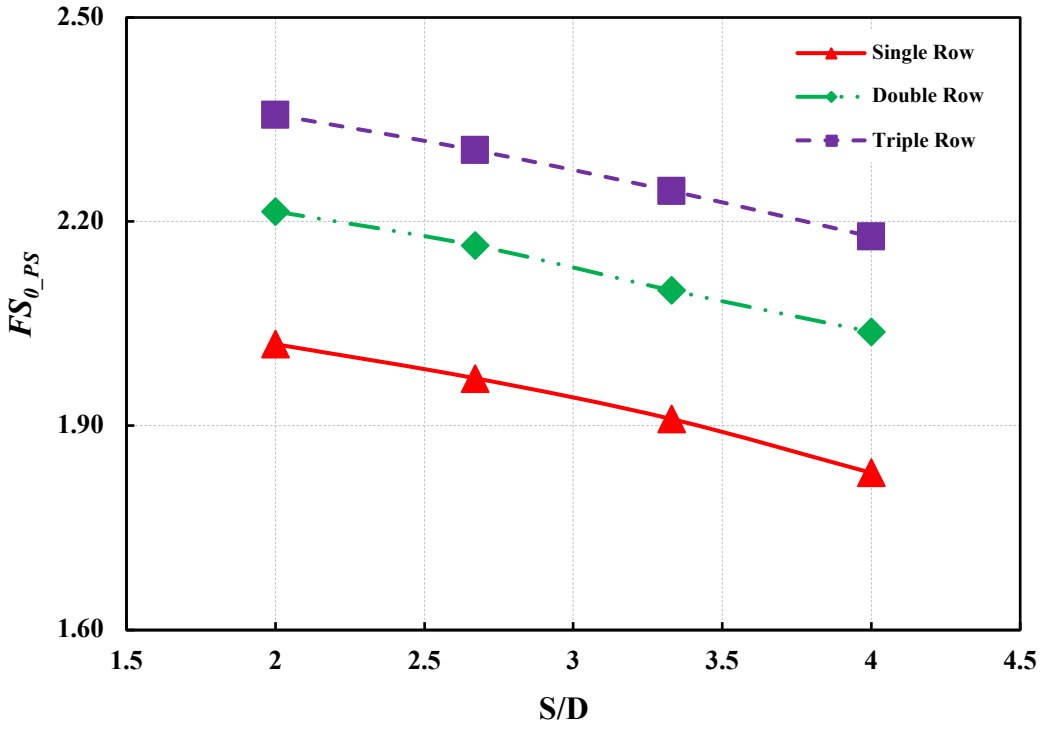


Figure 4.1. S/D ratio versus FS_{0_PS} (slice model cases, S_u=40 kPa).

The *FS* (%) increase with respect to S/D = 4 in this context measures the percentage (%) change in the *FS* of pile-stabilized slope for various S/D ratios in a pile group. Specifically, it quantifies how much the *FS* increases in %, as the S/D ratio is reduced from the initial value of 4, which is the largest ratio considered in this study, and the lowest value of S/D ratio considered in this study is 2. The formula of *FS* (%) increase with respect to S/D = 4 can be written as

$$FS_{0_PS}\ (\%)\ increase\ w.r.t\ largest\ S/D\ ratio\ (S/D=4) = 100 \times \left(\frac{FS_{0_PS\ (S/D=x)} - FS_{0_PS\ (S/D=4)}}{FS_{0_PS\ (S/D=4)}} \right). \quad (4.1)$$

Figure 4.2 illustrates the relationship between the S/D ratio and the % increase attained for FS_{0_PS} (S_u=40 kPa) due to the reduction of S/D ratio for cases with various numbers of rows. The analysis of the effect of the S/D ratio on the FS_{0_PS} for slope stability indicates a clear positive correlation between decreasing S/D ratios and increasing (%) FS_{0_PS}. Figure 4.2 shows a consistent trend across single, double, and triple row configurations, where reducing the S/D ratio results in an increase (%) of FS_{0_PS}. For single row configurations, reducing the S/D ratio leads to notable improvements in slope stability. In double row cases, the same trend is observed, although the improvements are slightly less pronounced than in the single row configuration. Triple row groups also follow this trend, (%) of FS_{0_PS} increases with a decrease in S/D ratio, however, the enhancements are more modest compared to single and double row configurations. Overall, the reduction in S/D ratio consistently enhances slope stability across all cases of number of rows, with the most significant improvements seen in single row configurations, followed by double row, and then triple row configurations. When considering the increase of FS_{0_PS}, it is also important to evaluate the increase in the required quantity of piles. When transitioning from S/D = 4 to S/D = 2, the number of piles also doubles. This indicates that for a the case of a pile configuration with a single row, to increase the FS_{0_PS} by 10.38%, it was necessary to almost double the materials required for piles.

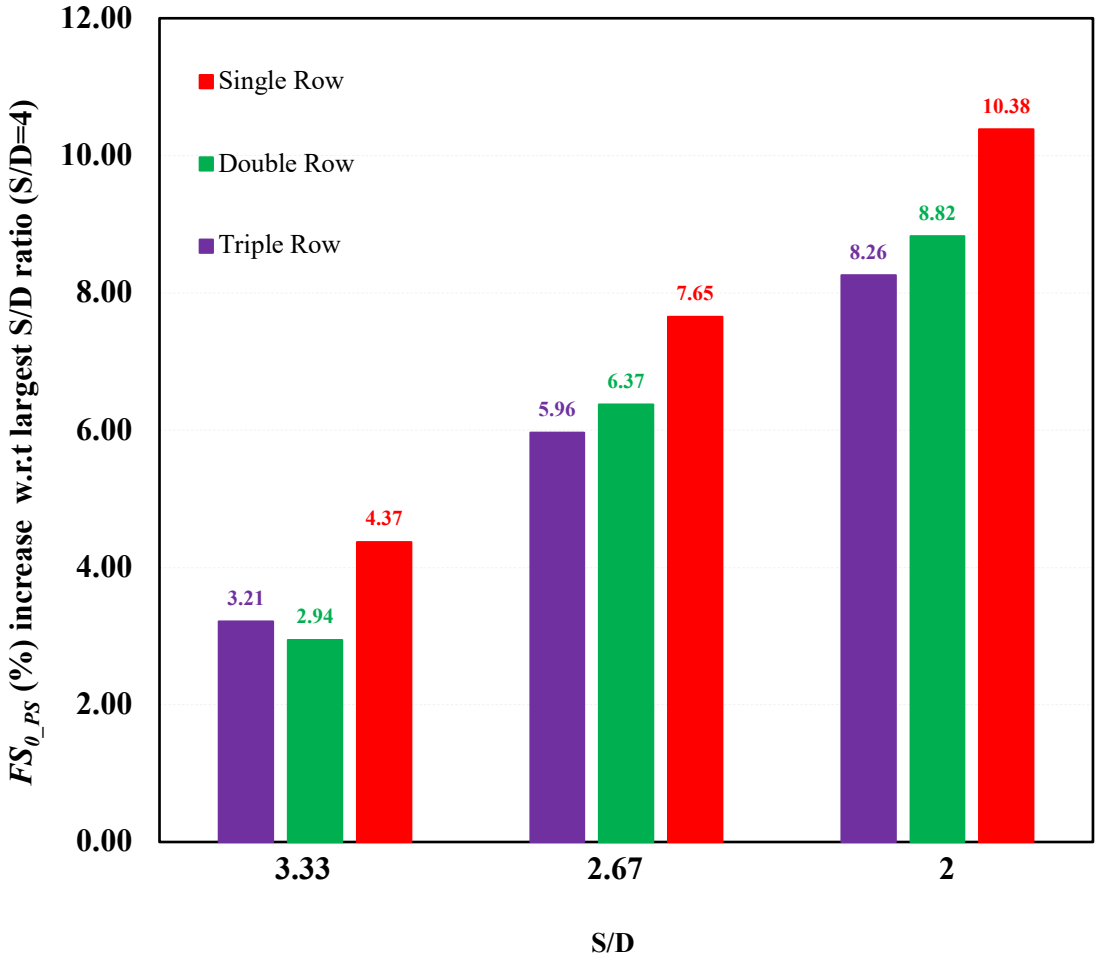


Figure 4.2. S/D ratio versus FS_{0_PS} (%) increase with respect to largest S/D ratio (S/D=4) (slice model cases, S_u=40 kPa).

The FS_{0_PS} values obtained from the analysis of the natural pile-stabilized slope cases considering various S/D ratios and numbers of rows are presented in Table 4.2 for the weaker soil case, S_u=30 kPa. Figure 4.3 presents S/D ratios versus FS_{0_PS} for S_u=30 kPa. There is a clear inverse correlation between the S/D ratio and FS_{0_PS}. When the S/D ratio decreases from 4 to 2 the FS_{0_PS} shows a significant increase.

Table 4.2. Results of safety analyses performed on the natural pile-stabilized slope (slice model cases, S_u=30 kPa).

Case No	Number of rows	Load Condition	S_u (kPa)	Model	Pile Position	S/D	FS_{0_PS}
77	Single Row	No Load	30	Slice	Middle	2.00	1.67
78	Single Row	No Load	30	Slice	Middle	3.00	1.50
79	Single Row	No Load	30	Slice	Middle	3.50	1.44
80	Single Row	No Load	30	Slice	Middle	4.00	1.39
81	Double Row	No Load	30	Slice	Middle	2.00	1.89
82	Double Row	No Load	30	Slice	Middle	3.00	1.79
83	Double Row	No Load	30	Slice	Middle	3.50	1.74
84	Double Row	No Load	30	Slice	Middle	4.00	1.68
85	Triple Row	No Load	30	Slice	Middle	2.00	2.04
86	Triple Row	No Load	30	Slice	Middle	3.00	1.95
87	Triple Row	No Load	30	Slice	Middle	3.50	1.89
88	Triple Row	No Load	30	Slice	Middle	4.00	1.83

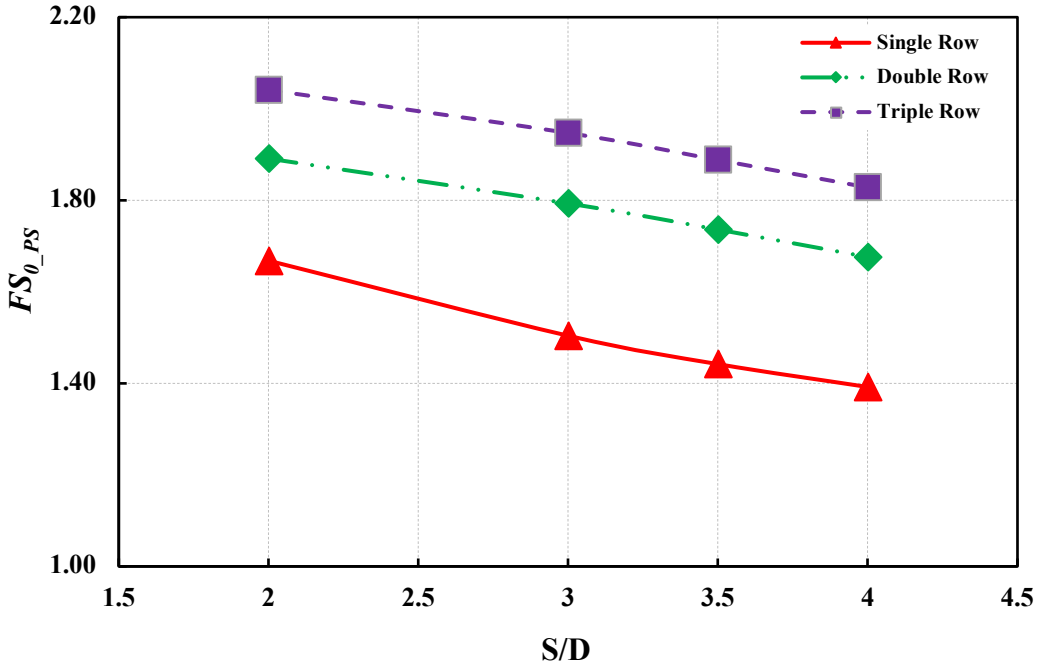


Figure 4.3. S/D ratio versus FS_{0_PS} (slice model cases, S_u=30 kPa).

Figure 4.4 illustrates the relationship between the S/D ratio and the % increase attained for FS_{0_PS} (S_u=30 kPa) due to reduction of S/D ratio for cases with various numbers of rows. The analysis of the effect of the S/D ratio on the FS_{0_PS} for slope stability indicates a clear

positive correlation between reducing S/D ratio and increasing (%) of FS_{0_PS}. The analysis indicates that reducing the S/D ratio consistently enhances FS_{0_PS} for single, double, and triple row configurations. In single row configurations, the reduction in the S/D ratio results in significant improvements in slope stability, with the most substantial increases observed. Double row cases show a similar trend, though the increases (%) in FS_{0_PS} are slightly less pronounced compared to single row configurations. Triple row groups also follow this trend, with improvements in FS_{0_PS}, although more modest than those seen in single and double row configurations. Overall, reducing the S/D ratio improves slope stability across the cases with vaious numbers of rows, with the greatest benefits seen in single row configurations, followed by double row, and then triple row configurations.

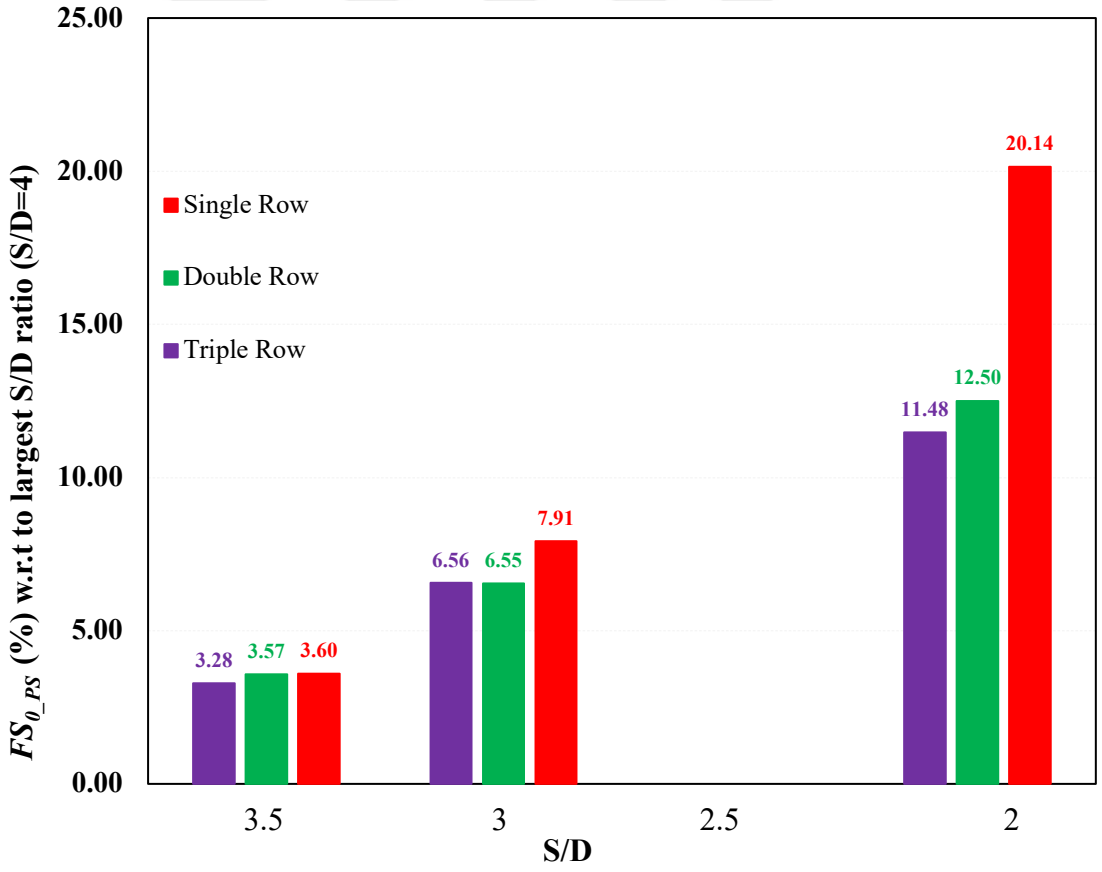


Figure 4.4. S/D ratio versus FS_{0_PS} (%) increase with respect to largest S/D ratio (S/D=4) (slice model cases, S_u=30 kPa).

The FS_{CL_PS} values obtained from the analysis of the continuously loaded pile-stabilized slope cases considering various S/D ratios and numbers of rows are presented in Table 4.3 for S_u=40 kPa. Figure 4.5 presents S/D ratios verus FS_{CL_PS} for S_u=40 kPa. There is a clear inverse correlation between the S/D ratio and FS_{CL_PS}. As the S/D ratio decreases from 4 to 2, there is an observed increase in FS_{CL_PS}.

Table 4.3. Results of the safety analyses performed on the continuously loaded pile-stabilized (slice model cases, S_u=40 kPa).

Case No	Number of rows	Load Condition	S_u (kPa)	Model	Pile position	S/D	FS_{CL_PS}
59	Single Row	Continuous Load	40	Slice	Middle	2.00	1.26
60	Single Row	Continuous Load	40	Slice	Middle	2.67	1.20
61	Single Row	Continuous Load	40	Slice	Middle	3.33	1.17
62	Single Row	Continuous Load	40	Slice	Middle	4.00	1.14
63	Double Row	Continuous Load	40	Slice	Middle	2.00	1.49
64	Double Row	Continuous Load	40	Slice	Middle	2.67	1.40
65	Double Row	Continuous Load	40	Slice	Middle	3.33	1.32
66	Double Row	Continuous Load	40	Slice	Middle	4.00	1.27
67	Triple Row	Continuous Load	40	Slice	Middle	2.00	1.58
68	Triple Row	Continuous Load	40	Slice	Middle	2.67	1.55
69	Triple Row	Continuous Load	40	Slice	Middle	3.33	1.48
70	Triple Row	Continuous Load	40	Slice	Middle	4.00	1.39

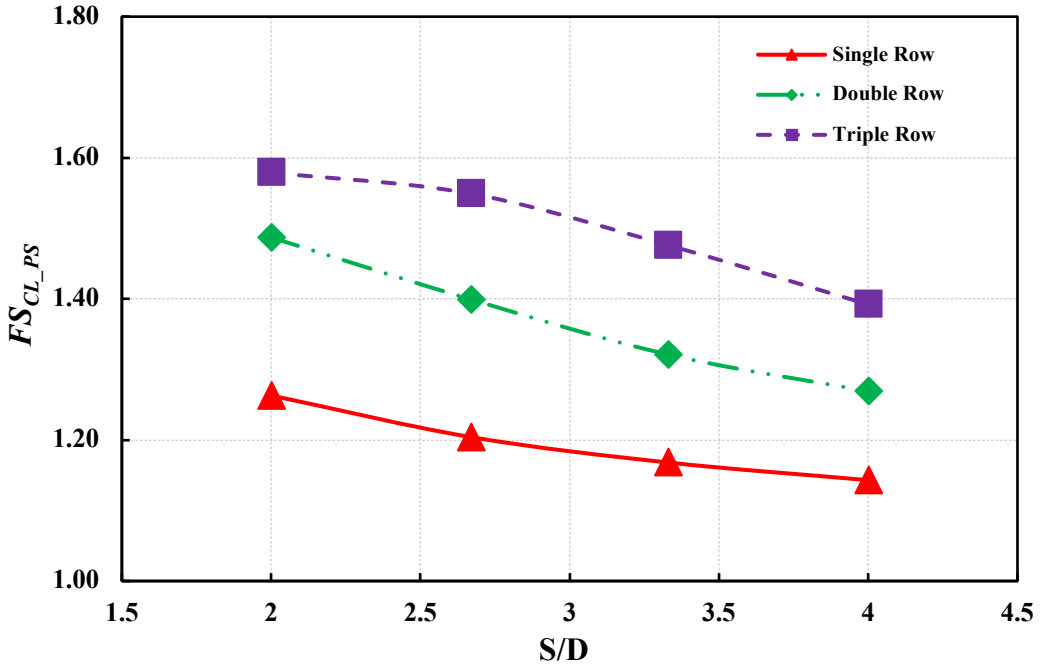


Figure 4.5. S/D ratio versus FS_{CL_PS} (slice model cases, S_u=40 kPa).

Figure 4.6 illustrates the relationship between the S/D ratio and the % increase attained for FS_{CL_PS} (S_u=40 kPa) due to reduction of S/D ratio for cases with various numbers of rows. The analysis of the effect of the S/D ratio on the FS_{CL_PS} for slope stability indicates a clear positive correlation between decreasing S/D ratios and increasing (%) FS_{CL_PS}. The analysis indicates that decreasing the S/D ratio consistently enhances FS_{CL_PS} for single, double, and triple row configurations. In single row configurations, reducing the S/D ratio significantly improves slope stability. Double row cases follow this trend, showing even more pronounced increases (%) in FS_{CL_PS}. Triple row groups also exhibit improvements with decreasing S/D ratios, although these enhancements are slightly less pronounced compared to double row configurations. Overall, decreasing the S/D ratio improves slope stability across all cases with various numbers of rows, with the greatest benefits seen in double row configurations, followed by triple row, and then single row configurations. Generally, as the number of rows of piles increases, the percentage increase in FS_{CL_PS} tends to be higher for similar reductions in the S/D ratio. This suggests that denser configurations (more rows) benefit more from reduced S/D ratio in terms of slope stability improvement for the continuously loaded slopes.

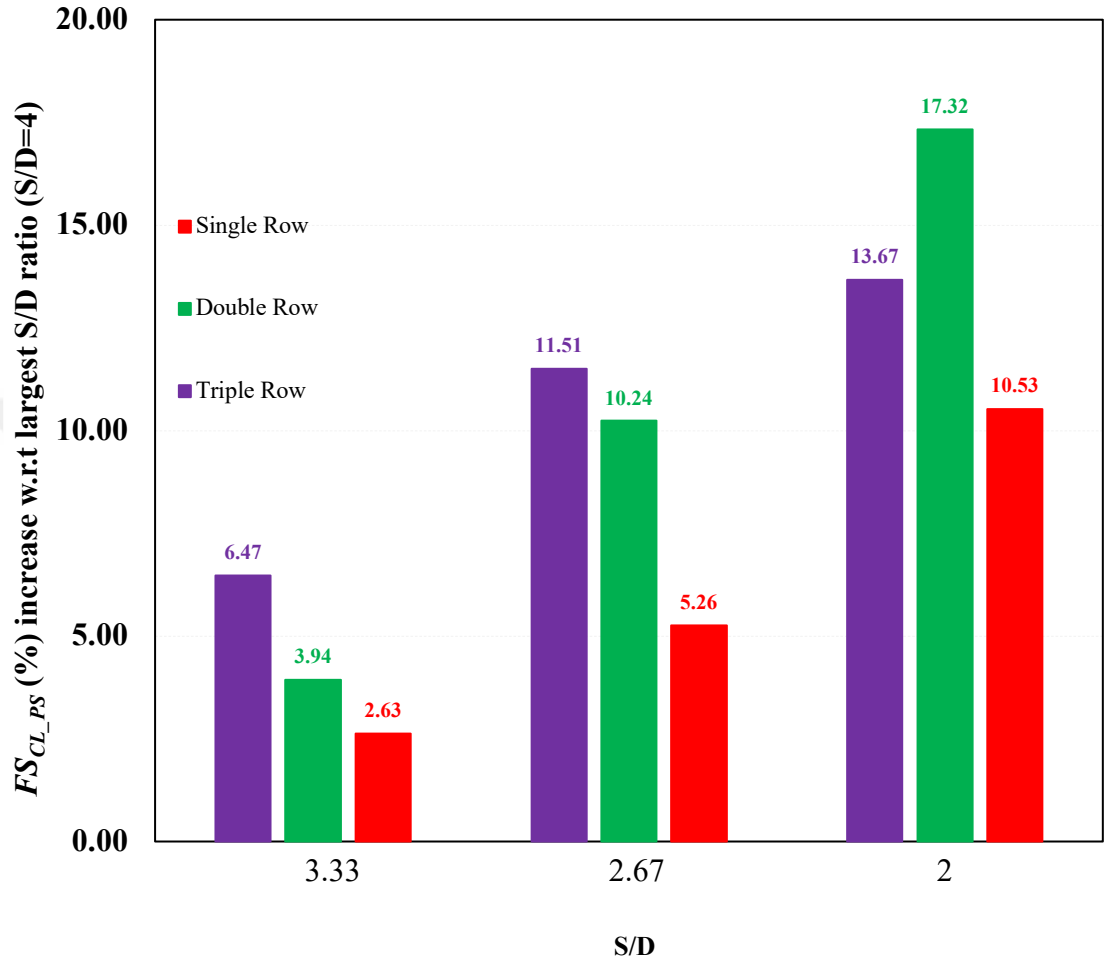


Figure 4.6. S/D ratio versus FS_{CP_PS} (%) increase with respect to largest S/D ratio (S/D=4) (slice model cases, S_u=40 kPa).

Once the trends presented in Figure 4.2 and Figure 4.4 are evaluated, one can conclude that the S/D ratio becomes more prevalent for stabilizing slopes with weaker soil (S_u=30 kPa), while the number of rows of piles serves as a secondary element, in other words it is a less effective factor for stabilizing the natural slopes that have no surcharge load on them. This conclusion is based on the consistent trend observed for both cases in both cases natural slopes (no surcharge), but the sensivity of the FS_{0_PS} with respect to the changes in S/D ratio is higher for the slope with weaker soil (S_u=30 kPa). Mainly, reduction of S/D ratio prevents flow of soil between piles. When the trend for the continuously loaded slope is examined, a very interesting

result can be observed. As can be seen in Figure 4.6, unlike the trend observed in natural slopes with no surcharge load, the increase in FS_{CL_PS} is more sensitive to the changes in the number of rows compared to the changes in S/D ratio, showcasing the different behavior of the pile groups in stabilizing the natural versus continuously loaded slopes.

The *FS* values obtained from the analysis of the full model cases of locally loaded pile-stabilized cases considering various S/D ratio, pile group position and pile head conditions are presented in Table 4.4 for S_u=40 kPa. Figure 4.7 presents S/D ratio versus factor of safety of locally loaded pile-stabilized slope (FS_{LPS}) for three different pile group positions along the slope with free pile head condition. A clear inverse relationship between S/D ratio and FS_{LPS} exists in groups placed at the crest and in the middle of the slope. For groups placed at the toe of the slope reduction of S/D ratio did not bring any change in FS_{LPS}. Additionally it can be said that the effect of S/D on the stability is equal for groups placed at the crest and in the middle of the slope as the data lines for these two cases are approximately parallel in Figure 4.7. In the case of pile groups installed at the crest of the slope, FS_{LPS} increases by 9 % when S/D ratio decreases from four (4) to two (2). For piles placed in middle of the slope same S/D reduction results in an increase of 8 %. Figure 4.8 shows S/D ratio versus FS_{LPS} for three different pile group positions, this time with a constrained pile head condition. A clear inverse relationship between S/D ratio and FS_{LPS} exists in groups placed at the crest. For groups placed in the middle of the slope this inverse relationship is not so distinct. For groups placed at the toe there is an absence of any dependence between S/D ratio and FS_{LPS}. In the case of groups installed at the crest of the slope, FS_{LPS} increases by 10 % when S/D ratio decreases from four (4) to two (2). For piles placed in middle of the slope same S/D reduction results in a FS_{LPS} an increase of 4 %.

Table 4.4. Results of the safety analyses performed on locally loaded pile-stabilized slope (full model cases, S_u=40 kPa, single row configurations).

Case No	Case Name	Load Condition	S_u (kPa)	Model	Pile Position	S/D	FS_{LPS}
16	S/D2_PN13_RN1_36_C	Local Load	40	Full	Crest	2	1.314
17	S/D3_PN9_RN1_36_C	Local Load	40	Full	Crest	3	1.248
18	S/D4_PN7_RN1_36_C	Local Load	40	Full	Crest	4	1.213
1	S/D2_PN13_RN1_36_M	Local Load	40	Full	Middle	2	1.290
19	S/D3_PN9_RN1_36_M	Local Load	40	Full	Middle	3	1.228
20	S/D4_PN7_RN1_36_M	Local Load	40	Full	Middle	4	1.191
21	S/D2_PN13_RN1_36_T	Local Load	40	Full	Toe	2	1.100
22	S/D3_PN9_RN1_36_T	Local Load	40	Full	Toe	3	1.100
23	S/D4_PN7_RN1_36_T	Local Load	40	Full	Toe	4	1.100
26	S/D2_PN13_RN1_36_C_HPC	Local Load	40	Full	Crest	2	1.446
27	S/D3_PN9_RN1_36_C_HPC	Local Load	40	Full	Crest	3	1.368
28	S/D4_PN7_RN1_36_C_HPC	Local Load	40	Full	Crest	4	1.314
13	S/D2_PN13_RN1_36_M_HPC	Local Load	40	Full	Middle	2	1.320
29	S/D3_PN9_RN1_36_M_HPC	Local Load	40	Full	Middle	3	1.303
30	S/D4_PN7_RN1_36_M_HPC	Local Load	40	Full	Middle	4	1.265
31	S/D2_PN13_RN1_36_T_HPC	Local Load	40	Full	Toe	2	1.100
32	S/D3_PN9_RN1_36_T_HPC	Local Load	40	Full	Toe	3	1.100
33	S/D4_PN7_RN1_36_T_HPC	Local Load	40	Full	Toe	4	1.100

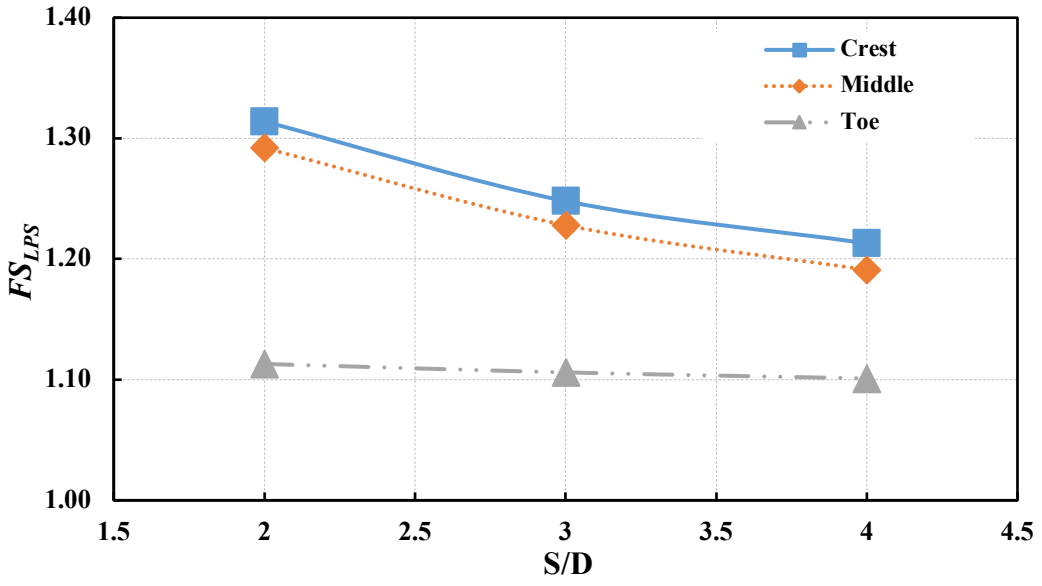


Figure 4.7. S/D ratio versus FS_{LPS} (full model cases, S_u=40 kPa, single row configurations, free pile head condition).

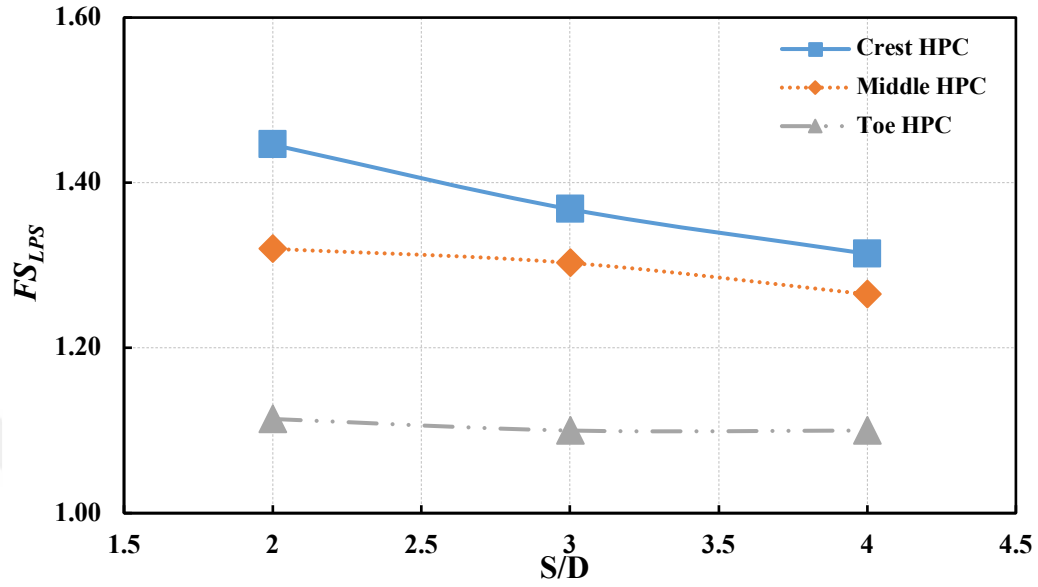


Figure 4.8. S/D ratio versus FS_{LPS} (full model cases, S_u=40 kPa, single row configurations constrained pile head condition).

4.1.2. Pile Internal Forces

The maximum pile internal force (bending moment and shear force) values obtained from the analysis of the continuously loaded pile-stabilized slope cases considering various S/D ratios and numbers of rows are presented in Table 4.5 for S_u=40 kPa. Figure 4.9 presents S/D ratio versus maximum pile bending moment values. A clear direct relationship exists between S/D ratio and maximum pile bending moment values. As expected, reducing S/D ratio has a positive effect on the maximum pile bending moment values, as such maximum pile bending moment values decrease. In case of pile groups with single row, maximum pile bending moment values decreasesd by 30% when the S/D reduced from four (4) to two (2). For pile groups with double and triple rows, this decrease in maximum pile bending moment values, was 38% and 39%, respectively. Figure 4.10 presents S/D ratio versus maximum pile shear force values. For the maximum pile shear force values, a similar pattern was observed. For example, in case of pile groups with the single row, maximum pile shear force values decreased by 37% when the S/D decreased from four (4) to two (2). For pile groups with double and triple rows, this decrease in maximum pile shear force value, was 44% and 45%, respectively. Notably, the decrease in shear

forces is more pronounced than the decreases in bending moments across all configurations, emphasizing the critical role of shear force considerations in design of slopes stabilized with pile groups.

Table 4.5. Maximum pile internal forces of continuously loaded pile-stabilized slopes (slice models, S_u=40 kPa).

Case No	Number of rows	Pile position	S/D	Maximum pile internal forces	
				Bending moment (kNm)	Shear force (kN)
59	Single Row	Middle	2.00	3672	965
60	Single Row	Middle	2.67	4393	1217
61	Single Row	Middle	3.33	4889	1397
62	Single Row	Middle	4.00	5251	1526
63	Double Row	Middle	2.00	1992	545
64	Double Row	Middle	2.67	2490	712
65	Double Row	Middle	3.33	2910	851
66	Double Row	Middle	4.00	3215	965
67	Triple Row	Middle	2.00	1589	428
68	Triple Row	Middle	2.67	1973	564
69	Triple Row	Middle	3.33	2312	678
70	Triple Row	Middle	4.00	2604	781

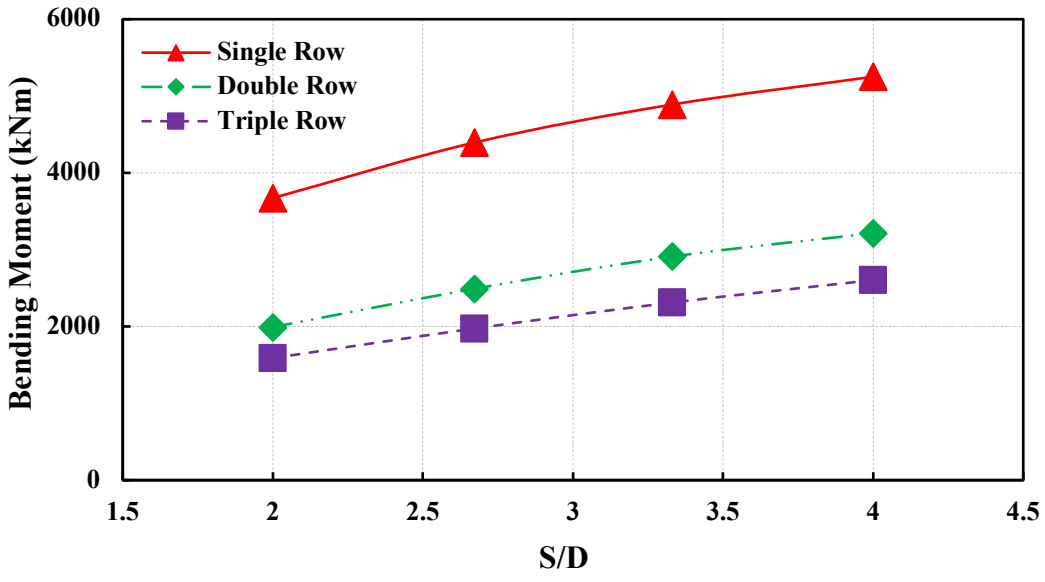


Figure 4.9. S/D ratio versus maximum pile bending moment values of continuously loaded pile-stabilized slope (slice model cases, S_u=40 kPa).

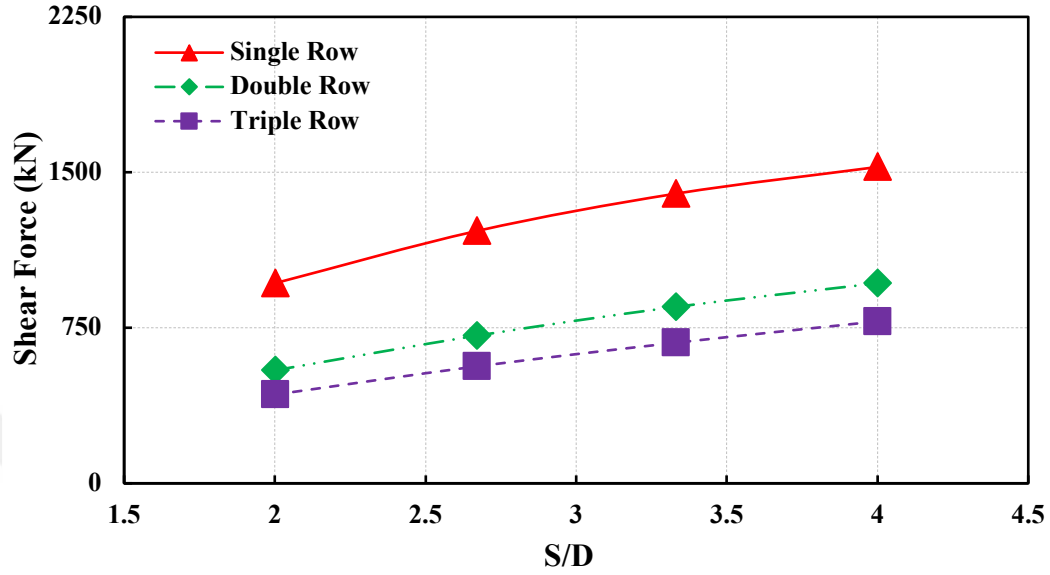


Figure 4.10. S/D ratio versus maximum pile shear force values of continuously loaded pile-stabilized slope (slice model cases, S_u=40 kPa).

The maximum pile internal force (bending moment and shear force) values obtained from the analysis of the locally loaded pile-stabilized slope cases considering various S/D ratios and pile group positions are presented in Table 4.6 for free pile head condition. Figure 4.11 presents S/D ratio versus maximum pile bending moment values for three different pile group position with free pile head condition. A clear direct relationship exists between S/D ratio and maximum pile bending moment values in all pile groups. In the case of groups installed at the crest and in the middle of the slope, maximum pile bending moment values decreased by 24 % when S/D ratio decreased from four (4) to two (2). For piles placed at the toe of the slope same S/D reduction resulted in decrease of about 20%. Figure 4.12 presents S/D ratio versus maximum pile shear force values for three different pile group position with free pile head condition. A clear direct relationship between S/D ratio and maximum pile shear force values exists in all pile groups. In the case of groups installed at the crest and in the middle of the slope , maximum pile shear force values decreased by 31% when S/D ratio was reduced from four (4) to two (2). For piles placed at the toe of the slope same S/D reduction resulted in a decrease of about 25% in maximum pile shear forces.

Table 4.6. Maximum pile internal forces of locally loaded pile-stabilized slopes (full model cases, S_u=40 kPa, single row configuration free pile head condition).

Case No	Case Name	Pile Position	S/D	Maximum Pile Internal Forces	
				Bending Moment (kNm)	Shear Force (kN)
16	S/D2_PN13_RN1_36_C	Crest	2	3923	892
17	S/D3_PN9_RN1_36_C	Crest	3	4730	1145
18	S/D4_PN7_RN1_36_C	Crest	4	5175	1286
1	S/D2_PN13_RN1_36_M	Middle	2	3749	1005
19	S/D3_PN9_RN1_36_M	Middle	3	4512	1289
20	S/D4_PN7_RN1_36_M	Middle	4	4951	1446
21	S/D2_PN13_RN1_36_T	Toe	2	1870	665
22	S/D3_PN9_RN1_36_T	Toe	3	2185	817
23	S/D4_PN7_RN1_36_T	Toe	4	2326	883

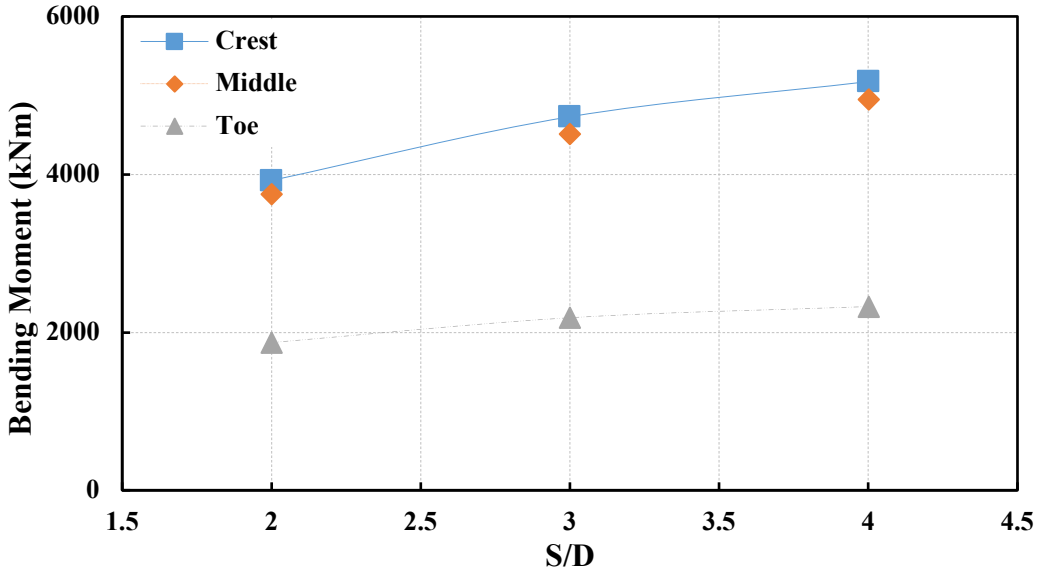


Figure 4.11. S/D ratio versus maximum pile bending moment values of locally loaded pile-stabilized slope (full model cases, S_u=40 kPa, single row configuration free pile head condition).

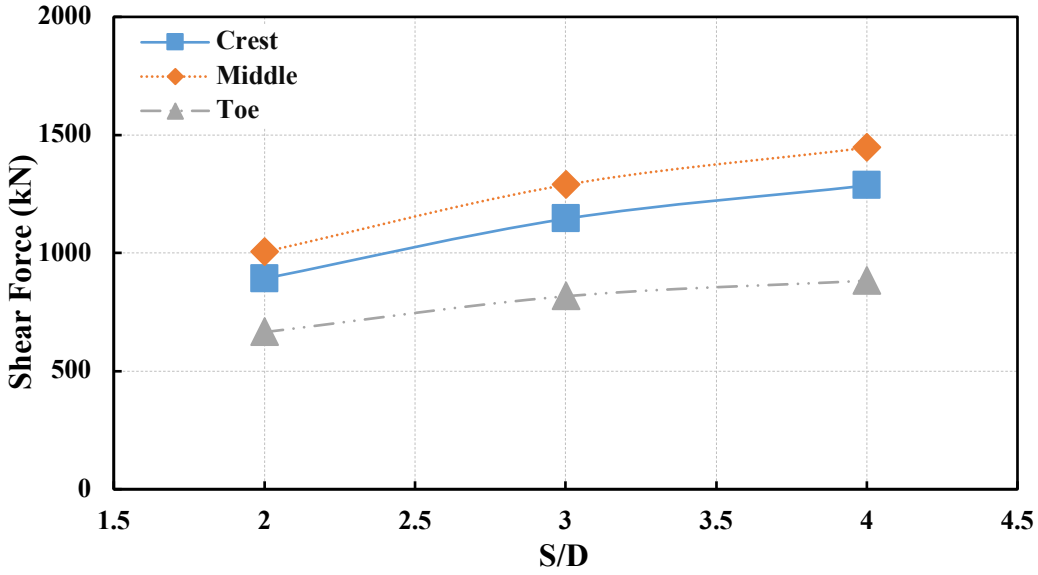


Figure 4.12. S/D ratio versus maximum pile shear force values of locally loaded pile-stabilized slope (full model cases, S_u=40 kPa, single row configurations, free pile head condition).

Figure 4.13 represents the influence of the S/D ratio on the distribution of bending moment within a pile (free pile head condition). Upon detailed examination, it can be observed that the S/D ratio does not affect the zone of distribution of the highest bending moment values, only the maximum value increases. In other words, the critical zone of the pile remains unchanged. This observation is significant as it suggests that while the S/D ratio impacts the magnitude of the bending moment, it does not alter the location along the pile where these maximum moments occur. This implies that the structural integrity and potential failure points of the pile remain consistent, regardless of the changes in the S/D ratio.

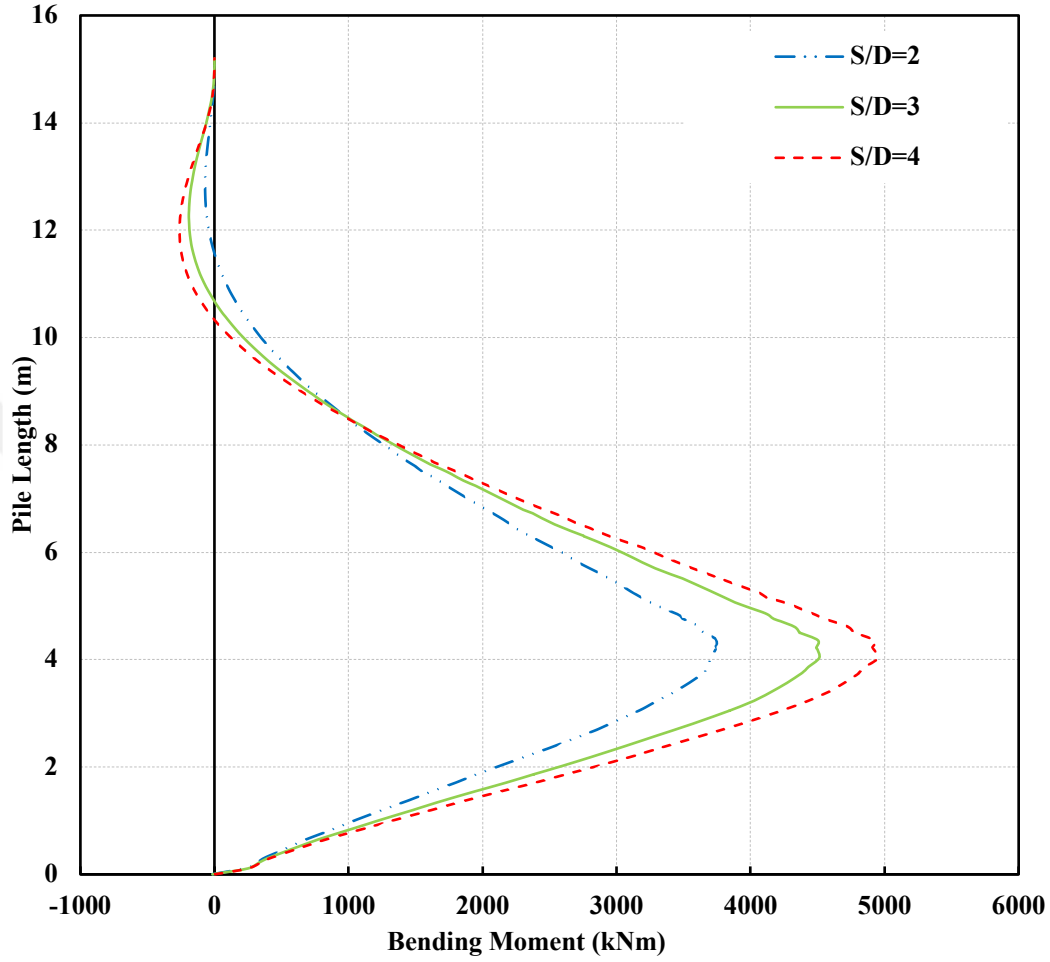


Figure 4.13. Bending moment diagram of central piles in single row configurations in locally loaded pile-stabilized slopes (full model cases, S_u=40 kPa, free pile head condition).

4.1.3. Displacements

The maximum diplacements (pile head, slope crest and slope toe) values obtained from the analysis of the locally loaded pile-stabilized slope cases considering various S/D ratio and numbers of rows are presented in Table 4.7 for S_u=40 kPa.

Table 4.7. Displacements values of continuously loaded pile-stabilized slopes (slice model cases, S_u=40 kPa).

Case No	Number of rows	Pile Position	S/D	Maximum Displacements (mm)		
				Pile Head U_{PH}	Slope Crest U_{SC}	Slope Toe U_{ST}
59	Single Row	Middle	2.00	11.2	7.9	5.6
60	Single Row	Middle	2.67	12.4	8.6	6.3
61	Single Row	Middle	3.33	13.7	9.3	7.0
62	Single Row	Middle	4.00	14.9	10	8.0
63	Double Row	Middle	2.00	8.7	6.2	3.9
64	Double Row	Middle	2.67	9.6	6.8	4.6
65	Double Row	Middle	3.33	10.5	7.3	5.1
66	Double Row	Middle	4.00	11.5	7.9	5.6
67	Triple Row	Middle	2.00	7.2	5.2	3.5
68	Triple Row	Middle	2.67	8.0	5.7	4.2
69	Triple Row	Middle	3.33	8.7	6.2	4.7
70	Triple Row	Middle	4.00	9.6	6.7	5.2

Figure 4.14 shows S/D ratio versus maximum pile head displacement (U_{PH}) values, Figure 4.15 presents S/D ratio versus maximum slope crest displacement (U_{SC}) values and Figure 4.16 presents S/D ratio versus maximum slope toe displacement (U_{ST}) values for the cases with three different numbers of rows. Slope and pile head displacements also depend on the S/D ratio, just as in the case with internal forces in the piles, the relationship between the S/D ratio and the displacements is direct, with greater S/D ratio resulting in larger displacements (*see* Figure 4.14, Figure 4.15 and Figure 4.16). U_{PH}, increased by 33% , with an increase in S/D ratio from two (2) to four (4). This increase is observed for configurations in two and three rows. The same trend was identified for displacements in crest and toe parts of the slope. With an increase of S/D ratio from two (2) to four (4), the increase in U_{SC} for configurations with single and double row is 27%, and for triple row configuration, it is 29%. In the case of U_{ST}, an increase of 43% and 44% was calculated for configurations with double and triple rows, and for configurations with triple rows, the increase is 49% .

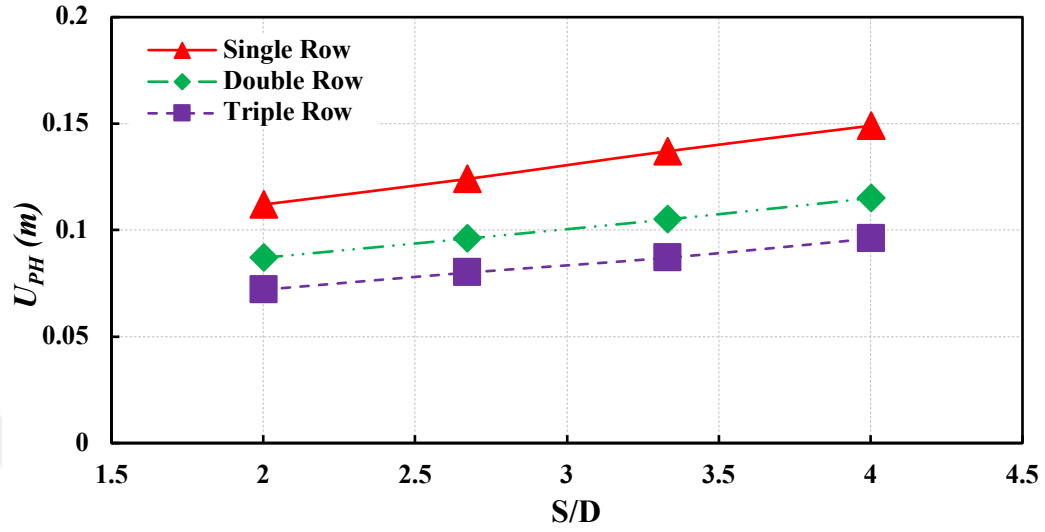


Figure 4.14. S/D ratio versus maximum U_{PH} values of continuously loaded pile-stabilized slope (slice model cases, S_u=40 kPa).

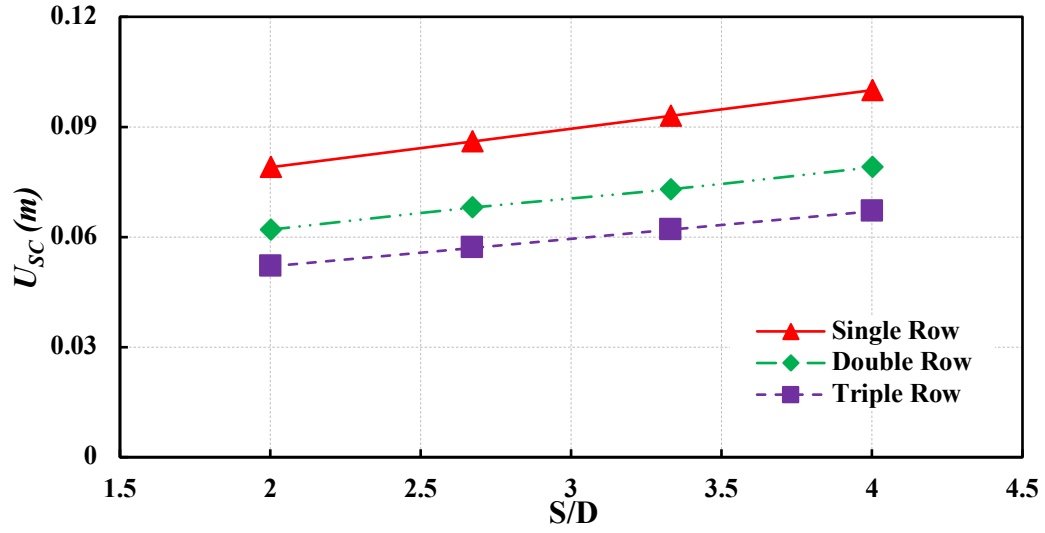


Figure 4.15. S/D ratio versus maximum U_{SC} values of continuously loaded pile-stabilized slope (slice model cases, S_u=40 kPa).

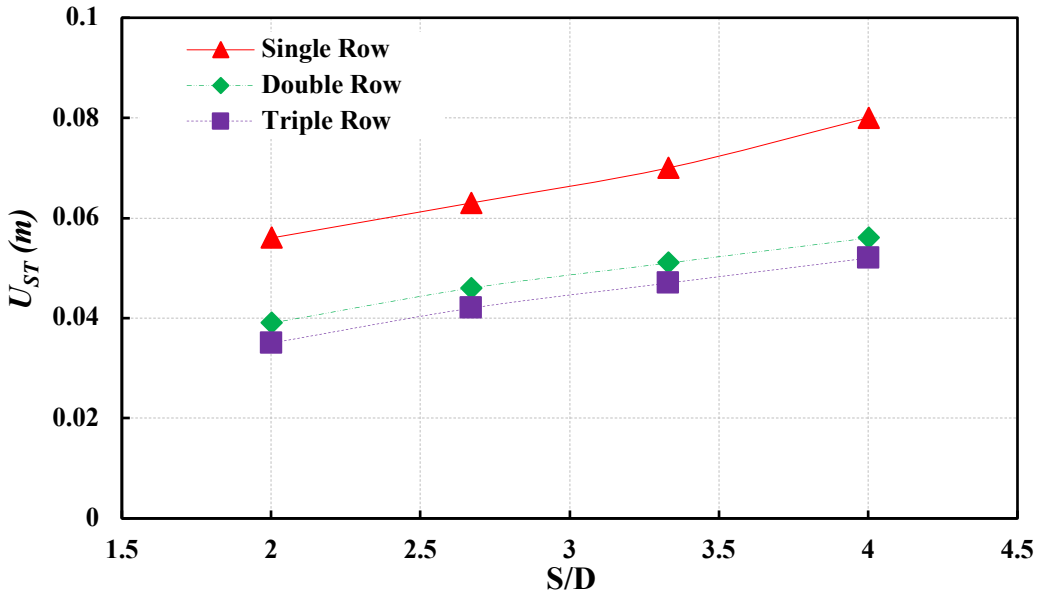


Figure 4.16. S/D ratio versus maximum U_{ST} values of continuously loaded pile-stabilized slope (slice model cases, S_u=40 kPa).

The maximum diplacements (pile head, slope crest and slope toe) values obtained from the analysis of the full models with locally loaded pile-stabilized slope cases considering various S/D ratio and pile group position are presented in Table 4.8 for free pile head condition.

Table 4.8. Displacements values of locally loaded pile-stabilized slopes (full model, S_u=40 kPa, single row configurations, free pile head condition).

Case No	Case Name	Pile Position	S/D	Maximum Displacements (mm)		
				Pile Head U_{PH}	Slope Crest U_{SC}	Slope Toe U_{ST}
16	S/D2_PN13_RN1_36_C	Crest	2	10.6	8.4	4.4
17	S/D3_PN9_RN1_36_C	Crest	3	12.1	8.8	5.0
18	S/D4_PN7_RN1_36_C	Crest	4	13.2	10.0	5.8
1	S/D2_PN13_RN1_36_M	Middle	2	11.4	8.2	5.0
19	S/D3_PN9_RN1_36_M	Middle	3	12.9	9.1	5.7
20	S/D4_PN7_RN1_36_M	Middle	4	14.3	9.8	6.4
21	S/D2_PN13_RN1_36_T	Toe	2	6.8	11.1	5.8
22	S/D3_PN9_RN1_36_T	Toe	3	7.6	11.8	6.5
23	S/D4_PN7_RN1_36_T	Toe	4	8.1	12.3	7.0

Figure 4.17 shows S/D ratio versus U_{PH} values, Figure 4.18 presents S/D ratio versus U_{SC} values and Figure 4.19 presents S/D ratio versus U_{ST} values for three different pile group positions for the free pile head condition. The results of the analyses indicate the following: regardless of the position of the pile groups, there is a direct relationship between the S/D ratio and U_{PH} (*see* Figure 4.17). For example, in the case of piles installed at the crest of the slope, there was a 25% increase in the U_{PH} when the S/D increased from two (2) to four (4). The same increase is observed for piles installed in the middle of the slope. And in the case of piles at the toe of the slope, this increase was 20%. A direct relationship was also observed for U_{SC} and U_{ST} (*see* Figure 4.18 and Figure 4.19). Changes in U_{SC} amount to a 9% increase for groups installed at the crest and in the middle of the slope. When piles are installed in the lower part of the slope, the increase in U_{SC} was 11%. Because the values of U_{ST} are smaller than U_{SC} and U_{PH}, the increases measured in percentages is greater is greater for U_{ST}. For example, for groups installed at the crest, the increase of U_{ST} is 32%, while for groups in the middle of the slope, it is 28%. A smaller increase of 21% was observed for the case of groups installed at the toe of the slope. While the percentage increase in displacements may be similar across different parts of the slope, the absolute increase in displacement varies. For instance, despite the similar percentage increases observed in displacement of piles located at three different locations along the slope, the absolute increase in displacements is greater for the case of piles located at the toe of the slope due to the relatively lower initial displacements. This underscores the need to consider both relative and absolute displacement changes in slope stability analyses.

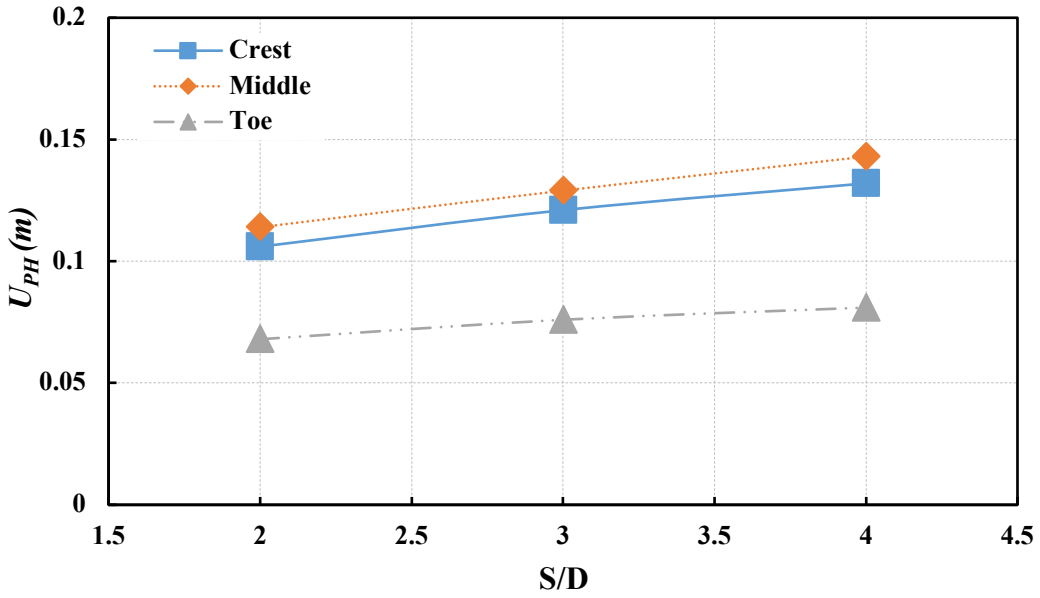


Figure 4.17. S/D ratio versus maximum U_{PH} of locally loaded pile-stabilized slope (full model cases, S_u=40 kPa, single row configurations, free pile head condition).

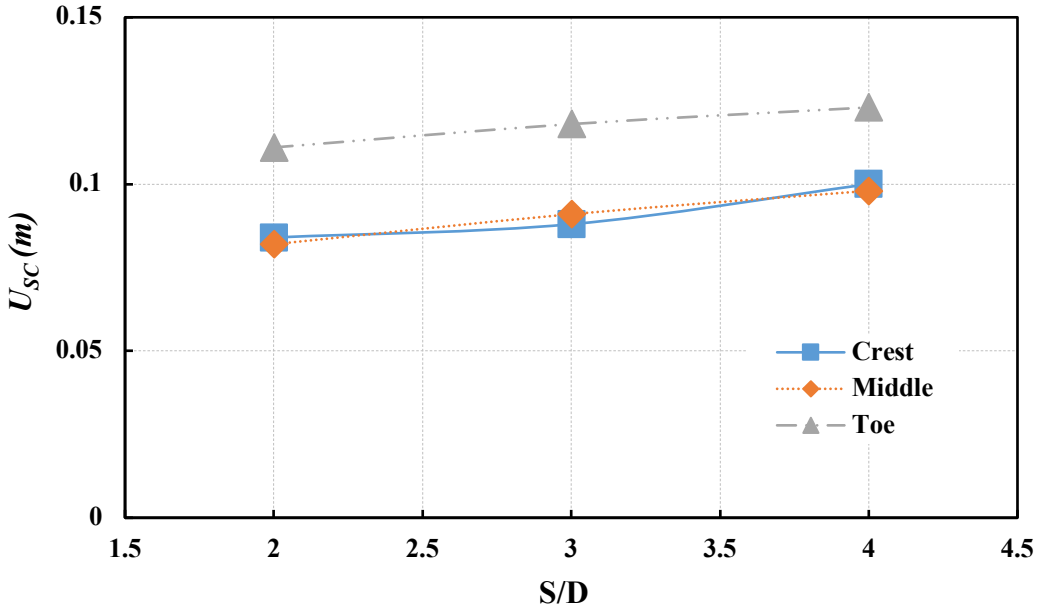


Figure 4.18. S/D ratio versus maximum U_{SC} values of locally loaded pile-stabilized slope (full model cases, S_u=40 kPa, single row configurations, free pile head condition).

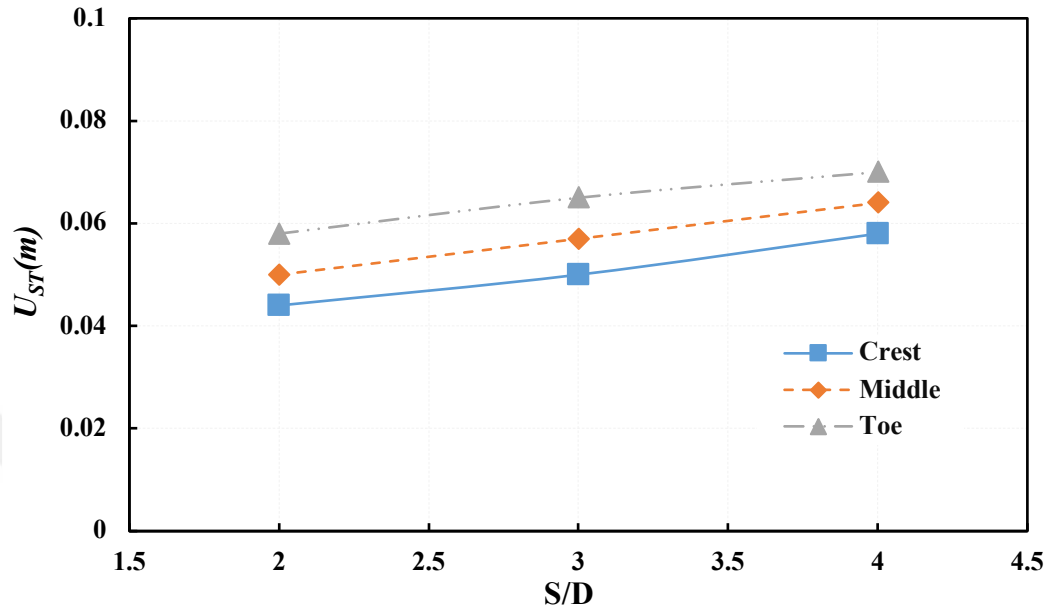


Figure 4.19. S/D ratio versus maximum U_{ST} values of locally loaded pile-stabilized slope (full model cases, S_u=40 kPa, single row configurations, free pile head condition).

The effect of the S/D ratio on the distribution of U_{PH} for three different pile group position is shown Figure 4.20 for the case of a free pile head. Figure 4.20a, Figure 4.20b and Figure 4.20c shows pile head displacements for pile groups placed at the crest, in the middle and at the toe of the slope, respectively. The effect of the S/D ratio on the distribution of U_{PH} for three different pile group position is shown in Figure 4.21 for the case of a constrained pile head. Figure 4.21a, Figure 4.21b and Figure 4.21c shows this distribution for piles placed at the crest, in the middle and at the toe of the slope, respectively. A common feature of these two graphs is that as the S/D ratio decreases, all U_{PH} values decrease, regardless of their distance from the load application zone. However, upon closer examination, it can be observed that the effect of S/D ratio is observed mainly in the piles located in the load application zone. While the overall trend of decreasing displacements with a reduction of S/D ratio is observed across the entire pile group, the variations in the S/D ratio have a more pronounced impact on U_{PH} near the load application zone compared to outer piles.

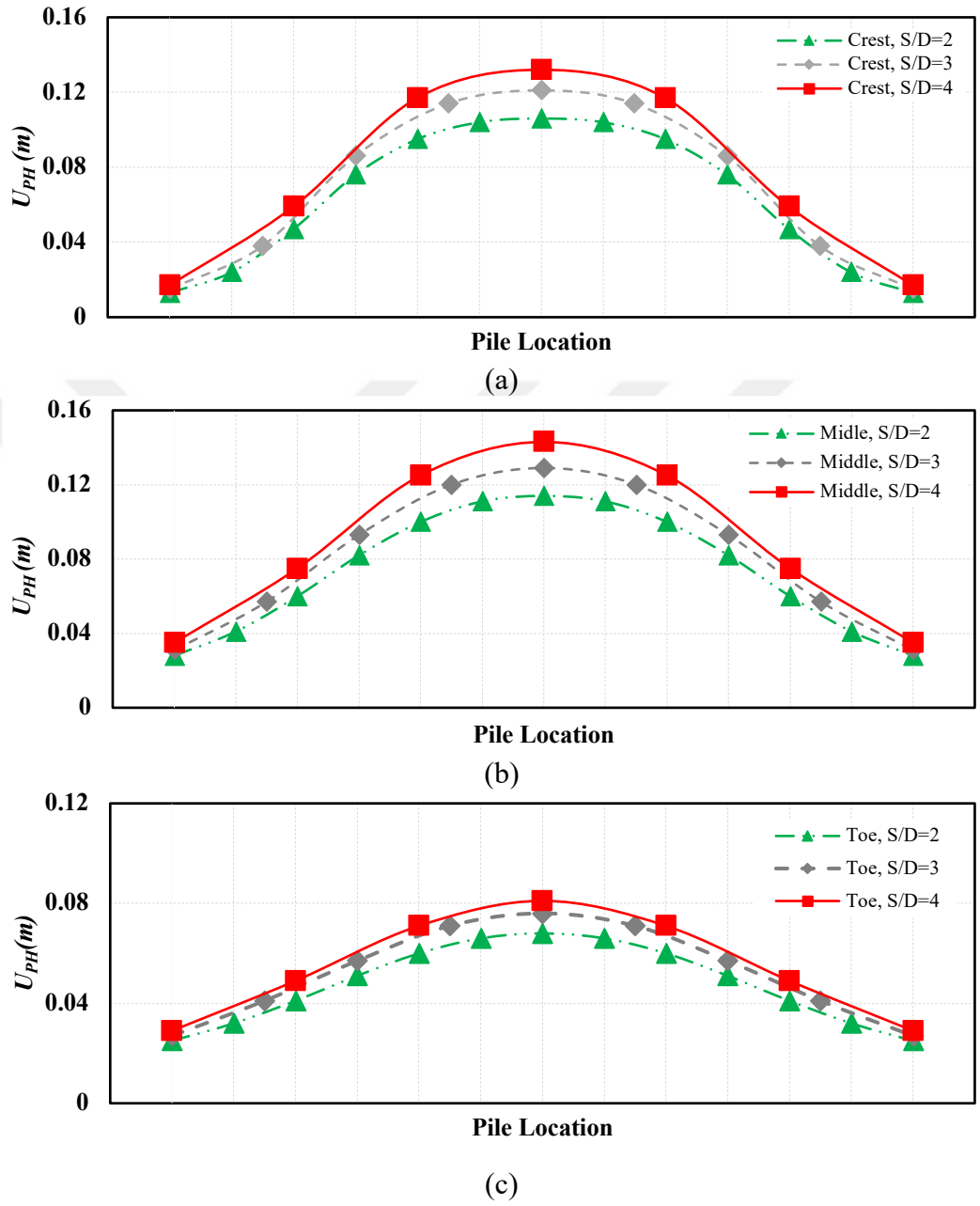
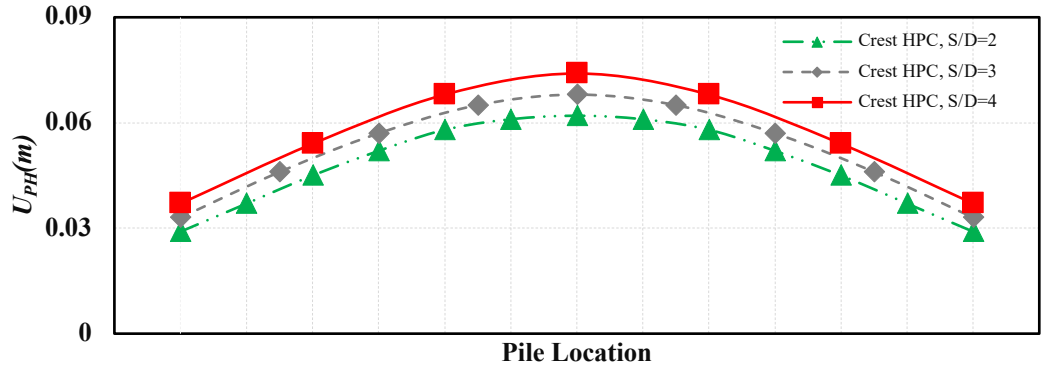
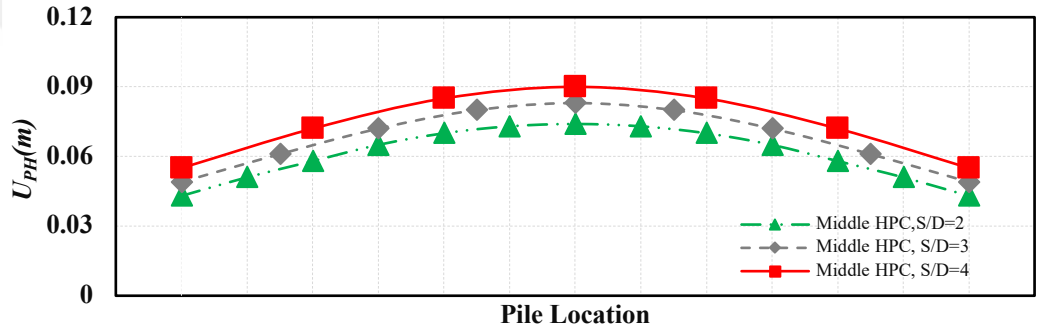


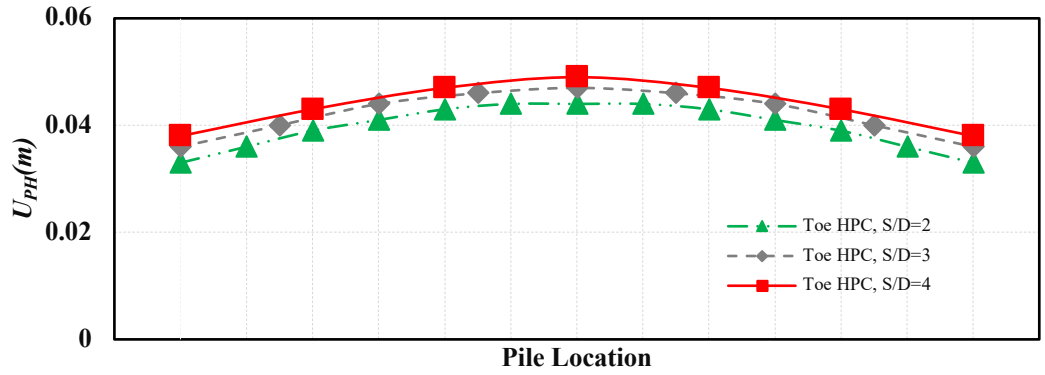
Figure 4.20. Pile location versus U_{PH} of locally loaded pile-stabilized slope (full model cases, S_u=40 kPa, single row configurations, free pile head condition): (a) crest , (b) middle , (c) toe.



(a)



(b)



(c)

Figure 4.21. Pile location versus U_{PH} of locally loaded pile-stabilized slope (full model cases, S_u=40 kPa, single row configurations, constrained pile head condition): (a) crest , (b) middle , (c) toe.

Figure 4.22 shows incremental displacements obtained from the safety phase of the analyses of single row configurations for pile groups placed at the crest and in the middle of the slope, and for both free and constrained pile head conditions. When the influence of S/D ratio on the critical zone is examined, a clear trend is observed, as such with an increase in the S/D ratio, the extent of the critical zone (the area affected by the load) also increases. However, it is also worth noting that this increase occurs in two directions: both horizontal and vertical, however a greater increase was observed in the horizontal direction. This conclusion applies to cases with all pile head conditions.

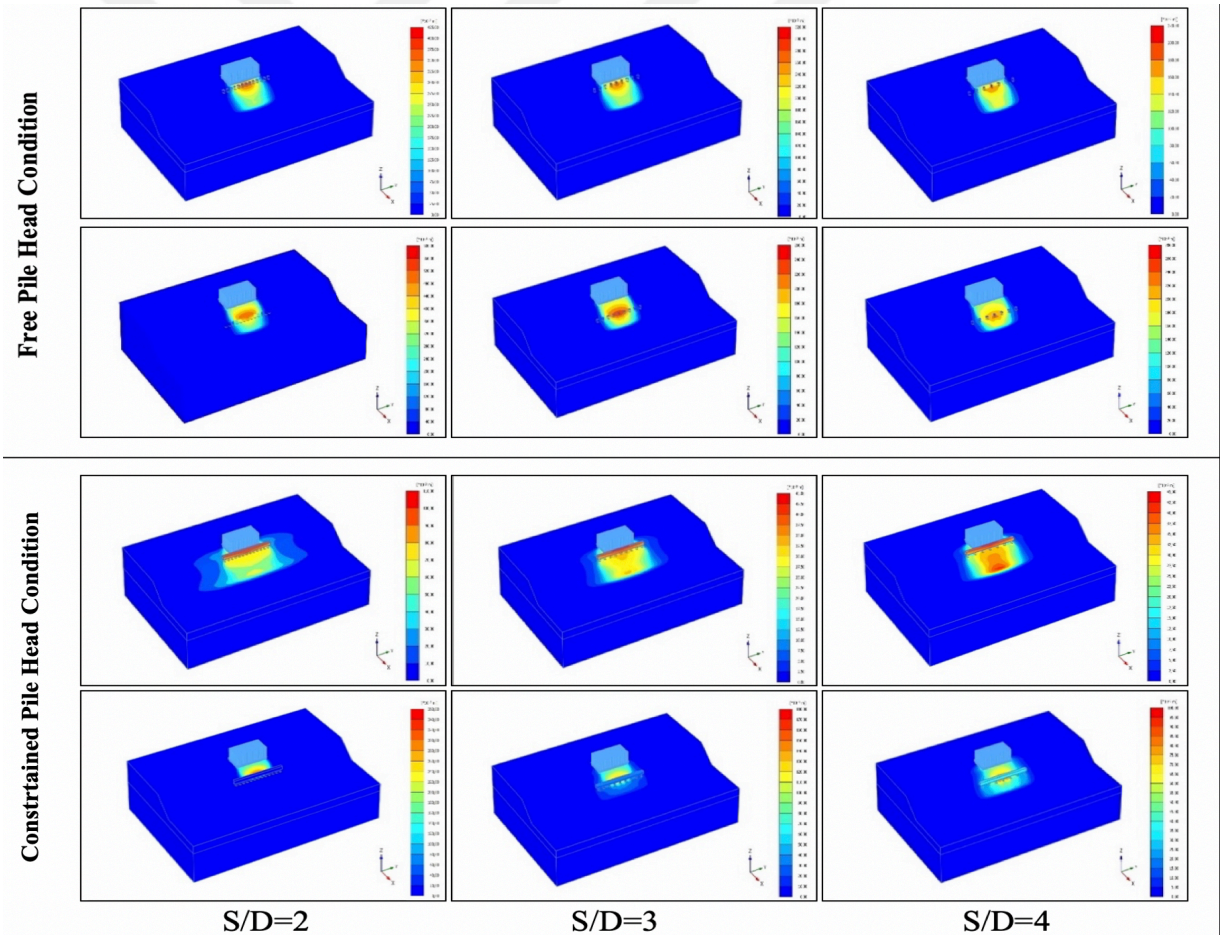


Figure 4.22. Effect of S/D ratio on critical surface, incremental displacements (full model cases, S_u=40 kPa, single row configurations).

4.2. Effect of Number of Rows

This section presents the influence of the number of rows on the *FS*, internal pile forces, and slope deformations. To study the effect of the number of rows on the stabilization of slopes three separate slice models with different loading and soil conditions, as well as full models with the condition of a free pile head were utilized. The results of these studies are explained below. For a more detailed assessment, the results of the analyses were grouped based on S/D ratios as such the only variable was the number of rows of piles.

4.2.1. Factor of Safety

The FS_{0_PS} values obtained from the analysis of the natural pile-stabilized slope cases considering various numbers of rows and S/D ratios are presented in Table 4.9 for S_u=40 kPa. Figure 4.23 presents number of rows versus FS_{0_PS} for S_u=40 kPa. A clear direct relationship exists between number of rows and FS_{0_PS}. As expected, increasing number of rows has a positive effect on slope stabilization, as such FS_{0_PS} clearly increases.

Table 4.9. Results of the study analyses performed on natural pile-stabilized slope (slice model cases, S_u=40 kPa).

Case No	Number of rows	Pile position	S/D	*FS*
-	0	-	-	1.45
39	Single Row	Middle	2.00	2.02
43	Double Row	Middle	2.00	2.22
47	Triple Row	Middle	2.00	2.36
40	Single Row	Middle	2.67	1.97
44	Double Row	Middle	2.67	2.17
48	Triple Row	Middle	2.67	2.31
41	Single Row	Middle	3.33	1.91
45	Double Row	Middle	3.33	2.10
49	Triple Row	Middle	3.33	2.25
42	Single Row	Middle	4.00	1.83
46	Double Row	Middle	4.00	2.04
50	Triple Row	Middle	4.00	2.18

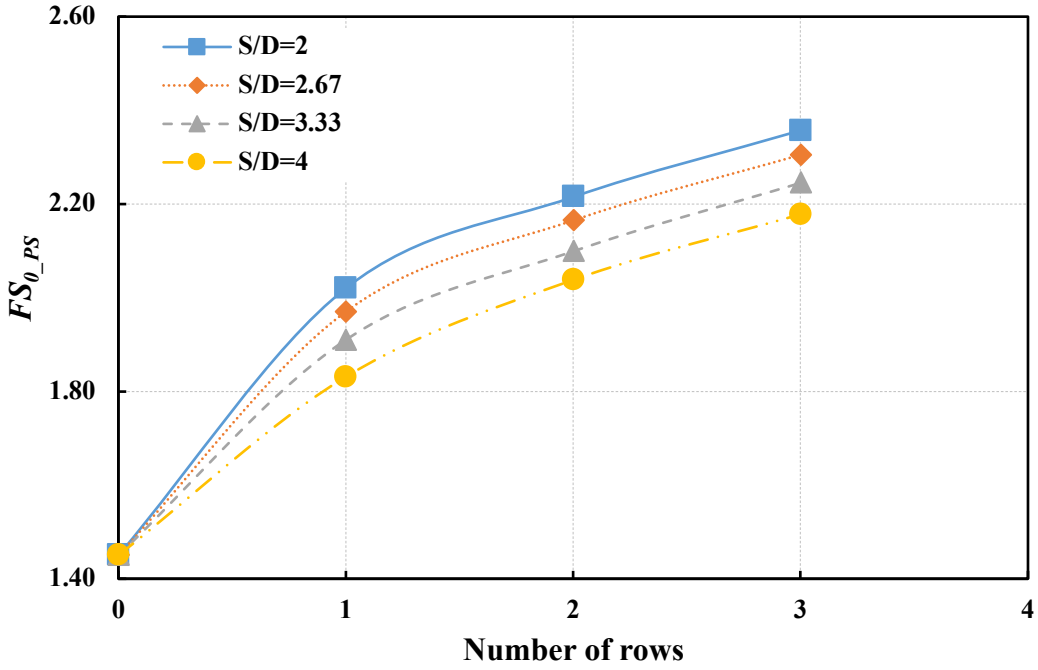


Figure 4.23. Number of rows versus FS_{0_PS} (slice model cases, S_u=40 kPa).

The *FS* (%) increase measures the percentage change in the factor of safety of pile-stabilized slope as a result of varying numbers of rows in a pile group with respect to the *FS* of the unstabilized slope, prior to stabilization. The formula can be written as

$$FS\ (\%)\ increase\ w.r.t.unstabilized\ slop = 100 \times \left(\frac{FS_{0_PS(row\ number=x)} - FS}{FS}\right), \quad (4.2)$$

where the initial value of number of row is 0 , which refers to the natural unstabilized slope (slope prior to the pile stabilization), and the final value of the number of rows investigated in this study is 3. Figure 4.24 illustrates the relationship between the number of rows and the % increase attained for *FS* of natural slope with S_u=40 kPa for various S/D ratios. The Figure 4.24 shows that as the number of rows of piles increases, there is a consistent increase (%) in *FS*. This indicates improved stability across varying S/D ratios. At lower S/D ratios, such as 2, the increase in *FS* is more pronounced with each additional row, demonstrating significant stability gains. As the S/D ratio increases, the of increase (%) of *FS* tends to diminish slightly, suggesting

that while additional rows still improve stability, the effect is somewhat reduced compared to with the effect of varying S/D ratios.

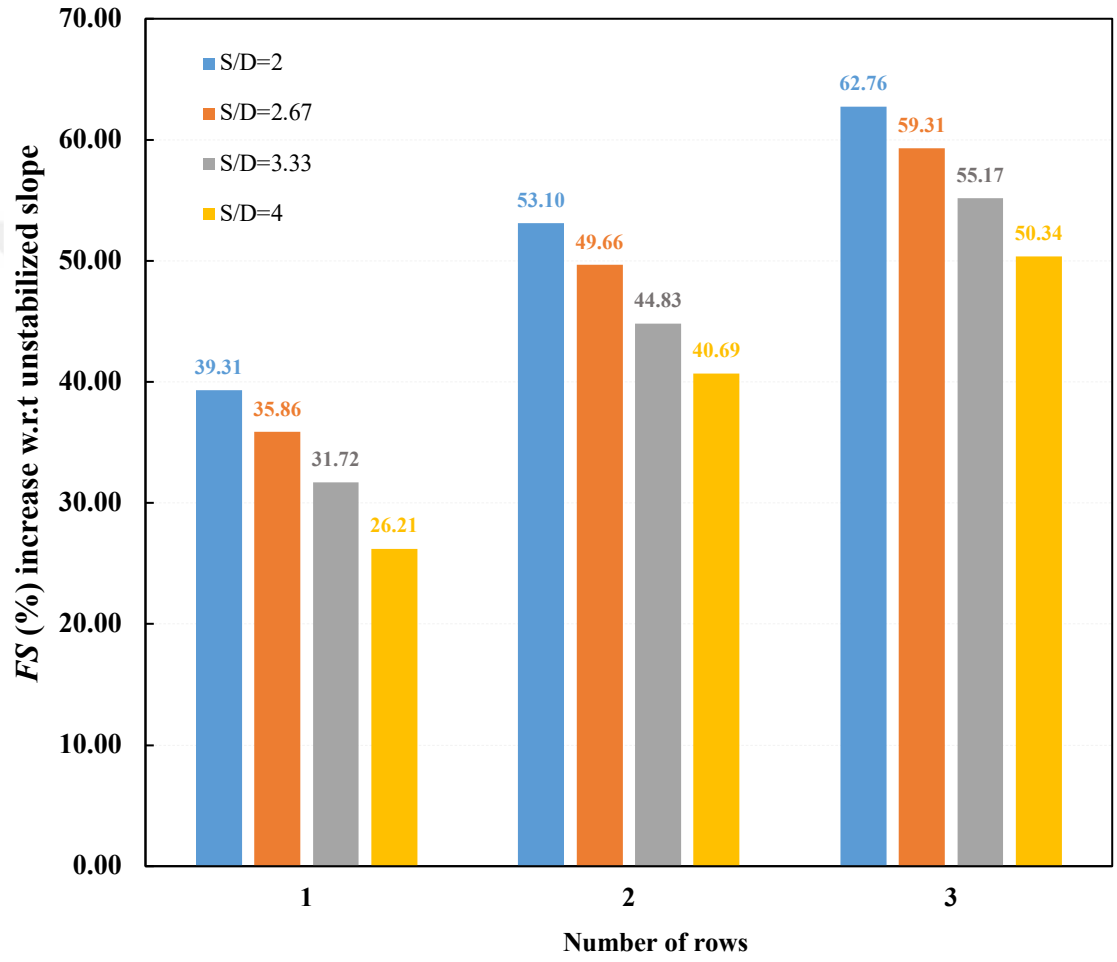


Figure 4.24. Number of rows versus *FS* (%) increase with respect to natural unstabilized slope (slice model cases, S_u=40 kPa).

The FS_{0_PS} values obtained from the analysis of the natural pile-stabilized slope cases considering various numbers of rows and S/D ratios are presented in Table 4.10 ,for S_u=30 kPa. Figure 4.25 presents number of rows versus FS_{0_PS} for S_u=30 kPa. A clear direct relationship between number of rows and FS_{0_PS} exists. As expected, increasing number of rows has a positive effect on slope stabilization, as such FS_{0_PS} increases.

Table 4.10. Results of the safety analyses performed on natural pile-stabilized slope (slice model cases, S_u=30 kPa).

Case No	Number of rows	Pile position	S/D	*FS*
-	0	-	-	1.10
77	Single Row	Middle	2.0	1.67
81	Double Row	Middle	2.0	1.89
85	Triple Row	Middle	2.0	2.04
78	Single Row	Middle	3.0	1.50
82	Double Row	Middle	3.0	1.79
86	Triple Row	Middle	3.0	1.95
79	Single Row	Middle	3.5	1.44
83	Double Row	Middle	3.5	1.74
87	Triple Row	Middle	3.5	1.89
80	Single Row	Middle	4.0	1.39
84	Double Row	Middle	4.0	1.68
88	Triple Row	Middle	4.0	1.83

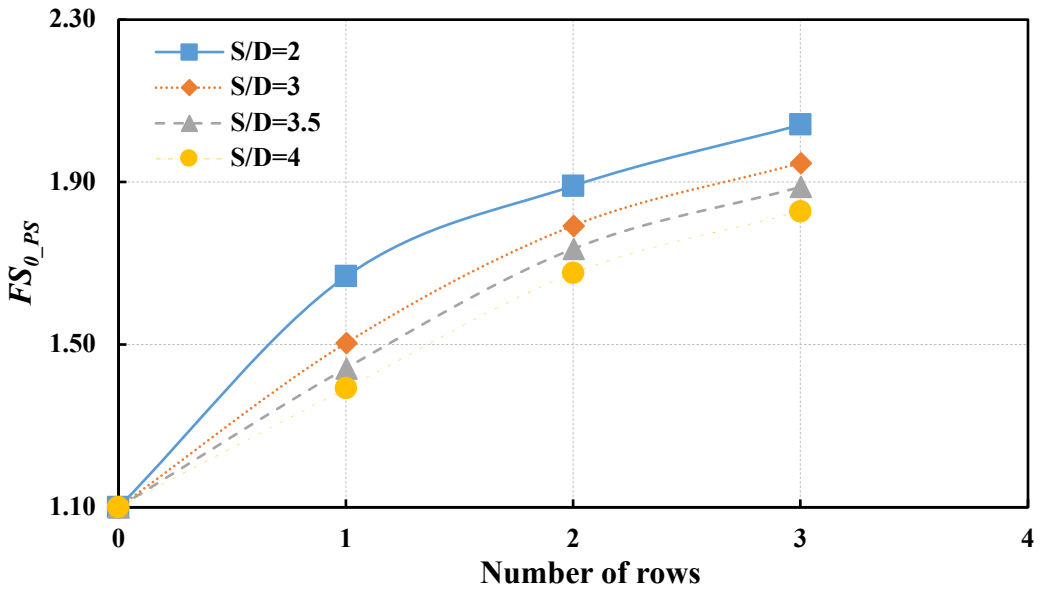


Figure 4.25. Number of rows versus FS_{0_PS} (slice model cases, S_u=30 kPa).

Figure 4.26 illustrates the relationship between the number of rows and the % increase attained for *FS* of natural slope with S_u=30 kPa for various S/D ratios. Figure 4.26 illustrates that increasing the number of rows of piles consistently enhances *FS* across all cases with various S/D ratios. At lower S/D ratios, such as 2, each additional row results in substantial

increases in *FS*, highlighting significant stability improvements. As the S/D ratio increases, the percentage increase of *FS* generally diminishes with each additional row, though still showing notable enhancements in stability. This trend underscores the effectiveness of multiple rows of piles in increasing *FS*, with the magnitude of improvement influenced by the specific S/D ratio of the pile configuration. More rows of piles consistently lead to higher increases in *FS*, similar to the previous case with S_u=40 kPa. This indicates that additional rows significantly enhance slope stabilization, however, the % increase diminishes as the number of rows increases. Increasing the S/D ratio reduces the % increase in *FS* for all numbers of rows, emphasizing the importance of lower S/D ratio for optimal slope stabilization. For the case of lower soil strength (for S_u = 30 kPa) % increases of *FS* are higher compared to the % increases of *FS* observed for the higher soil strength cases (for S_u=40 kPa) for all pile configurations and S/D ratios.

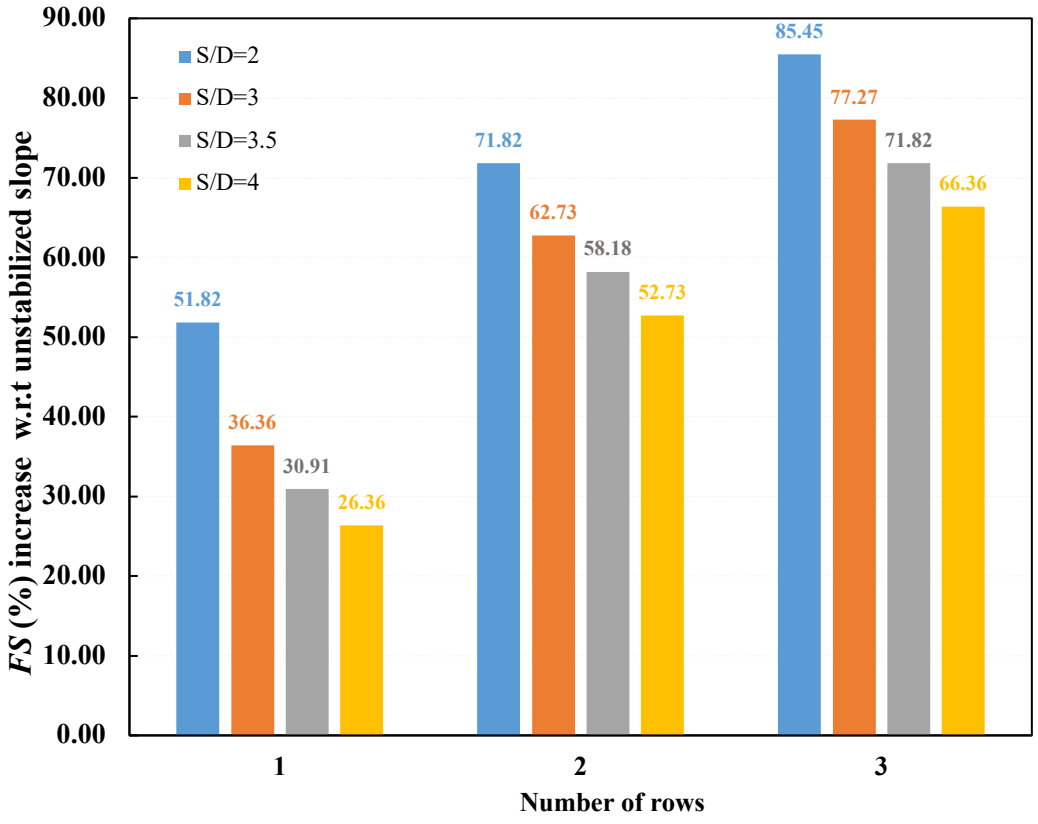


Figure 4.26. Number of rows versus *FS* (%) increase with respect to natural unstabilized slope, S_u=30 kPa.

The FS_{CL_PS} values obtained from the analysis of the continuously loaded pile-stabilized slope cases considering various numbers of rows and S/D ratios are presented in Table 4.11, for S_u=40 kPa. Figure 4.27 presents the number of rows versus FS_{CL_PS} for S_u=40 kPa. A distinct direct relationship is observed between the number of rows and FS_{CL_PS}. As expected, increasing number of rows has a positive effect on slope stabilization, F_{CL_PS} increases.

Table 4.11. Results of the safety analyses performed on continuously loaded pile-stabilized slope (slice model case, S_u=40 kPa).

Case No	Number of rows	Pile position	S/D	*FS*
-	0	-	-	1.00
59	Single Row	Middle	2.00	1.26
63	Double Row	Middle	2.00	1.49
67	Triple Row	Middle	2.00	1.58
60	Single Row	Middle	2.67	1.20
64	Double Row	Middle	2.67	1.40
68	Triple Row	Middle	2.67	1.55
61	Single Row	Middle	3.33	1.17
65	Double Row	Middle	3.33	1.32
69	Triple Row	Middle	3.33	1.48
62	Single Row	Middle	4.00	1.14
66	Double Row	Middle	4.00	1.27
70	Triple Row	Middle	4.00	1.39

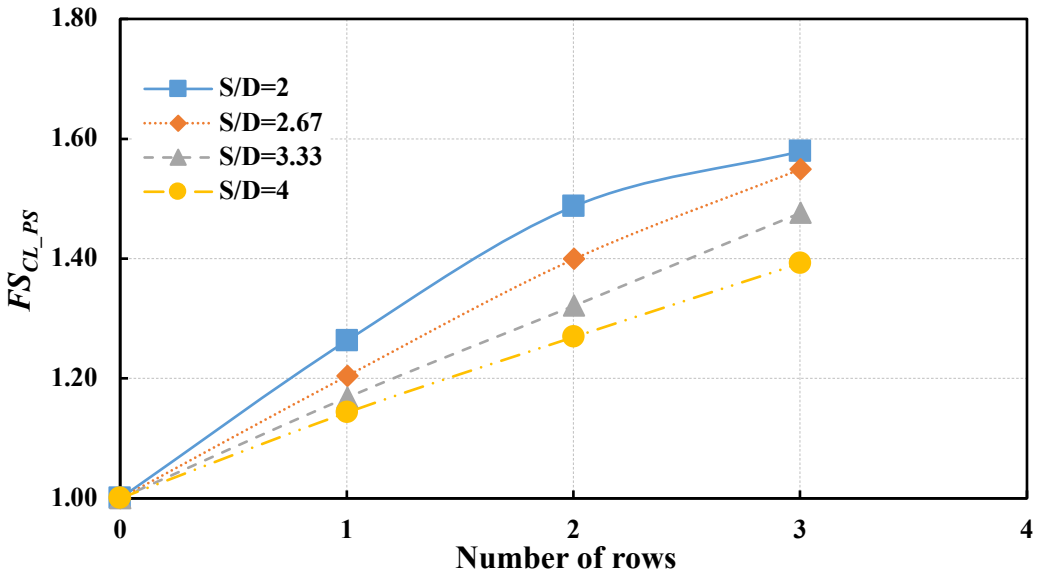


Figure 4.27. Number of rows versus FS_{CL_PS} (slice model cases, S_u=40 kPa).

Figure 4.28 illustrates the relationship between the number of rows and the % increase obtained for *FS* in continuously loaded slope with S_u=40 kPa for various S/D ratios 4. Increasing the number of rows of piles generally results in higher increases (%) of *FS* across all S/D ratios. At lower S/D ratios, such as S/D=2, each additional row notably boosts *FS*. As the S/D ratio increases, the increase (%) in *FS* per additional row diminishes, though there remains a clear trend of improved stability with more rows. This trend underscores the effectiveness of multiple rows of piles in enhancing *FS*, with the extent of improvement moderated by the specific S/D ratio of the pile configuration. Lower S/D ratios results in greater increases in *FS*. The effectiveness of pile row installation in increasing *FS* of diminishes as the S/D ratio increases. Adding more rows of piles (especially from single to double) has a more pronounced effect on increasing the *FS* compared to changing the S/D ratio. While the S/D ratio also impacts *FS*, its effect is smaller compared to the number of rows.

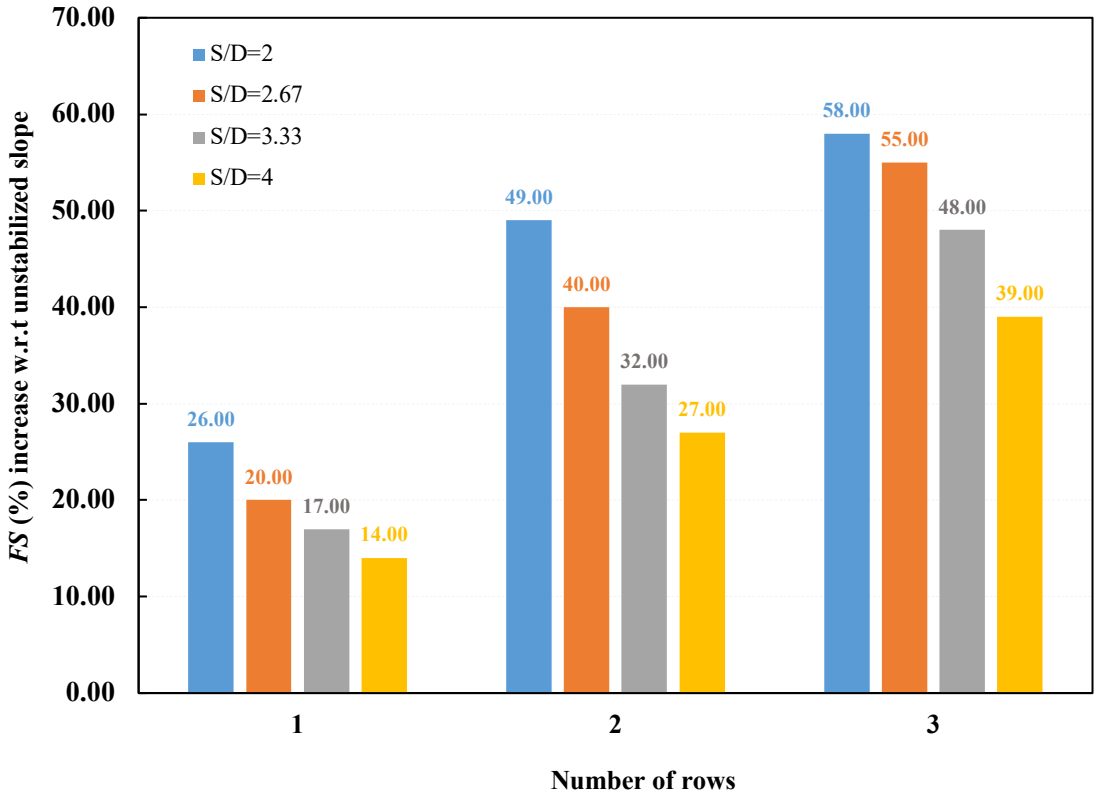


Figure 4.28. Number of rows versus *FS* (%) increase with respect to continuously loaded unstabilized slope (slice model cases, S_u=40 kPa).

The FS_{LPS} values obtained from the analysis of the locally loaded pile-stabilized slope cases considering various numbers of rows are presented in Table 4.12. The cases presented in Table 4.12 pertrain to S/D=3. Installing the single row resulted in a 16% increase in FS_{LPS} and when pile groups were configurated in double row and triple row the increase was 26% and 31%, respectively.

Table 4.12. Results of the safety analyses performed on locally loaded pile-stabilized slope (full model cases, S_u=40 kPa, S/D=3, free pile head condition).

Case No	Case Name	Number of rows	FS_{LPS}
11	S/D3_PN21_RN3_36_M	3	1.45
2	S/D3_PN14_RN2_36_M	2	1.34
19	S/D3_PN9_RN1_36_M	1	1.228

4.2.2. Internal Forces

The maximum pile internal force (bending moment and shear force) values obtained from the analysis of the continuously loaded pile-stabilized slope cases considering various numbers of rows and S/D values are presented in Table 4.13 for S_u=40 kPa. Figure 4.29 presents number of rows versus maximum pile bending moment values. Figure 4.30 illustrates the relationship between number of rows and maximum pile shear force values. There is a clear connection between the number of rows and the maximum pile internal force values. As anticipated, increasing the number of rows positively impacts these values, resulting in a decrease. Specifically, the addition of more rows in pile groups consistently lowers both maximum pile bending moment and shear force values across different S/D ratios. This trend demonstrates significant reductions in these internal forces with each additional row. However, the rate of reduction diminishes with subsequent additions of rows.

Table 4.13. Maximum pile internal forces of continuously loaded pile-stabilized slope (slice models, S_u=40 kPa).

Case No	Number of rows	Pile position	S/D	Maximum internal forces	
				Bending moment (kNm)	Shear force (kN)
59	Single Row	Middle	2.00	3672	965
63	Double Row	Middle	2.00	1992	545
67	Triple Row	Middle	2.00	1589	428
60	Single Row	Middle	2.67	4393	1217
64	Double Row	Middle	2.67	2490	712
68	Triple Row	Middle	2.67	1973	564
61	Single Row	Middle	3.33	4889	1397
65	Double Row	Middle	3.33	2910	851
69	Triple Row	Middle	3.33	2312	678
62	Single Row	Middle	4.00	5251	1526
66	Double Row	Middle	4.00	3215	965
70	Triple Row	Middle	4.00	2604	781

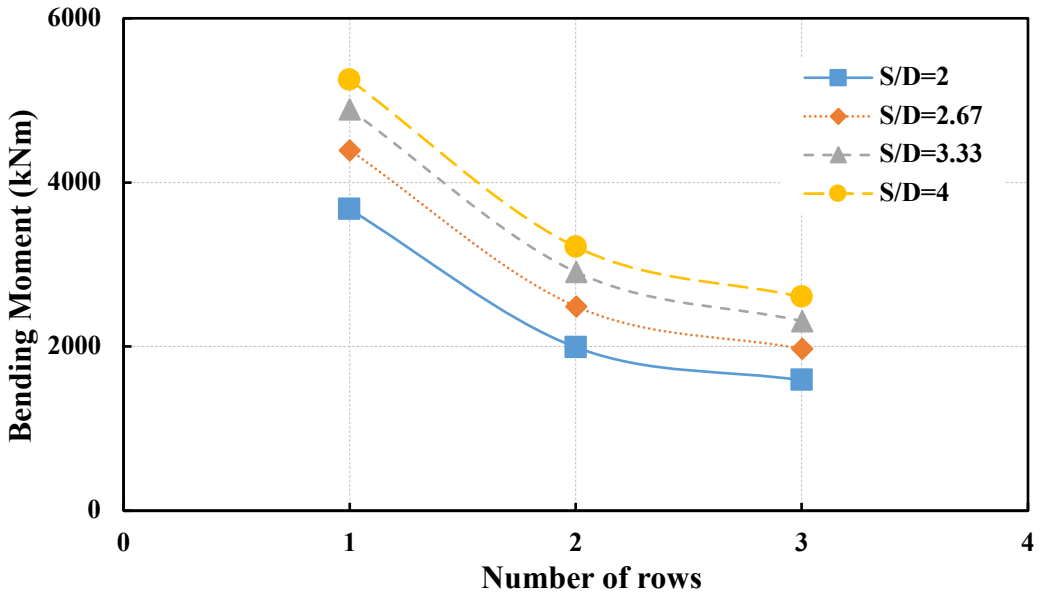


Figure 4.29. Number of rows versus maximum pile bending moment values of continuously loaded pile-stabilized slope (slice model cases, S_u=40 kPa).

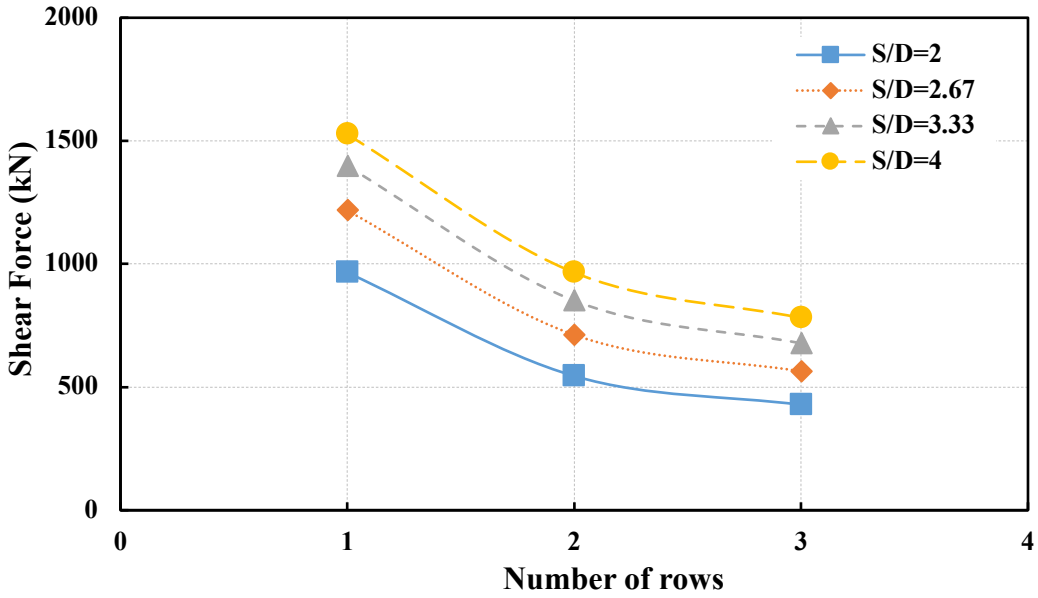


Figure 4.30. Number of rows versus maximum pile shear force values of continuously loaded pile-stabilized slope (slice model cases, S_u=40 kPa).

The maximum pile internal force values (bending moment and shear force) obtained from the analysis of locally loaded pile-stabilized slopes, considering various numbers of rows, are presented in Table 4.14. The results of the analysis of three slope models stabilized with pile groups with S/D =3, and various rows were examined first . With the installation of the first row, there was a 29% decrease in the maximum pile bending moment. As the number of rows increased from single to double, the maximum bending moment further decreased by 29%. However, when the number of rows increased from double to triple, the maximum bending moment decreased only by 13%. The changes in maximum shear force values followed a very similar pattern.

Table 4.14. Maximum pile internal forces of locally loaded pile-stabilized slope (full model cases, S_u=40 kPa, S/D=3, free pile head condition).

Case No	Case Name	Number of rows	Maximum Internal Forces	
			Bending moment (kNm)	Shear force (kN)
11	S/D3_PN21_RN3_36_M	3	2771	787
2	S/D3_PN14_RN2_36_M	2	3199	912
19	S/D3_PN9_RN1_36_M	1	4512	1289

4.2.3. Displacements

The maximum diplacements (pile head, slope crest and slope toe) values obtained from the analysis of the continuously loaded pile-stabilized slope cases considering various numbers of rows and S/D ratios are presented in Table 4.15 for S_u=40 kPa. Figure 4.31 shows the number of rows versus U_{PH} values, Figure 4.32 presents number of rows versus U_{SC} values and Figure 4.33 shows number of rows versus U_{ST}. The analysis reveals that the U_{PH} decreases significantly with the increase in pile rows. Results show that increasing the number of rows consistently decreases the U_{PH}, U_{SC}, and U_{ST}. This reduction trend is observed consistently regardless of the S/D ratio, with the most significant decreases occurring with the change from single to double row cases. However, the effectiveness of further reducing displacements diminishes with third row. This is due to the fact that total concrete volume used represent the amount of reinforcement in the slope. Accordingly, % increase in total concrete volume used is 100% when the number of rows changes from single row to double row. However % increase of total concrete used, and hence the increase in reinforcement is only 50% when number of rows changes from double to triple row.

Table 4.15 Maximum displacement values of continuously loaded pile-stabilized slopes (slice model cases, S_u=40 kPa).

Case No	Number of rows	Pile Position	S/D	Maximum Displacements (mm)		
				Pile Head U_{PH}	Slope Crest U_{SC}	Slope Toe U_{ST}
59	Single Row	Middle	2.00	11.2	7.9	5.6
63	Double Row	Middle	2.00	8.7	6.2	3.9
67	Triple Row	Middle	2.00	7.2	5.2	3.5
60	Single Row	Middle	2.67	12.4	8.6	6.3
64	Double Row	Middle	2.67	9.6	6.8	4.6
68	Triple Row	Middle	2.67	8.0	5.7	4.2
61	Single Row	Middle	3.33	13.7	9.3	7.0
65	Double Row	Middle	3.33	10.5	7.3	5.1
69	Triple Row	Middle	3.33	8.7	6.2	4.7
62	Single Row	Middle	4.00	14.9	10.0	8.0
66	Double Row	Middle	4.00	11.5	7.9	5.6
70	Triple Row	Middle	4.00	9.6	6.7	5.2

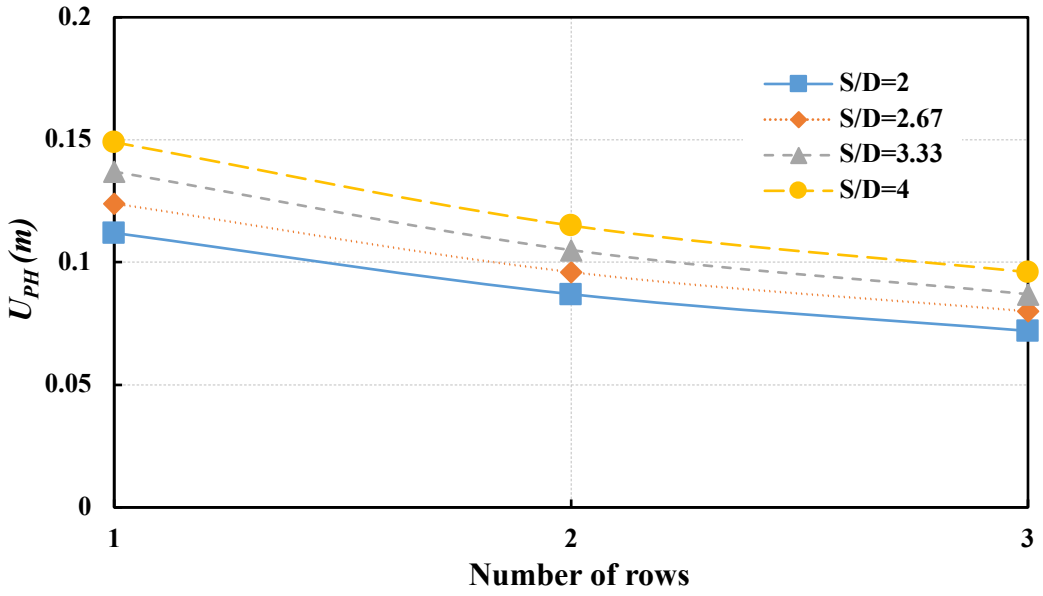


Figure 4.31. Number of rows versus maximum U_{PH} values of continuously loaded pile-stabilized slope (slice model cases, S_u=40 kPa).

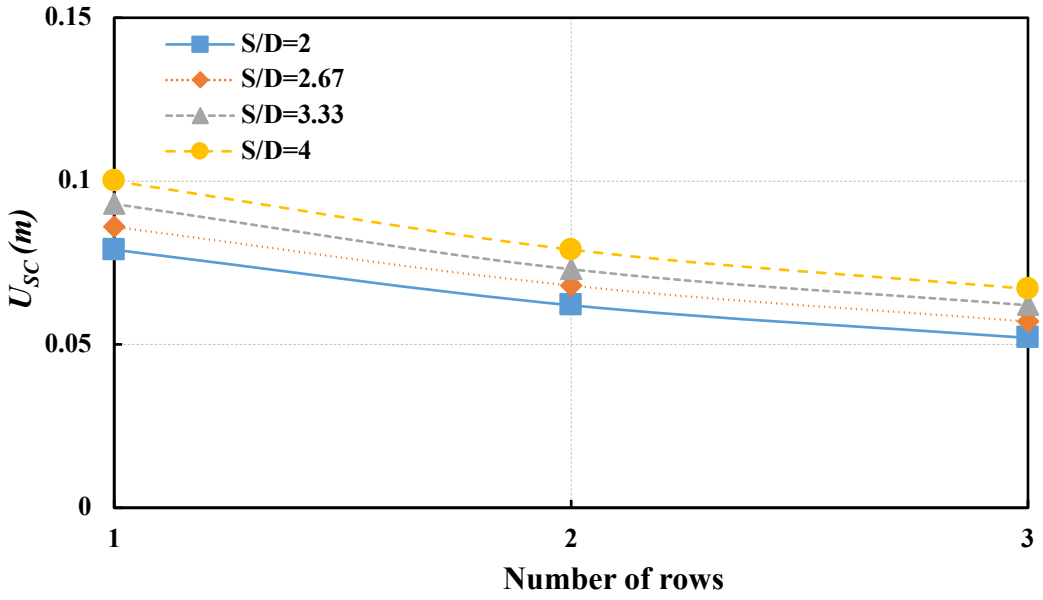


Figure 4.32. Number of rows versus maximum U_{SC} values of continuously loaded pile-stabilized slope (slice model cases, S_u=40 kPa).

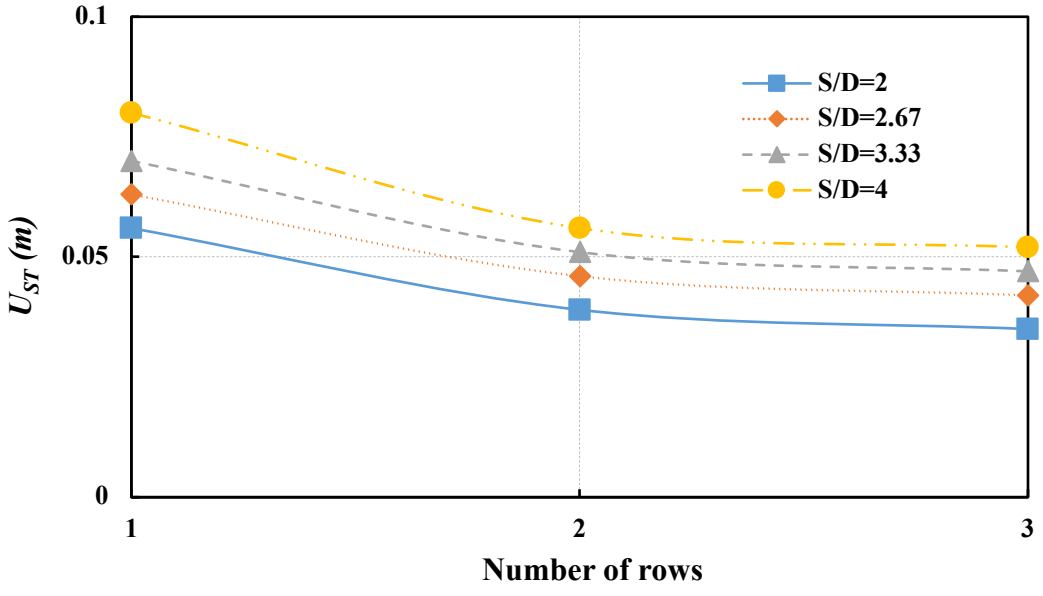


Figure 4.33. Number of rows versus maximum U_{ST} values of continuously loaded pile-stabilized slope (slice model cases, S_u=40 kPa).

In the case of the full model where a localized load was applied, the displacement values listed in Table 4.16 were obtained. Upon reviewing the displacement values, a gradual decrease in the magnitude of U_{SC} and U_{PH} can be observed with an increase in the number of rows. However, when analyzing the U_{PH}, a sharp drop is observed with the installation of third row.

Table 4.16. Maximum displacements values of locally loaded pile-stabilized slopes (full model cases, S_u=40 kPa, S/D=3, free pile head condition).

Case No	Case Name	Number of rows	Maximum Displacements (mm)		
			Pile Head, U_{PH}	Slope Crest, U_{SC}	Slope Toe, U_{ST}
11	S/D3_PN21_RN3_36_M	3	10.1	7.0	3.1
2	S/D3_PN14_RN2_36_M	2	11.2	7.9	5.1
19	S/D3_PN9_RN1_36_M	1	12.9	9.1	5.7

The effect of the number of rows on the distribution of pile head displacements is shown in Figure 4.34. Please note that the the displacements pertain to the front row, that is closer to the crest for each case. The increase of number of rows decreases the magnitude of U_{PH}, rather than the distribution itself. In other words, the difference between the displacements of the central and outermost piles remains constant in all groups regardless of the number of rows in the group.

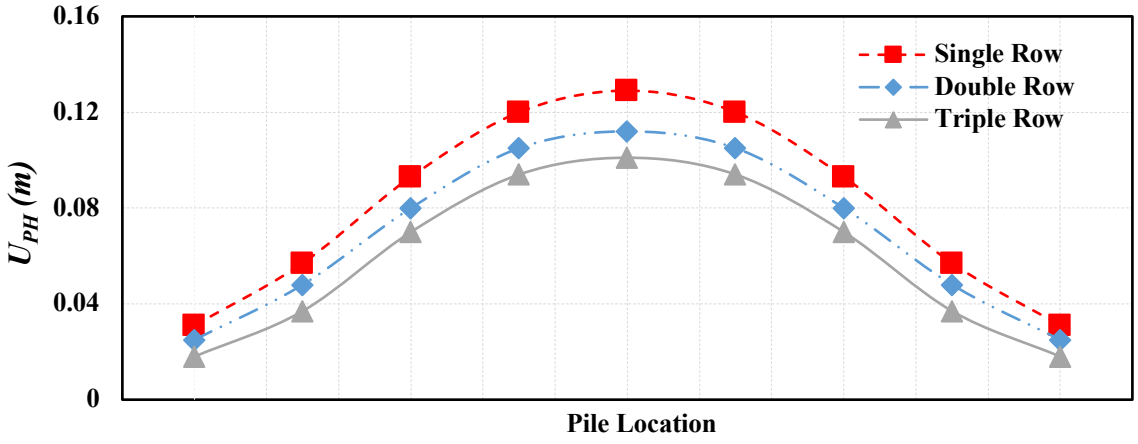
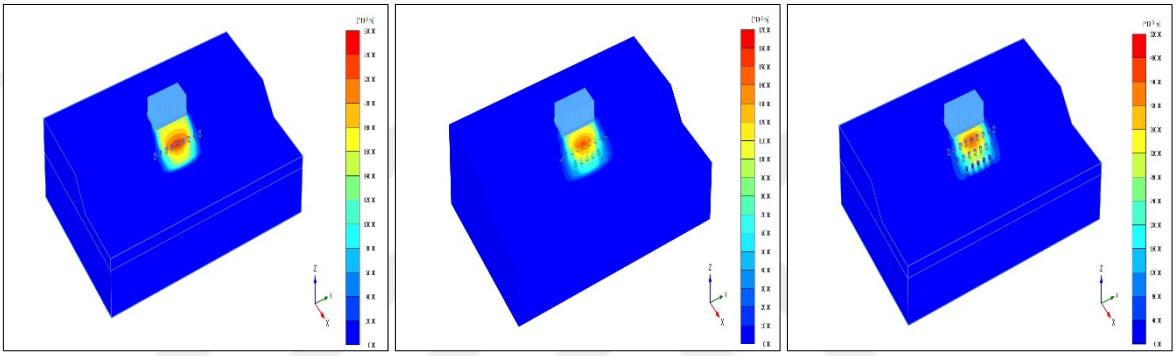


Figure 4.34. Pile location versus U_{PH} of locally loaded pile-stabilized slope (full model cases, S_u=40 kPa, S/D=3, free pile head condition).

Figure 4.35 shows incremental displacements obtained from the safety phase of the FE analysis of various S/D=3 configurations. Upon reviewing the incremental displacements, one can see that as the number of rows increases, the area experiencing the greatest displacement, in essence, the criticial failure volume reduces. It is important to note that this reduction was more prevalent in the vertical direction.



Single Row Double Row Triple Row

Figure 4.35. Effect of number of rows on critical surface of locally loaded pile-stabilized slope on incremental displacements (full model cases, S_u=40 kPa, S/D=3, free pile head condition).

4.3. Effect of Pile Position

This section of this Chapter 4 examines in detail the strategic placement of piles in different positions of the slope especially at the crest, middle, and toe and explores their respective effects on slope stabilization. By examining the mechanisms by which piles interact with the soil and the slope failure surface, this study aims to provide a comprehensive understanding of how efficient pile placement can reduce the risks of slope failure while reducing the cost. Slice models were used when considering continuous loading and natural slope cases. The full models were used for local loading cases. Two different load conditions were considered in slice model cases and two pile head conditions in full models (*i.e.*, free and constrained head) were investigated.

4.3.1. Factor of Safety of Pile-Stabilized Slopes

The *FS* values obtained from the analysis of the natural pile-stabilized slopes (FS_{0_PS}) and continuously loaded pile-stabilized slope cases considering various pile group positions along the slope are presented in Table 4.17 for S_u=40 kPa. Figure 4.36 presents number of rows versus FS_{0_PS} and FS_{CL_PS} for S_u=40 kPa. Based on the results of the analysis, it can be said that piles located at the crest of the slope provide greater *FS* values than those located in the middle and toe of the slope. However, it should be noted that the differences between the *FS* values obtained from the stabilization of the slope with piles located at the crest are not significantly different from those obtained from the case with piles in the middle of the slope. On the other hand, a noticeable differences were observed when piles are placed at toe of the slope. Especially with a continuous load on the slope, the installation of piles at the toe practically has almost no effect. On the other hand when the piles are placed at the same location without this continuous surcharge load, in the natural slope case a noticeable reinforcement is observed. In the absence of piles, the *FS* of this natural slope is 1.45, and when piles are installed at the toe of the slope, *FS* increases to 1.75 which corresponds to an increase of 21%.

Table 4.17. Results of the analyses performed on natural and continuously loaded pile-stabilized slopes (slice models cases, S_u=40 kPa).

Case No	Number of Rows	Load Condition	Pile Position	S/D	*FS*
-	0	No Load	-	-	1.45
56	Single Row	No Load	Crest	2	2.07
39	Single Row	No Load	Middle	2	2.02
55	Single Row	No Load	Toe	2	1.75
-	0	Continuous Load	-	-	1.00
76	Single Row	Continuous Load	Crest	2	1.30
59	Single Row	Continuous Load	Middle	2	1.26
75	Single Row	Continuous Load	Toe	2	1.07

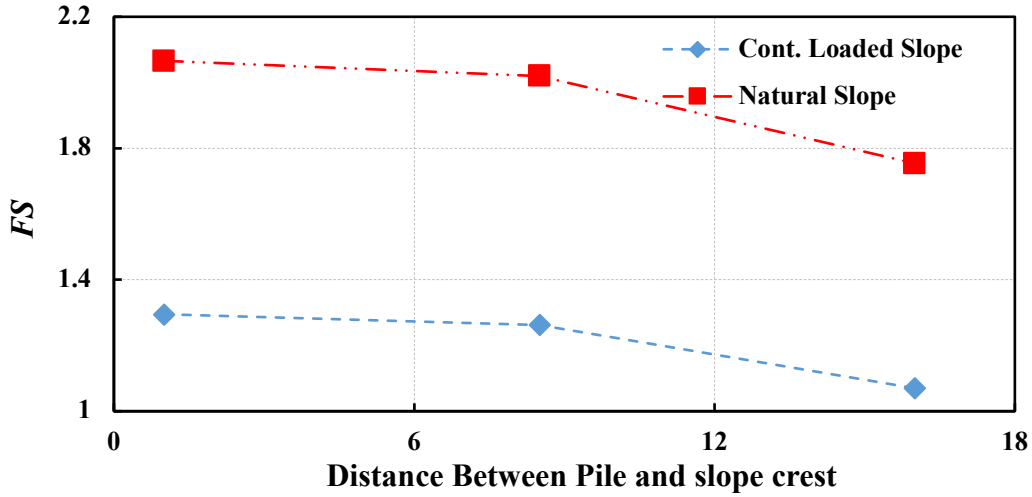


Figure 4.36. Pile position versus FS_{0_PS} and FS_{CL_PS} (slice models cases, S_u=40 kPa).

In this section, the influence of pile group position on FS_{LPS} values was investigated using full models with local loading. Models of pile groups in single and double row were created. In single row groups, configurations with varying S/D ratios were modeled, while in the case of double row, the S/D ratio remained constant (S/D=3). Additionally, two pile head condition were utilized: free and constrained. Results are shown in Table 4.18. Figure 4.37 presents pile position versus FS_{LPS} for free pile head condition. The analysis of FS_{LPS} values for single row groups reveals a consistent trend across all S/D ratios, where the FS_{LPS} is highest when piles are placed at the crest, FS_{LPS} slightly decreases when piles are at the middle, and reaches lowest at the toe. This trend holds for all S/D ratios examined. These findings indicate that stability, as

measured by FS_{LPS}, is strongly dependent on the pile group position along the slope, with the piles located at the toe yielding the lowest FS_{LPS} and the piles located at the crest yielding the highest FS_{LPS} across different S/D configurations for locally loaded slope. While the absolute difference between FS_{LPS} values obtained from the piles located at the crest and in the middle of the slope varies, these differences are not substantial in absolute terms. For the double row cases, the crest position exhibits the highest FS_{LPS} value of 1.352, indicating the most stable condition within the double row configuration. In contrast, the toe position displays the lowest FS_{LPS} value at 1.213, signifying lower stability compared to both the middle (FS_{LPS}=1.33) and crest positions. This gradient from crest to toe underscores the critical influence of pile position on stability, emphasizing the vulnerabilities associated with the toe position.

Table 4.18. Results of the analyses performed on locally loaded pile-stabilized slopes (full model cases, S_u=40 kPa).

Case No	Case Name	Pile Position	S/D	FS
16	S/D2_PN13_RN1_36_C	Crest	2	1.314
1	S/D2_PN13_RN1_36_M	Middle	2	1.290
21	S/D2_PN13_RN1_36_T	Toe	2	1.113
17	S/D3_PN9_RN1_36_C	Crest	3	1.248
19	S/D3_PN9_RN1_36_M	Middle	3	1.228
22	S/D3_PN9_RN1_36_T	Toe	3	1.106
18	S/D4_PN7_RN1_36_C	Crest	4	1.213
20	S/D4_PN7_RN1_36_M	Middle	4	1.191
23	S/D4_PN7_RN1_36_T	Toe	4	1.101
24	S/D3_PN13_RN2_36_C	Crest	3	1.352
4	S/D3_PN13_RN2_36_M	Middle	3	1.330
25	S/D3_PN13_RN2_36_T	Toe	3	1.213
26	S/D2_PN13_RN1_36_C_HPC	Crest	2	1.446
13	S/D2_PN13_RN1_36_M_HPC	Middle	2	1.320
31	S/D2_PN13_RN1_36_T_HPC	Toe	2	1.114
27	S/D3_PN9_RN1_36_C_HPC	Crest	3	1.368
29	S/D3_PN9_RN1_36_M_HPC	Middle	3	1.303
32	S/D3_PN9_RN1_36_T_HPC	Toe	3	1.100
28	S/D4_PN7_RN1_36_C_HPC	Crest	4	1.314
30	S/D4_PN7_RN1_36_M_HPC	Middle	4	1.265
33	S/D4_PN7_RN1_36_T_HPC	Toe	4	1.100
34	S/D3_PN13_RN2_36_C_HPC	Crest	3	1.452
35	S/D3_PN13_RN2_36_M_HPC	Middle	3	1.401
36	S/D3_PN13_RN2_36_T_HPC	Toe	3	1.23

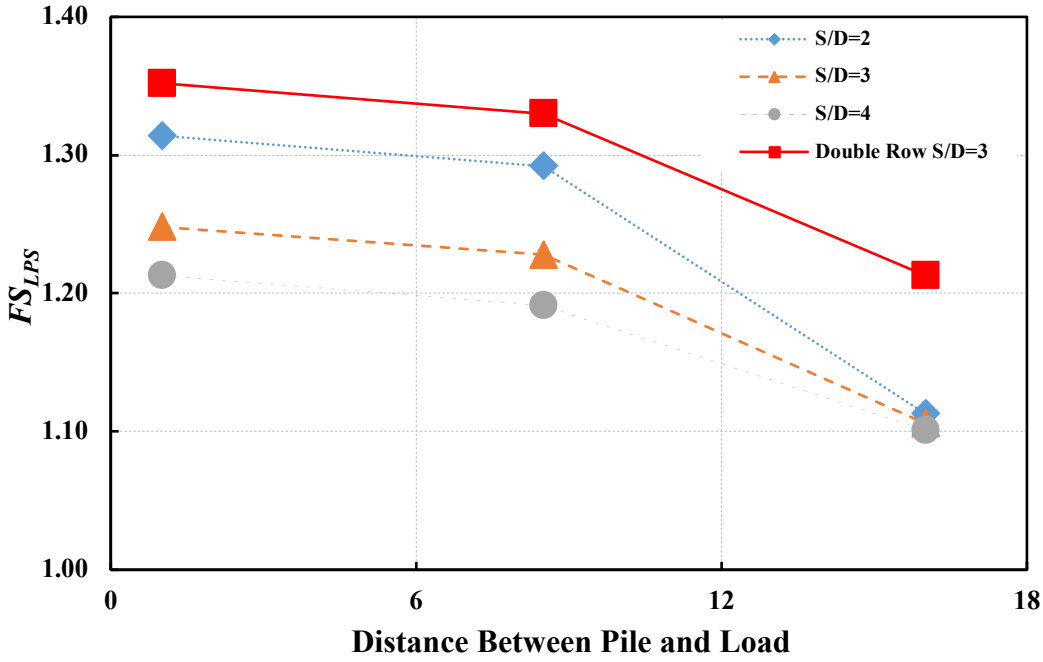


Figure 4.37. Pile position versus FS_{LPS} (full models cases, S_u=40 kPa, single and double row configurations, free pile head condition).

Figure 4.38 presents pile position versus FS_{LPS} for constrained pile head condition. Figure 4.38 presents a comparison of FS_{LPS} values across different S/D ratios in constrained pile head condition, highlighting distinct advantages and disadvantages based on pile group position. For all S/D ratios of 2, 3, and 4 , the crest position consistently demonstrates superior stability compared to the piles located at the middle of the slope. For S/D=2, the crest position exhibits FS_{LPS} of 1.446, which is higher than those obtained for piles placed at the middle position (1.320). Similarly, for S/D=3, the crest position maintains a higher FS_{LPS} of 1.368 compared to the case when piles are placed at the middle of the slope (1.303). This trend continues at S/D=4, where the case of the piles at the crest position yields an FS_{LPS} of 1.314, surpassing the one obtained for the piles middle position (1.265). These results underscore the advantage of positioning piles at the crest for maximizing stability and safety in stabilization of clayey slopes underlain by sand. The toe position consistently shows the lowest FS_{LPS} values across all S/D ratios, highlighting its vulnerability to potential failure. At S/D= 2, FS_{LPS} obtained for the slope stabilized with piles at the toe position is 1.114, that is notably lower than those obtained for the

cases with piles at the crest and middle positions. This pattern persists for S/D =3 and 4, where the toe position records FS_{LPS} value of 1.1, consistently lower than those of both the crest and middle positions.

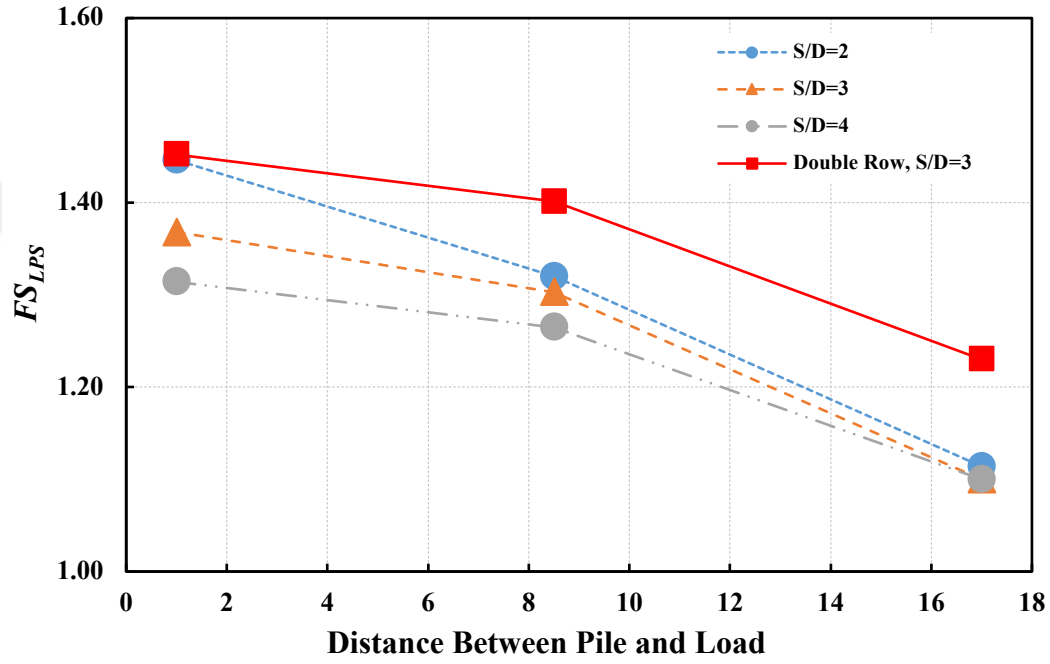


Figure 4.38. Pile position versus FS_{LPS} (full models cases, S_u=40 kPa, single and double row configurations, constrained pile head condition).

4.3.2. Internal Forces

The maximum pile internal force values obtained from the analysis of the locally loaded pile-stabilized slopes cases considering various pile group position along the slope, S/D ratio and pile head condition are presented in Table 4.19.

Table 4.19. Maximum pile internal force values of locally loaded pile-stabilized slopes (full model cases, S_u=40 kPa).

Case No	Case Name	Pile Position	S/D	Maximum Pile Internal Forces	
				Bending Moment (kNm)	Shear Force (kN)
16	S/D2_PN13_RN1_36_C	Crest	2	3923	892
1	S/D2_PN13_RN1_36_M	Middle	2	3749	1005
21	S/D2_PN13_RN1_36_T	Toe	2	1870	665
17	S/D3_PN9_RN1_36_C	Crest	3	4730	1145
19	S/D3_PN9_RN1_36_M	Middle	3	4512	1289
22	S/D3_PN9_RN1_36_T	Toe	3	2185	817
18	S/D4_PN7_RN1_36_C	Crest	4	5175	1286
20	S/D4_PN7_RN1_36_M	Middle	4	4951	1446
23	S/D4_PN7_RN1_36_T	Toe	4	2326	883
26	S/D2_PN13_RN1_36_C_HPC	Crest	2	2646	924
13	S/D2_PN13_RN1_36_M_HPC	Middle	2	2514	869
31	S/D2_PN13_RN1_36_T_HPC	Toe	2	1253	470
27	S/D3_PN9_RN1_36_C_HPC	Crest	3	3283	1169
29	S/D3_PN9_RN1_36_M_HPC	Middle	3	3080	1099
32	S/D3_PN9_RN1_36_T_HPC	Toe	3	1441	566
28	S/D4_PN7_RN1_36_C_HPC	Crest	4	3704	1344
30	S/D4_PN7_RN1_36_M_HPC	Middle	4	3408	1261
33	S/D4_PN7_RN1_36_T_HPC	Toe	4	1512	618

Figure 4.39 and Figure 4.40 present a comparison of maximum pile bending moment values obtained from analyses of the cases with different pile positions along the slope, for free pile head and for constrained pile head conditions, respectively. The analysis of maximum pile bending moment reveals a clear dependence of the maximum pile bending moment on the pile position. The highest values of maximum pile bending moment occur in the pile groups placed at the crest of the slope, a slightly lower values were obtained in the groups placed in the middle of the slope and the lowest at the toe. The differences between these values are more pronounced under constrained pile head conditions compared to free pile head conditions. This highlights

the significant influence of pile position on bending moment distribution. Figure 4.41 and Figure 4.42 compare the maximum pile shear force values across various S/D ratios. Figure 4.41 illustrates the advantages and disadvantages concerning pile position under free pile head conditions, while Figure 4.42 addresses the same under constrained pile head conditions. The analysis of maximum pile shear force reveals dependence of the maximum pile shear force on the pile position. Under free pile head conditions, maximum pile shear force values are slightly higher when they are placed in the middle of the slope. Pile shear forces are the lowest, when piles are placed at the toe of the slope. In contrast, with a constrained pile head condition, maximum pile shear forces consistently decrease as the pile position move from the crest of the slope to the toe of the slope. Placing piles at the toe of a slope should not be seen as advantageous solely because they exhibit low pile internal forces. These reduced forces are primarily due to the difference in the failure mechanism of the slope,the piles at the toe are not fully mobilized for stabilization and the applied loads do not directly interact with the piles positioned at the toe.

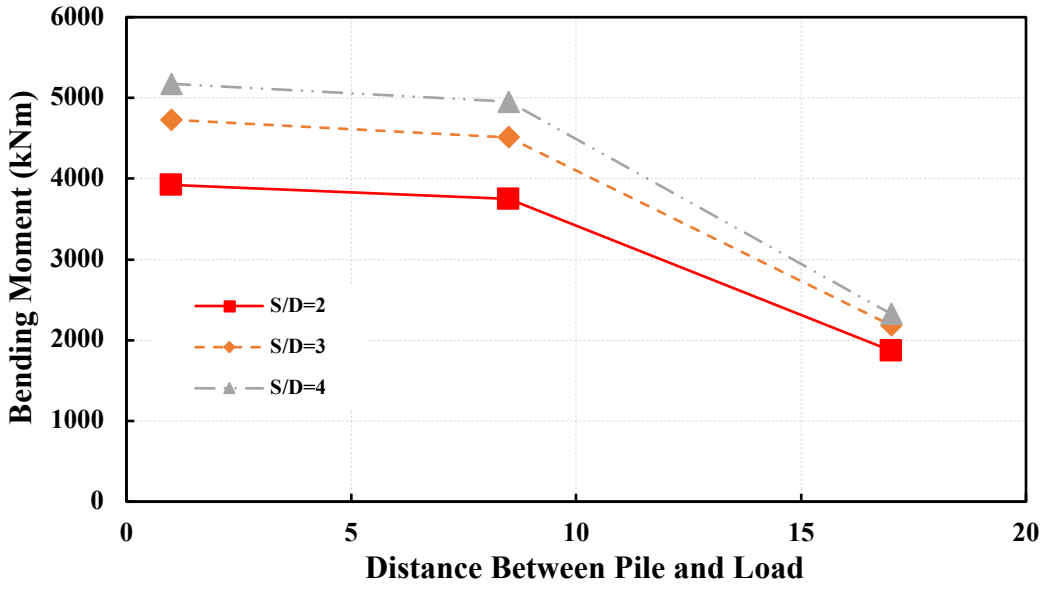


Figure 4.39. Pile position versus maximum pile bending moment values of locally loaded pile-stabilized slope (full model cases, S_u=40 kPa, single row configurations, free pile head condition).

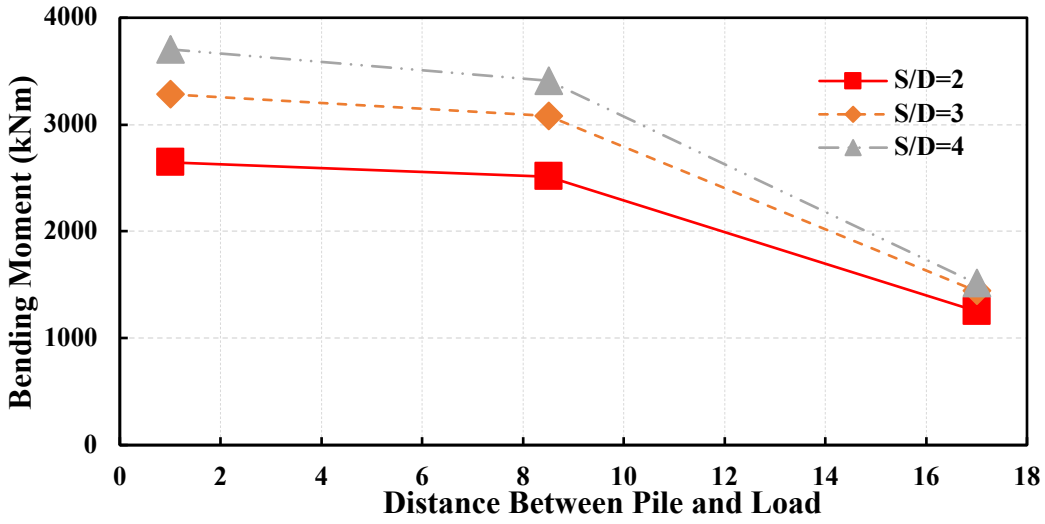


Figure 4.40. Pile position versus maximum pile bending moment values of locally loaded pile-stabilized slope (full model cases, S_u=40 kPa, single row configurations, constrained pile head condition).

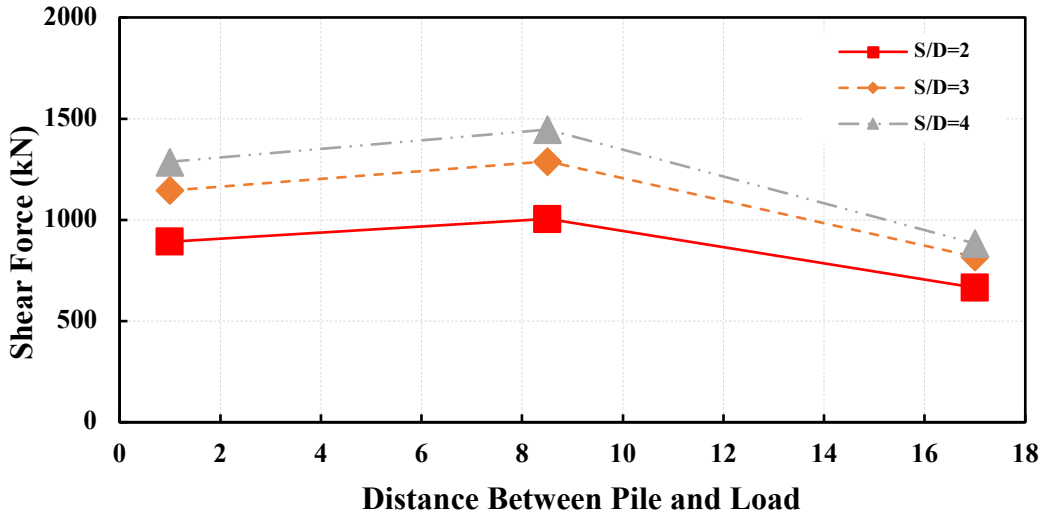


Figure 4.41. Pile position versus maximum pile shear force values of locally loaded pile-stabilized slope (full model cases, S_u=40 kPa, single row configurations, free pile head condition).

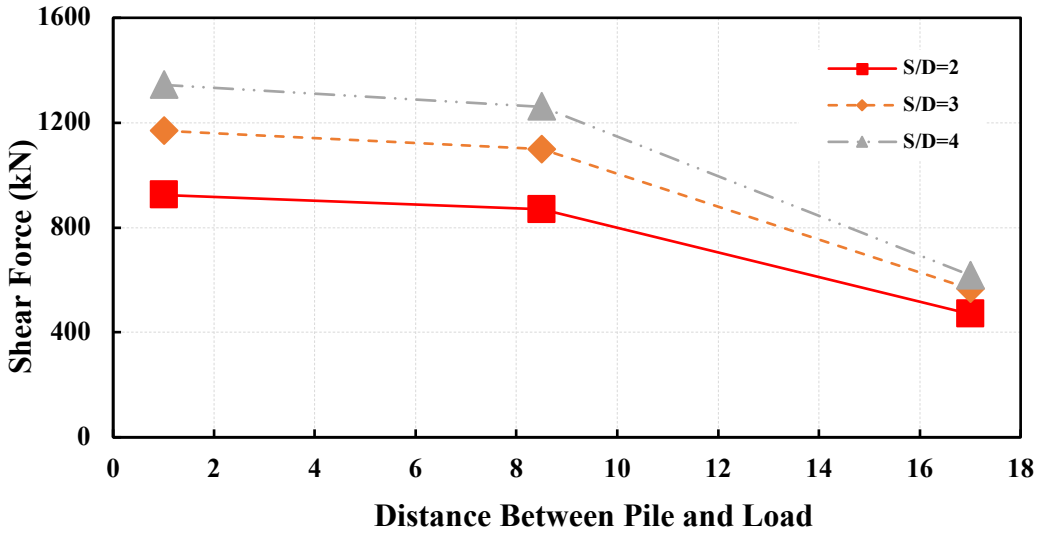


Figure 4.42. Pile position versus maximum pile shear force values of locally loaded pile-stabilized slope (full model cases, S_u=40 kPa, single row configurations, constrained pile head condition).

Figure 4.43 shows the distribution of pile bending moment of central pile for various pile group postions (crest, middle and toe). This figure demonstrates that placing piles closer to the crest results in an increased loading on the upper part of the pile. For piles installed in the lower and middle sections of the slope, there is a concentration of higher bending moment values around the location where the pile is socketed into the sand, while the load is practically negligible in the upper part of the pile. However, when the pile is installed at the crest of the slope, a significant load increase is observed on the upper part of the pile.

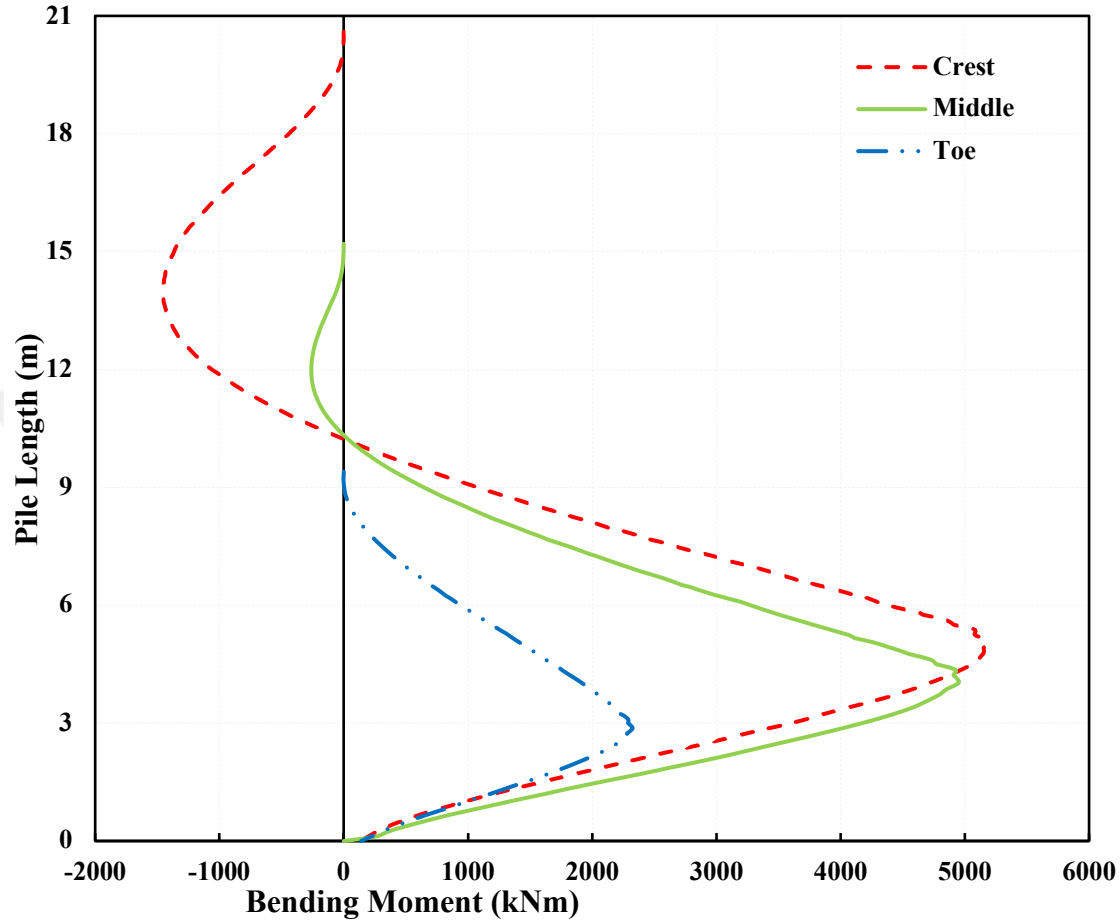


Figure 4.43. Pile bending moment diagram versus pile length for different pile positions (full model cases, S_u=40 kPa, free pile head condition).

4.3.3. Displacements

The maximum diplacements (pile head, slope crest and slope toe) values obtained from the analysis of the locally loaded pile-stabilized slope cases considering various pile group positions and S/D ratios are presented in Table 4.20 for S_u=40 kPa. Figure 4.44 and Figure 4.45 present a comparison of U_{PH} values for different pile positions (crest, middle toe) for free pile head conditions and constrained pile head conditions, respectively.

Table 4.20. Maximum displacement values of locally loaded pile-stabilized slopes (full model cases, S_u=40 kPa).

Case No	Case Name	Pile Position	S/D	Maximum Displacement (mm)		
				Pile Head U_{PH}	Slope Crest U_{SC}	Slope Toe U_{ST}
16	S/D2 PN13 RN1 36 C	Crest	2	10.6	8.4	4.4
1	S/D2 PN13 RN1 36 M	Middle	2	11.4	8.2	5.0
21	S/D2 PN13 RN1 36 T	Toe	2	6.8	11.1	5.8
17	S/D3 PN9 RN1 36 C	Crest	3	12.1	8.8	5.0
19	S/D3 PN9 RN1 36 M	Middle	3	12.9	9.1	5.7
22	S/D3 PN9 RN1 36 T	Toe	3	7.6	11.8	6.5
18	S/D4 PN7 RN1 36 C	Crest	4	13.2	10	5.8
20	S/D4 PN7 RN1 36 M	Middle	4	14.3	9.8	6.4
23	S/D4 PN7 RN1 36 T	Toe	4	8.1	12.3	7.0
26	S/D2 PN13 RN1 36 C HPC	Crest	2	6.2	4.9	3.3
13	S/D2 PN13 RN1 36 M HPC	Middle	2	7.4	6.4	3.9
31	S/D2 PN13 RN1 36 T HPC	Toe	2	4.4	10.9	3.8
27	S/D3 PN9 RN1 36 C HPC	Crest	3	6.8	5.8	4.0
29	S/D3 PN9 RN1 36 M HPC	Middle	3	8.3	7.0	4.4
32	S/D3 PN9 RN1 36 T HPC	Toe	3	4.7	11.6	4.1
28	S/D4 PN7 RN1 36 C HPC	Crest	4	7.4	6.3	4.6
30	S/D4 PN7 RN1 36 M HPC	Middle	4	9.0	7.7	5.0
33	S/D4 PN7 RN1 36 T HPC	Toe	4	4.9	12.1	4.2

For both free and constrained pile head conditions, the middle pile group position consistently exhibits the highest U_{PH}, while the toe position experiences the lowest U_{PH}. For instance, at S/D=2 with free pile head condition, the U_{PH} is 11.4 mm when piles are placed at the middle, 10.6 mm, when piles are placed at the crest, and 6.8 mm when piles are placed at the toe. With constrained pile head condition at the same S/D ratio, the U_{PH} reduces to 7.4 mm, 6.2 mm and 4.4 mm when piles are placed at the crest, at the middle and at the toe, respectively. Similar patterns were observed for pile groups with S/D=3 and S/D=4. Overall, the data indicates that the pile position significantly impacts U_{PH}. It is important to note that the lowest U_{PH} results were observed for toe pile positions, mainly because this pile position did not offer a substantial increase in FS_{LPS}, in essence an increase in stability is practically not observed in these cases. To optimize the design considering U_{PH}, pile positions in the middle and crest of the slope should be considered, as these cases correspond to better improvements in the FS_{LPS} compared to installing piles at the toe of the slope. These observations on U_{PH} apply to both free pile head conditions and constrained head conditions.

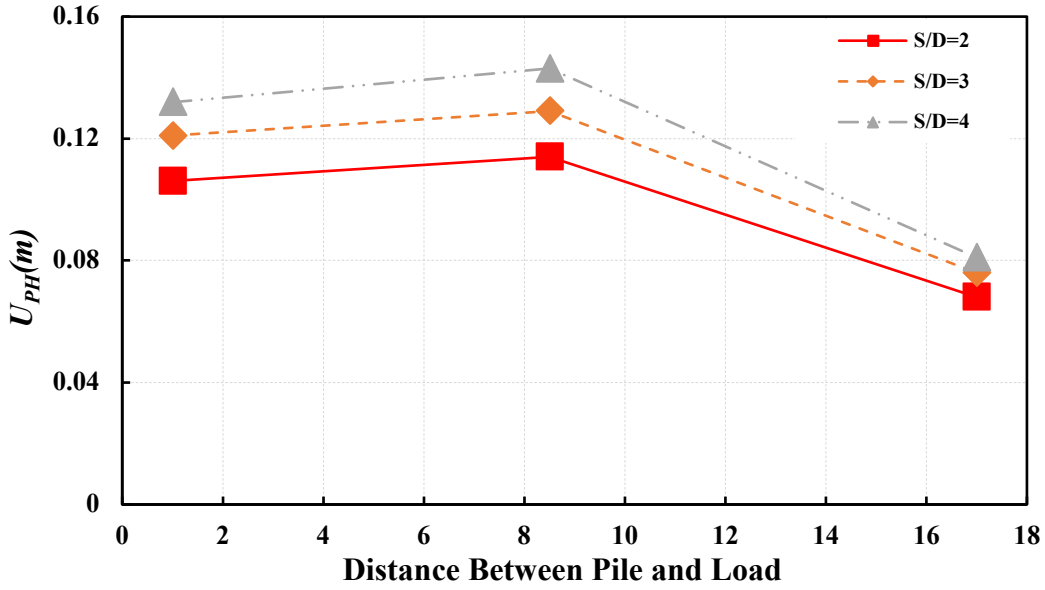


Figure 4.44. Pile position versus maximum U_{PH} of locally loaded pile-stabilized slope (full model cases, S_u=40 kPa, single row configurations, free pile head condition).

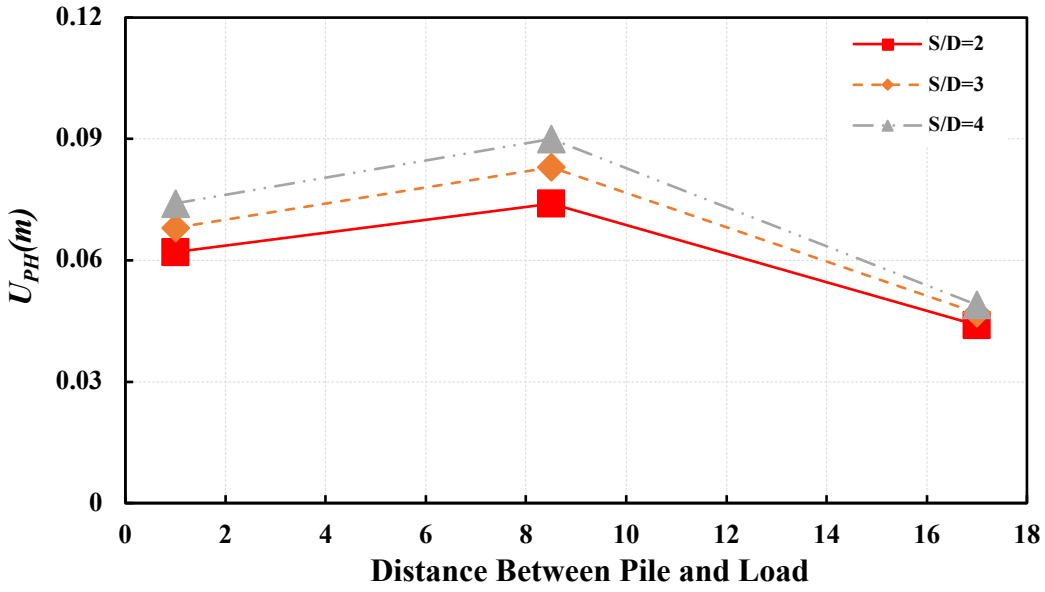


Figure 4.45. Pile position versus maximum U_{PH} of locally loaded pile-stabilized slope (full model cases, S_u=40 kPa, single row configuration, constrained pile head condition).

Figure 4.46 and Figure 4.47. present a comparison of U_{SC} values for three different pile group positions along the slope for free and constrained pile head conditions, respectively. Under both free pile head and constrained pile head condition, the position of pile groups influences U_{SC} values for all S/D ratio values considered. Figure 4.46 shows that the highest U_{SC} were consistently observed in the cases where piles were placed at the toe of the slope, indicating reduced stability of this case. In contrast, in the scenarios when piles were placed at the crest and in the middle of the slope U_{SC} values were comparable to each other. Figure 4.47 shows that, in constrained pile head condition, when piles are positioned at the crest of the slope, the U_{SC} is lowest, whereas placing them at the toe results in the highest U_{SC} observed.Specifically, under constrained head conditions, there is a distinct difference in U_{SC} values for piles positioned at the crest and middle of the slope, unlike the free pile head condition where these displacements were almost equal as shown in Figure 4.46.

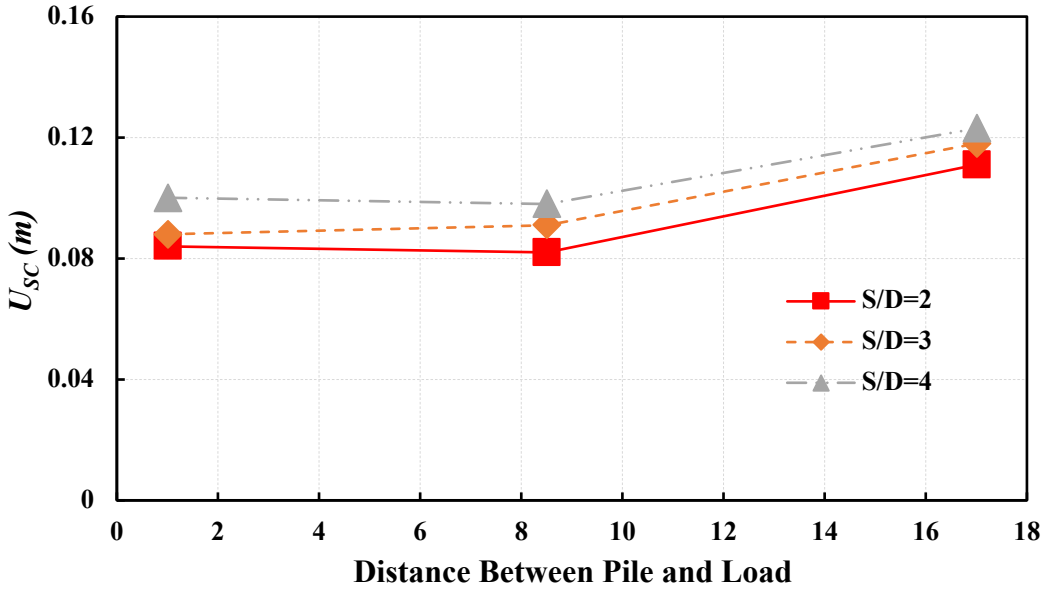


Figure 4.46. Pile position versus maximum U_{SC} of locally loaded pile-stabilized slope (full model cases, S_u=40 kPa, single row configurations, free pile head condition).

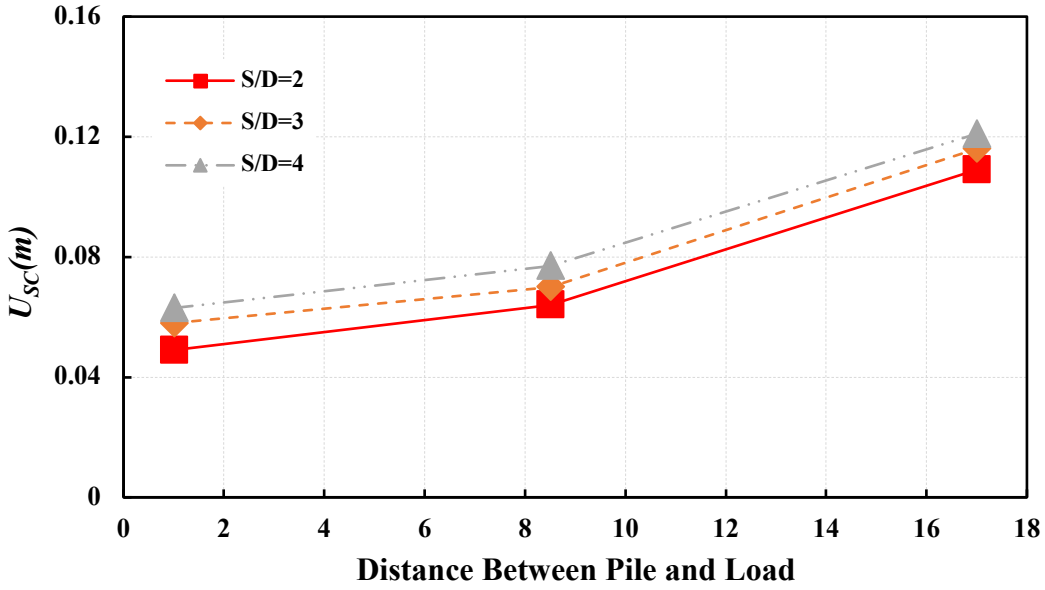


Figure 4.47. Pile position versus maximum U_{SC} of locally loaded pile-stabilized slope (full model cases, S_u=40 kPa, single row configurations, constrained pile head condition).

Figure 4.48 and Figure 4.49 present a comparison of U_{ST} values for different pile positions, considering free pile head condition and constrained pile head condition respectively. Figure 4.48 shows that the highest U_{ST} values were obtained in the cases where pile groups were placed at the toe of the slope and the lowest ones in cases where pile groups were installed at the crest of the slope. For constrained pile head conditions relatively higher U_{ST} values were achieved in the cases where piles were placed in the middle of the slope, and a clear trend between U_{ST} and pile group position could not be attained dissimilar to the free pile head condition (*see* Figure 4.48).

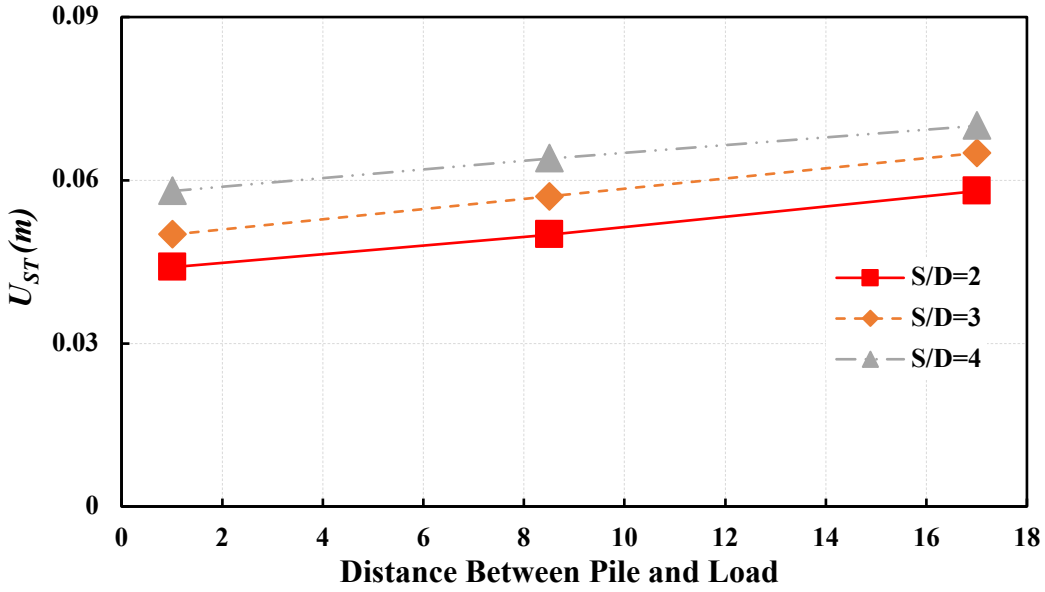


Figure 4.48. Pile position versus maximum U_{ST} of locally loaded pile-stabilized slope (full model cases, S_u=40 kPa, single row configurations, free pile head condition).

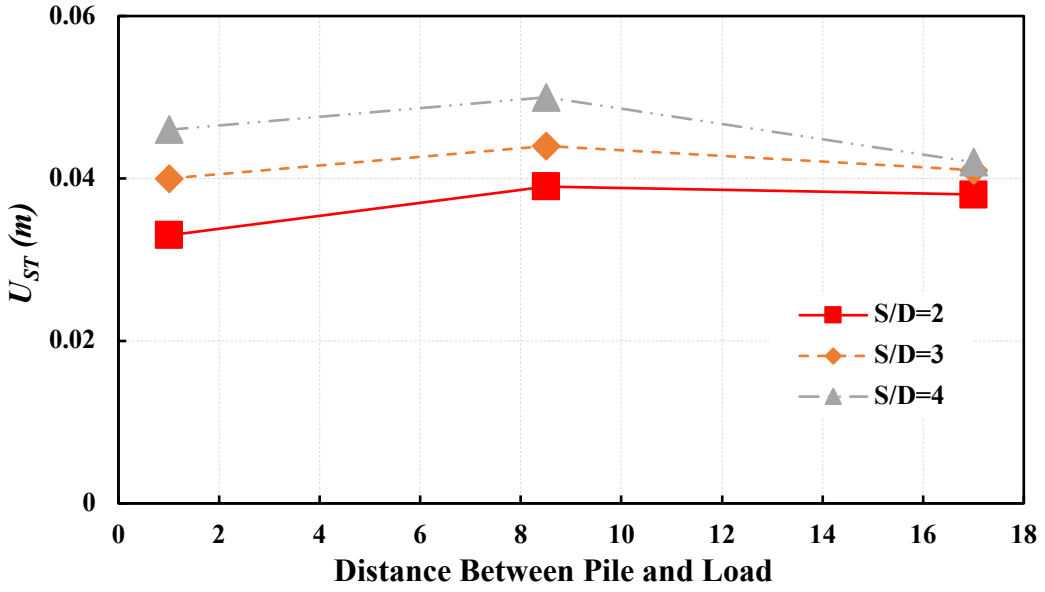
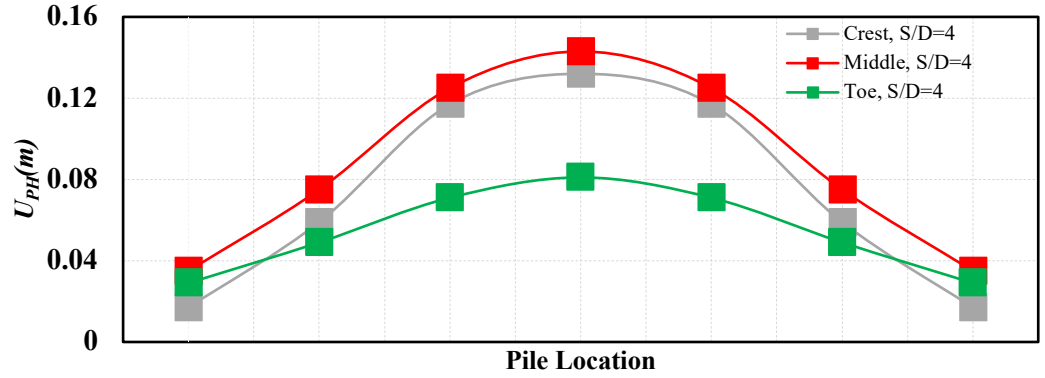
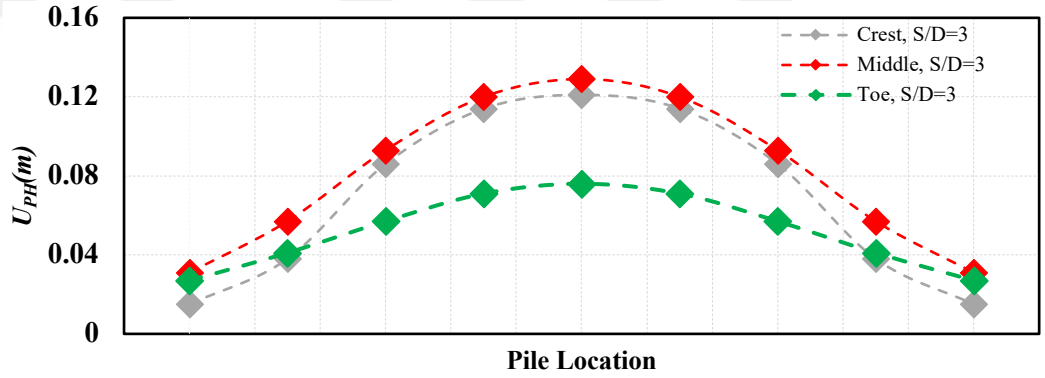


Figure 4.49. Pile position versus maximum U_{ST} of locally loaded pile-stabilized slope (full model cases, S_u=40 kPa, single row configurations, constrained pile head condition).

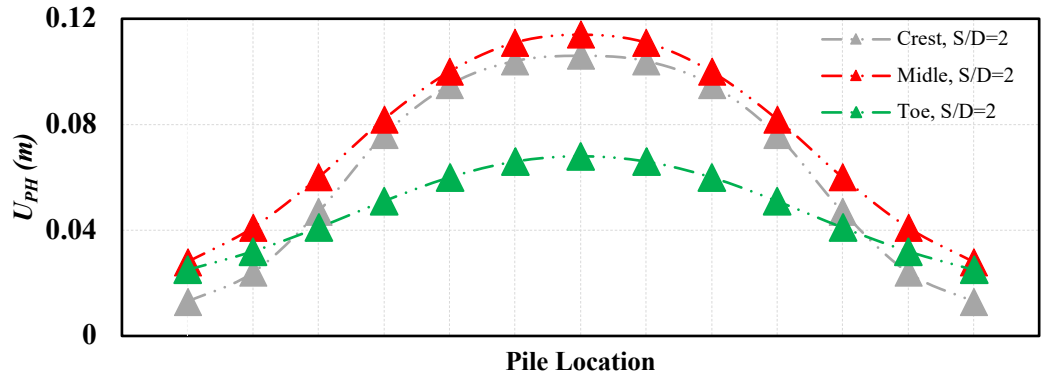
For the free pile head conditions, the effect of the pile group position on the U_{PH} distribution for S/D=2, S/D=3 and S/D=4 are shown in Figure 4.50a, Figure 4.50b, and Figure 4.50c, respectively. Regardless of the S/D ratio, U_{PH} values of the piles located at the central zone (that are located closer to the loading area) are higher than those of the outer piles located near the edges. There is a clear difference between U_{PH} of the outermost piles and the central piles for the pile groups located at the crest of the slope and in the middle of the slope. When piles are placed at the toe of the slope, U_{PH} is more evenly distributed. All these observations correspond to the free pile head condition. The effect of the pile group position on the U_{PH} distribution, in constrained pile head condition, for S/D=2, S/D=3, S/D=4 are shown in Figure 4.51a, Figure 4.51b and Figure 4.51c, respectively. Regardless of the S/D ratio and their distance from the central load zone of the slope, a consistent pattern emerges when a pile cap is placed: the U_{PH} of the piles located in the upper slope are consistently less than those placed in the middle portion.



(a)

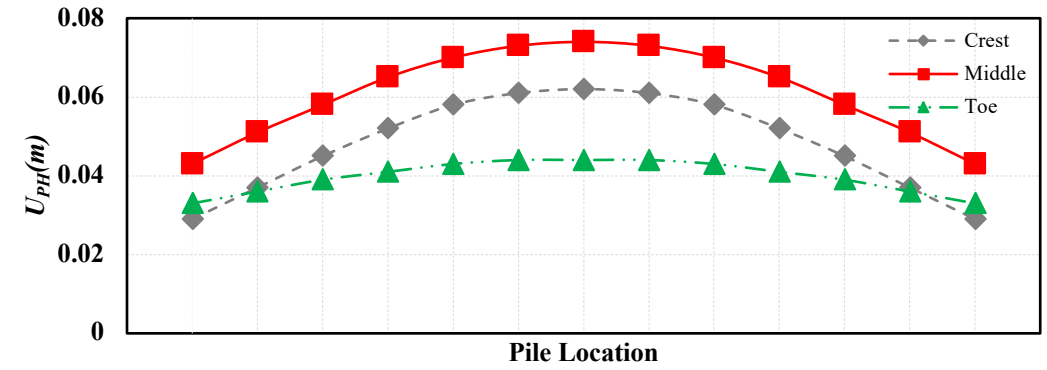


(b)

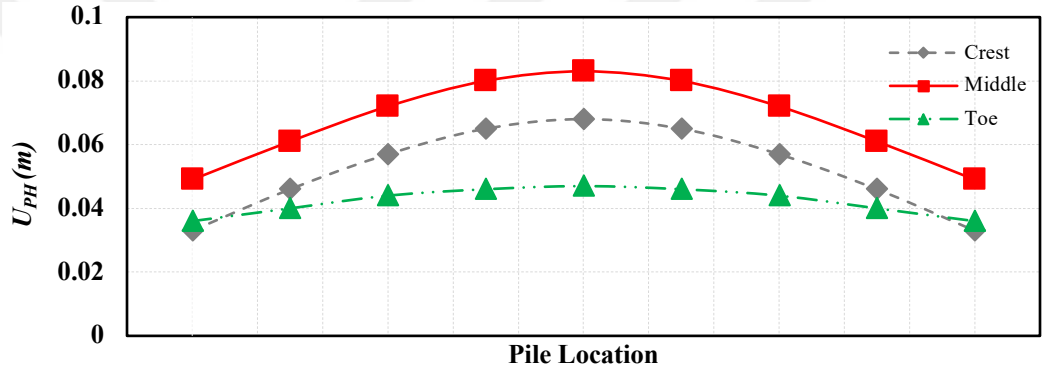


(c)

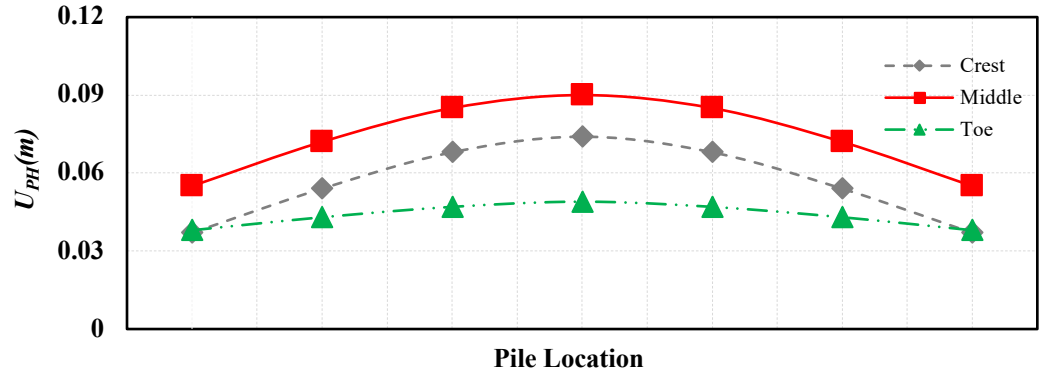
Figure 4.50. Pile location versus U_{PH} of locally loaded pile-stabilized slope (full model cases, S_u=40 kPa, single row configurations, free pile head condition) : (a) S/D=2 , (b) S/D=3, (c) S/D=4.



(a)



(b)



(c)

Figure 4.51. Pile location versus UP_H of locally loaded pile-stabilized slope (full model cases, S_u=40 kPa, single row configurations, constrained pile head condition) : (a) S/D=2 , (b) S/D=3, (c) S/D=4.

The Figure 4.52 show the influence of pile group position on the failure zone of the slope, for free pile head condition. Installing piles at the crest of the slope restricts the failure zone in the upper part of the slope, while placing the piles at the lower locations enlarges this critical failure zone, making it deeper and wider.

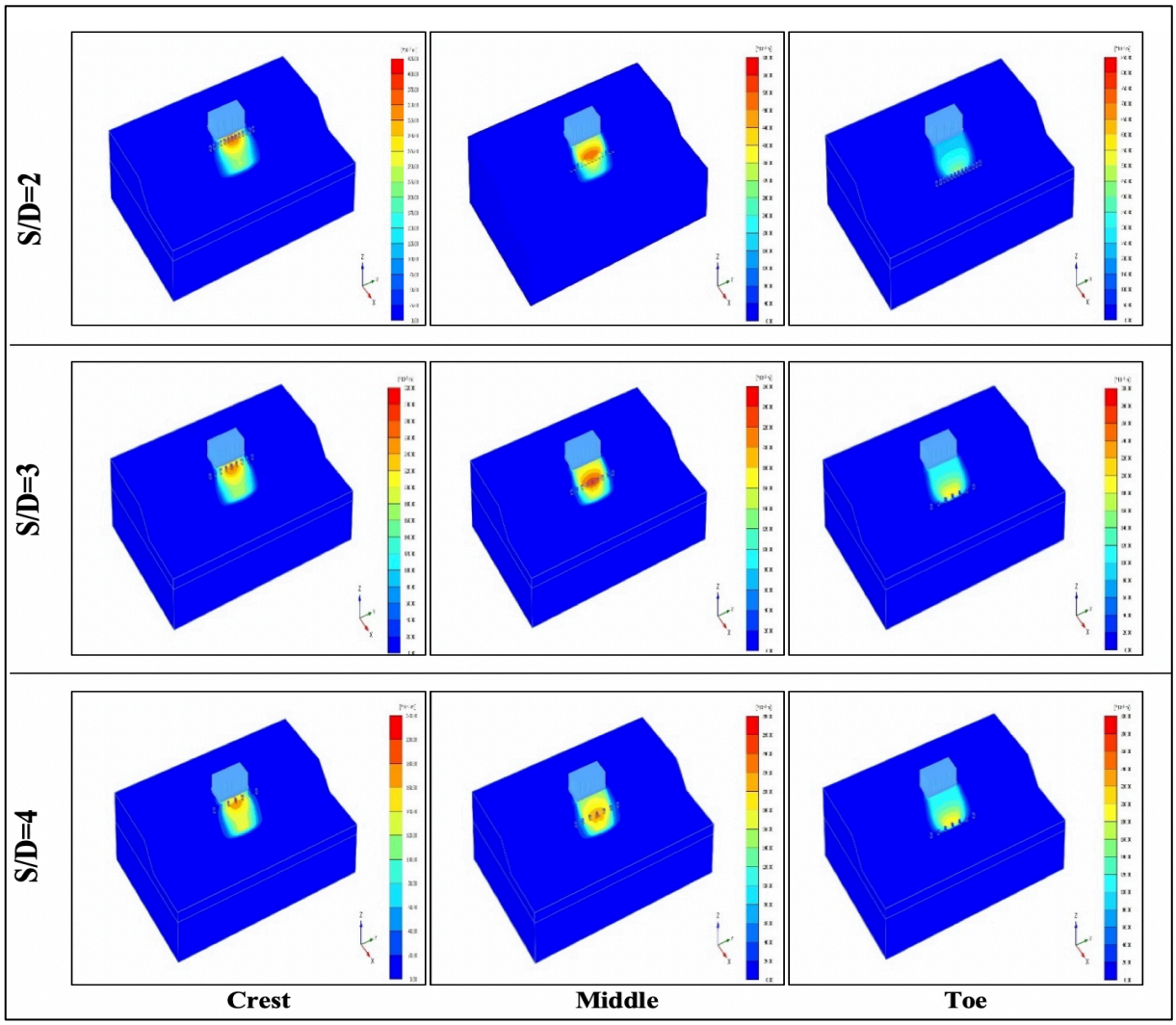


Figure 4.52. Effect of pile group position on the critical surface of locally loaded pile-stabilized slope, incremental displacements (full model cases, S_u=40 kPa single row configurations, free pile head condition).

4.4. Pile Cap Beam Placement

In this section, the effect of placement of the pile cap beam on the stability of the pile-stabilized slopes are discussed. Table 4.21 presents the maximum pile head displacements (U_{PH}) and maximum bending moment values before and after the installation of the pile cap for comparison purposes. For all of the cases analyzed, there is a clear reduction in U_{PH} after the placement of the pile cap. The U_{PH} values obtained for the pile groups with the pile cap is at the least 35% lower than the U_{PH} values obtained for the cases without the pile cap. The largest reductions in U_{PH} were observed in groups installed at the crest of the slope; in these groups, regardless of the S/D ratio and the number of rows, the reduction in displacement was more than 41%. In the case of a configuration in a single row, the highest reduction in U_{PH} was observed in groups with S/D = 3 and S/D = 4. As for the changes in the maximum pile bending moment, the pile cap placement caused similar reduction amounts in all of the cases analyzed. The placement of a pile cap reduced the maximum bending moments by 28%-35%. A clear trend between configuration components and % reduction in maximum bending moment and pile head displacements could not be attained.

Table 4.21. Maximum pile bending moment and pile head displacements of locally loaded pile-stabilized slopes.

S/D	Position	Number of Rows	Max Pile Head Displacement (mm)			Max Bending Moment (kNm)		
			Free Pile Head	Constrained Pile Head	% Decrease	Free Pile Head	Constrained Pile Head	% Decrease
2	Crest	1	10.6	6.2	42	3923	2646	33
3	Crest	1	12.1	6.8	44	4730	3283	31
4	Crest	1	13.2	7.4	44	5175	3704	28
2	Middle	1	11.4	7.4	35	3749	2514	33
3	Middle	1	12.9	8.3	36	4512	3080	32
4	Middle	1	14.3	9.0	37	4951	3408	31
2	Toe	1	6.8	4.4	35	1870	1253	33
3	Toe	1	7.6	4.7	38	2185	1441	34
4	Toe	1	8.1	4.9	40	2326	1512	35
3	Crest	2	10.3	6.1	41	3641	2542	30
3	Middle	2	11.3	7.4	35	3282	2258	31
3	Toe	2	11.4	7.4	35	3615	2386	34

Table 4.22 shows the changes in FS_{LPS} caused by installing a pile cap beam on the existing pile groups. The groups with the pile cap beam generally exhibits higher FS_{LPS}. However, a different scenario exists for the pile groups installed in the toe of the slope; as such installing the pile cap beam did not improve the stability of the slope . It is worth noting that this position of the piles was found to have a minimal stabilization effect prior to the placement of the cap beam, and hence, the expected additional benefit from installing the pile cap beam becomes negligible. The results indicate that cap beam placement was the most effective on the FS_{LPS} for groups in a single row installed at the crest of the slope, with an increase in FS_{LPS} ranging from 8% to 10%. It is worth noting the cardinal difference between the groups installed in the middle of the slope and those at the crest. In the groups installed in the middle of the slope, the increase in FS_{LPS} is only 2% for the group with a S/D = 2, while for S/D=3 and S/D= 4, the increase was 6%. In groups set in the middle of a slope, it can be said that the farther apart the piles are, the greater the effect of installing the pile cap beam will be. However, in the case where the piles are installed at the crest of the slope, an opposite effect is observed; as such the pile cap beam placement were more effective for piles placed closer.

Table 4.22. Results of the analyses performed on locally loaded pile-stabilized slopes (full model cases, S_u=40 kPa).

S/D	Position	Number of rows	Factor of Safety, FS_{LPS}		
			Free Pile Head	Constrained Pile Head	% Increase
2	Crest	1	1.314	1.446	10
3	Crest	1	1.248	1.368	10
4	Crest	1	1.213	1.314	8
2	Middle	1	1.292	1.32	2
3	Middle	1	1.228	1.303	6
4	Middle	1	1.191	1.265	6
2	Toe	1	1.110	1.110	0
3	Toe	1	1.100	1.100	0
4	Toe	1	1.100	1.100	0
3	Crest	2	1.352	1.452	7
3	Middle	2	1.330	1.401	5
3	Toe	2	1.213	1.230	1

Figure 4.53 shows differences in pile bending moment distribution for constrained and free pile head conditions. Installing the pile cap, causes a shift in the bending moment diagram of the pile. The zone of large bending moment values decreases, and greater loading takes place in the upper part of the pile. In other words, there is a redistribution of the load on the pile. A similar phenomenon was observed when comparing the internal forces of piles installed in the middle and crest of the slope. Analyzing these data, one can make the following comment: with the achievement of a more equal distribution of internal forces along the piles that stabilize slopes , the *FS* of the pile-slope system also increases. What makes this unique is the fact that this improvement in stability can occur without increasing the number of piles, but changing other configuration factors.

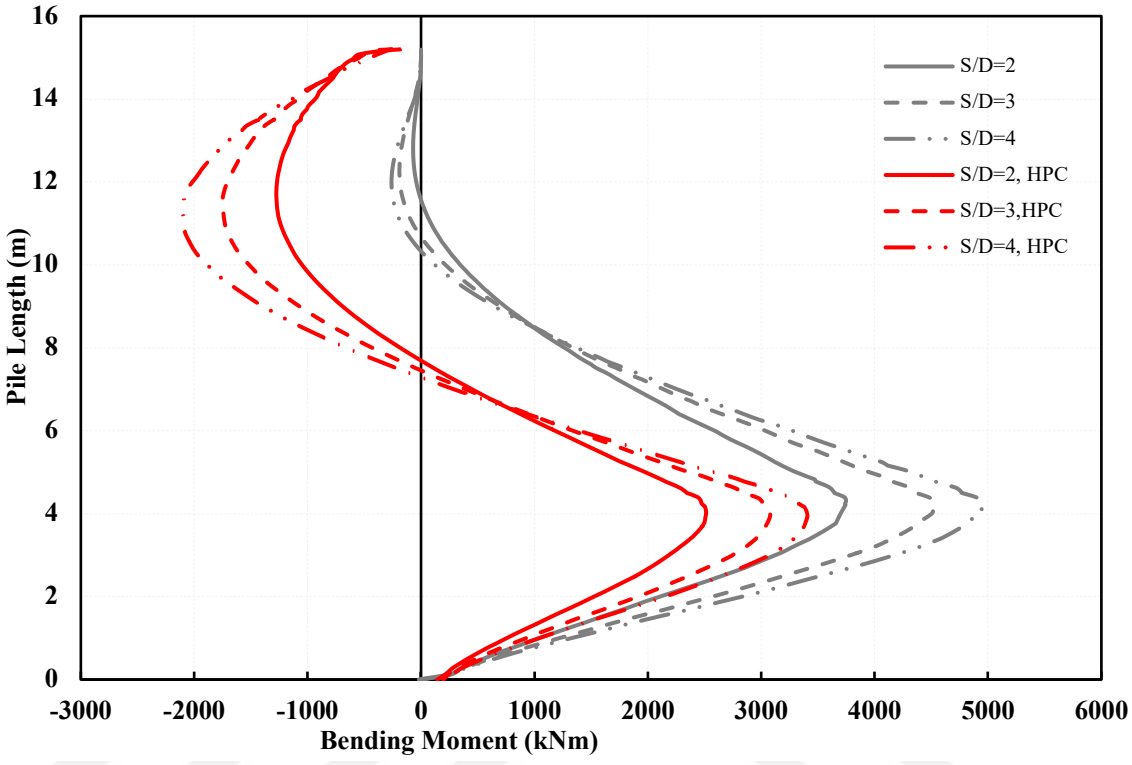
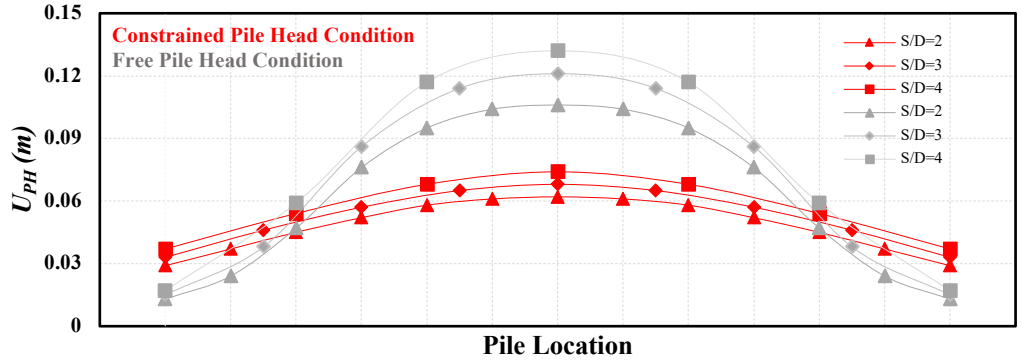
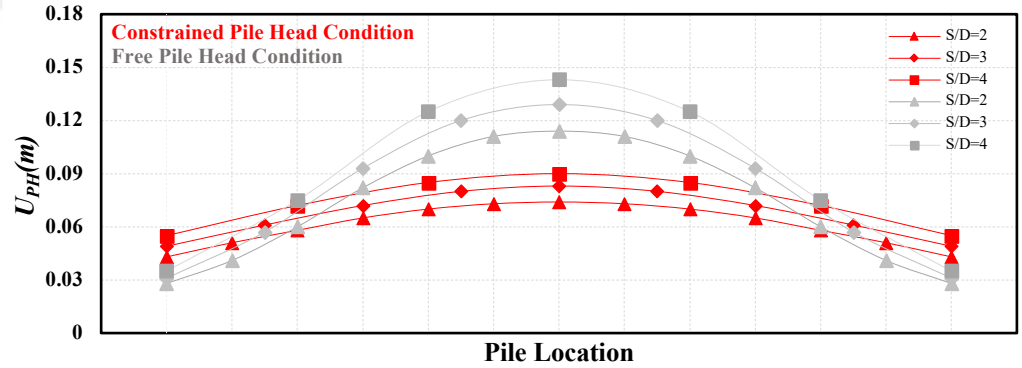


Figure 4.53. Pile bending moment diagram versus pile length for locally loaded pile-stabilized slope case (full model cases, S_u=40 kPa, single row configurations).

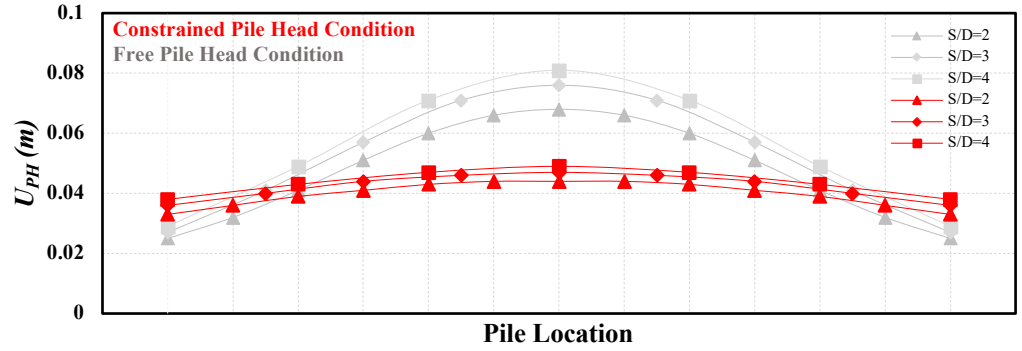
The installation of the pile cap also had a positive effect on the distribution of pile head displacements. Figure 4.54 shows a comparison of U_{PH} with and without the installation of the pile cap beam. From the graphs, it can be seen that the displacements in the central part were significantly reduced by the pile cap, in the zone where surcharge load is applied. However, when viewing the outermost piles, it can be seen that the U_{PH} of these piles increased. This indicates that achieving a uniform distribution of *UPH* (minimizing the difference between the largest and smallest U_{PH} values among the pile group) is preferable and it positively affectes the stabilization of the locally loaded slope. The main contribution of the pile cap beam was to mobilize the outermost piles in stabilization, as a consequence of this an even distribution of U_{PH} was observed among the piles in the front row.



(a)



(b)



(c)

Figure 4.54. Pile location versus U_{PH} of locally loaded pile-stabilized slope (full model cases, S_u=40 kPa, single row configurations): (a) crest, (b) middle, (c) toe.

4.5. Effectiveness of Pile Groups in Slope Stabilization

4.5.1. Slice Model Cases

The *FS* values obtained from the analysis of the natural pile-stabilized slope cases considering various pile group configuration (single row, staggered and double row) are presented in Table 4.23. for S_u=40 kPa. To be able to quantify the efficiency of these pile group configurations pile row length should also be determined. For this reason , reference pile row length of 180 meters was considered for this comparison. The cases were designed to have an approximately equal number of piles to better analyze the differences in FS_{0_PS} values obtained for various configurations investigated in this study: single row, staggered, and double row. Figure 4.55 illustrates the relationship between the number of piles and FS_{0_PS} for S_u=40 kPa. Figure 4.55 clearly demonstrates the superior performance of the staggered configuration. With a lower number of piles, the staggered configuration achieves higher FS_{0_PS} values. In other words, with a larger S/D ratio, the staggered configuration outperforms both the double row and single row configurations in terms of FS_{0_PS} values. Additionally, when comparing the single row and double row configurations, the double row configuration shows a distinct advantage.

Table 4.23. Results of the safety analysis performed on natural pile-stabilized slopes (slice model cases, S_u=40 kPa).

Number of Rows/ Staggered	S/D	Number of piles	FS_{0_PS}
Single Row	1.33	91	2.07
Staggered	2.67	91	2.16
Double Row	2.67	91	2.17
Single Row	1.67	73	2.05
Staggered	3.33	73	2.12
Double Row	3.33	73	2.10
Single Row	2.00	61	2.02
Staggered	4.00	61	2.07
Double Row	4.00	61	2.04

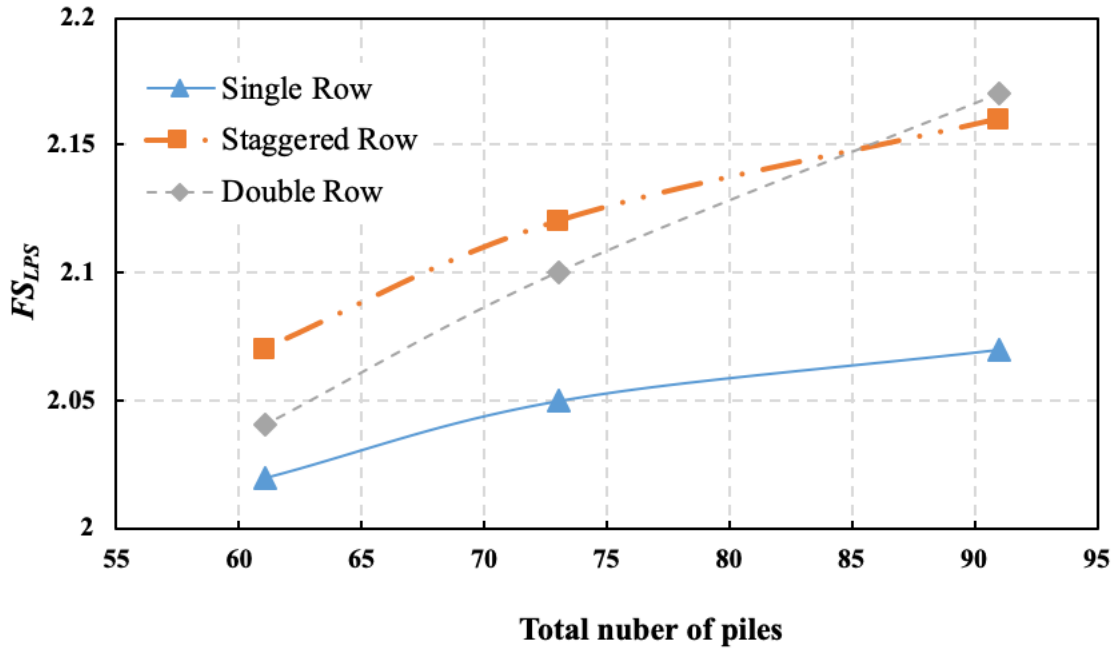


Figure 4.55. Number of piles versus FS_{0_PS}.

4.5.2. Full Model Cases

For a better understanding of the influence of configuration components such as S/D ratio, pile group position, number of rows and pile cap beam placement effect on locally loaded slopes, all FS_{LPS} values were plot in Figure 4.56, in which the y-axis on the graph represents FS_{LPS}, while the x-axis represents the configuration case number investigated (*see* Figure 3.17 and Figure 3.18 to see all configurations together). In Figure 4.57 the x-axis represents the number of piles in group and y-axis on the graph again represents FS_{LPS}. Figure 4.56 clearly indicates that different FS_{LPS} values can be achieved, by using the same number of piles. This observation primarily shows the influence of the pile group position and the placement of the pile cap beam on the pile group. The graph illustrates how varying the position of the pile group along the slope and placement of the pile cap beam with an identical number of piles yields markedly different outcomes. The second observation is that FS_{LPS} obtained with the efficient configurations with fewer piles, can easily exceed the FS_{LPS} obtained for other configurations that incorporate a greater number of piles. For further evaluation of configuration efficiency, it

is necessary to determine the required stability level of the slope, in other words, defining how much increase is required in FS_{LPS} becomes important. Once the level of required stability improvement is determined, then it is possible to identify the most effective configurations based on the target FS_{LPS}, by minimizing the number and length of piles to reduce the material cost.

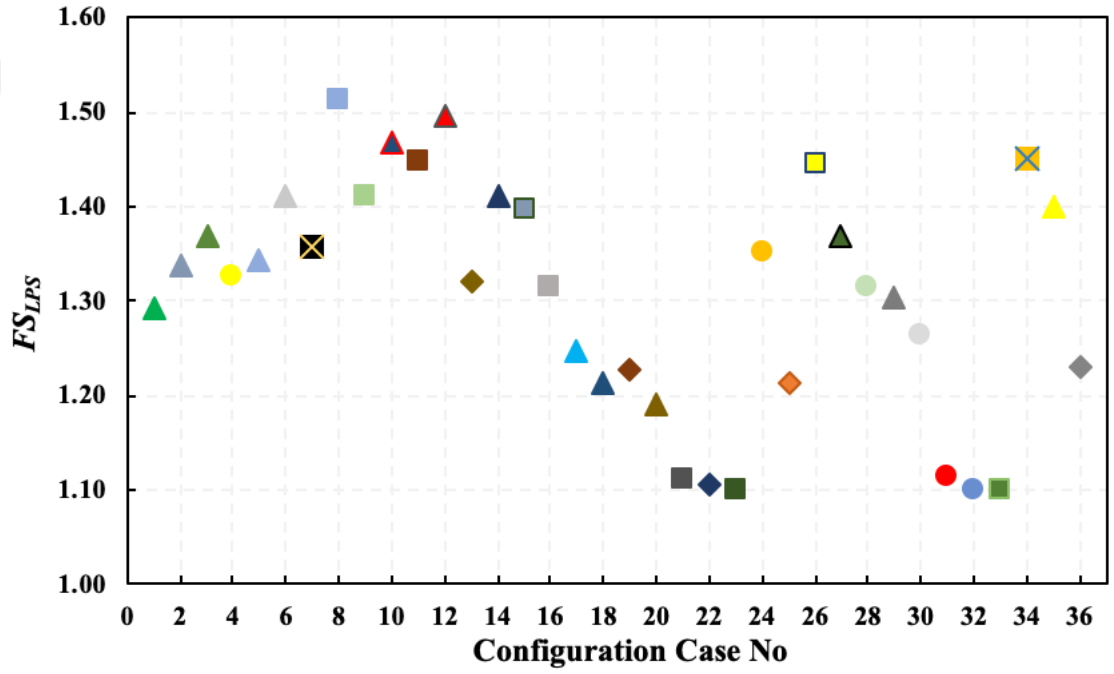


Figure 4.56. Pile configuration case number versus FS_{LPS}.

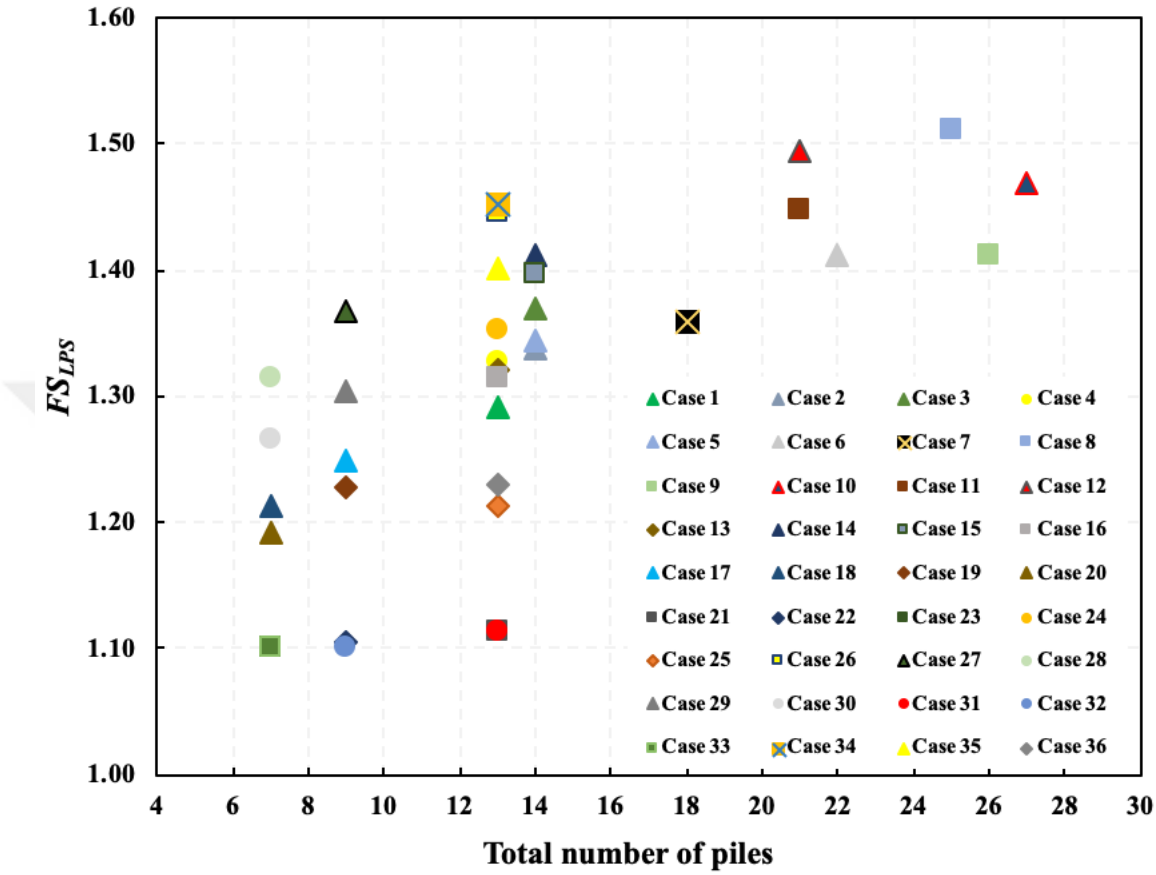
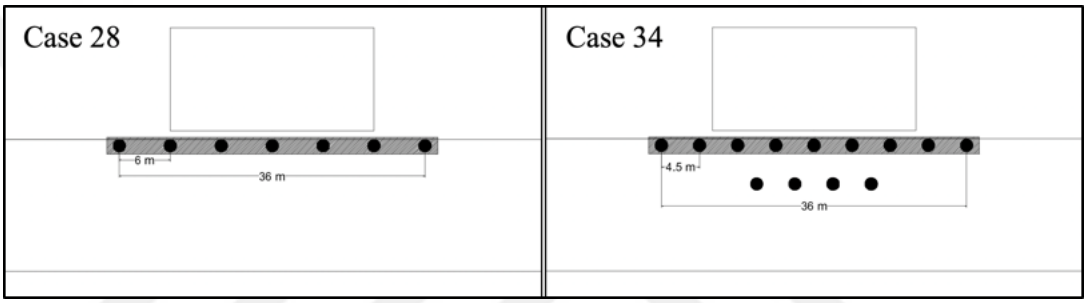


Figure 4.57. Total number of piles in pile group versus FS_{LPS}.

For a target short-term FS_{LPS} between 1.3 and 1.4, it can be clearly established that the pile cap beam has a greater influence on stabilization than other factors. It is possible to achieve higher FS_{LPS} with fewer piles, once a pile cap beam is installed. Under limited conditions, such as the absence of material for slope stabilization, the combined use of the pile cap beam and the installation of piles at the crest of the slope (*i.e.*, Cases 26, 27, 28, 34) proves to be the most effective method for stabilizing the locally loaded slope. Plan views of Cases 26, 27, 28, 34 is shown in Figure 4.58.



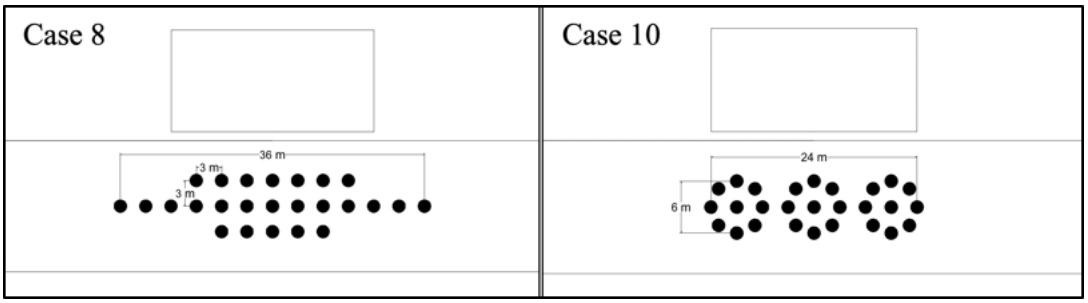
(a)



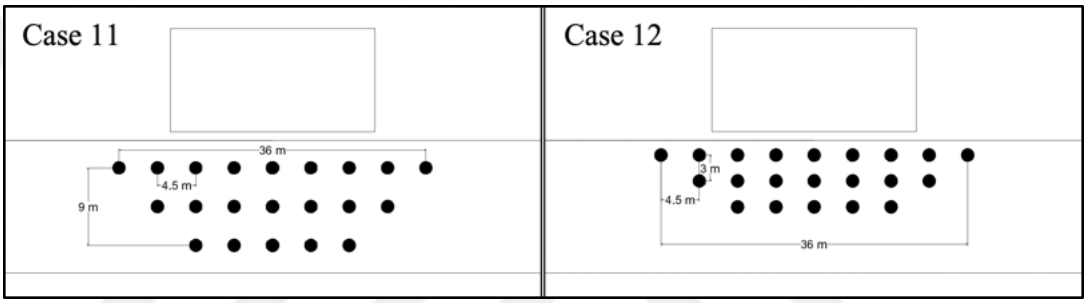
(b)

Figure 4.58. Plan views of configurations: (a) Cases 26 and 27, (b) Cases 28 and 34.

Generally, the configurations in three rows (*i.e.*, Cases 8, 10, 11, 12) provided the highest FS_{LPS} among the investigated configurations. Since these configurations do not include a pile cap beam, by analyzing the results of these models, we can assess the influence of the S/D ratio and the position of the configuration along the slope. Based on the results, the configurations installed in the upper part of the slope with a larger S/D ratio (*e.g.*, Case 12) is more effective than the configurations installed in the middle of the slope but with a smaller S/D ratio (*e.g.*, Case 8). Reason for this statement is that in the case with higher S/D ratio total number of piles is lower. Plan views of Cases 8, 10, 11, 12 is shown in Figure 4.59.



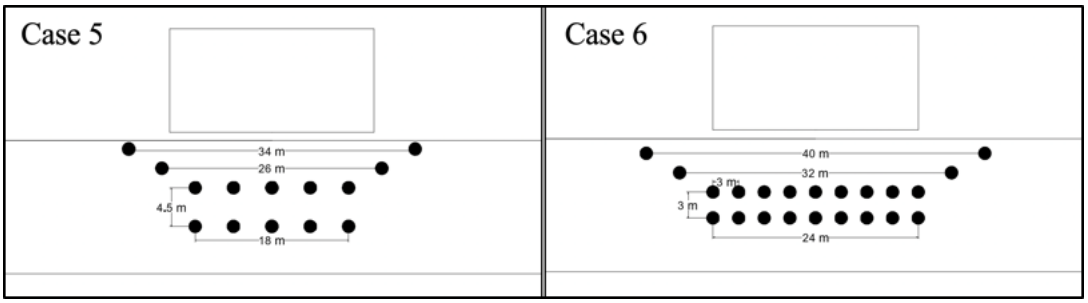
(a)



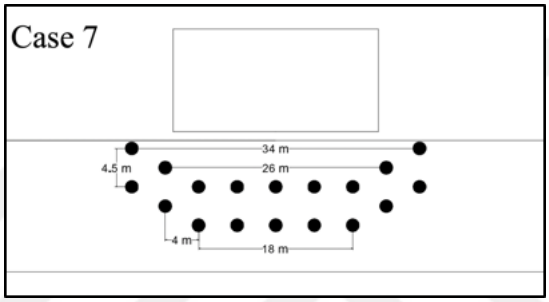
(b)

Figure 4.59. Plan views of configurations: (a) Cases 8 and 10, (b) Cases 11 and 12.

It is also worth noting the degree of influence of certain additional aspects of the configuration. As shown in Figure 4.60 which presents the plan views of Cases 5, 6, 7, one of these aspects is the placement of the outermost piles. The analysis results showed that the placement of the outermost piles has a minimal effect on the FS_{LPS} as such it remains the same, regardless of their placement is inclined (*i.e.*, Case 5, 6, 7) or paralel to the loading. The second aspect is for the unique configuration where the piles were arranged in the shape of three circles, with one pile placed in the center of each circle (*e.g*, Case 10). The analysis results showed that the circular arrangement of the piles did not offer a specific advantage on slope stabilization.



(a)



(b)

Figure 4.60. Plan views of configurations: (a) Cases 5 and 6, (b) Case 7.

To determine the most efficient pile group arrangements that uses the lowest number of piles and pile materials, three efficiency coefficients were derived in this study. The first efficiency factor is E1, that represents the ratio of the *FS* increase after attained by the installation of the pile group with respect to the original *FS* of the locally loaded unstabilized slope to the number of piles. Formula for this coefficient can be expressed as

$$E1 = \frac{(FS_{LPS} - FS)}{Pile\ Number}. \tag{4.3}$$

Figure 4.61 shows configuration case numbers versus values of E1. The graph can be investigated and explained by dividing it into the three main regions. Configurations with efficiency coefficients lower than 0.015 remained in the first region. All of these are installed at the toe of the slope, efficiency was not increased in the cases of this group due to the installation of the pile cap beam. The second region of the graph is defined for the cases with E1 values in the 0.015 to 0.025 range. The main feature of these configurations is that they are installed in the middle of the slope and they use greater number of piles. In configurations where a greater

number of piles were used, high FS_{LPS} values were obtained. However, these solutions were not the most efficient configurations because the number of piles averaged more than 20. The most efficient configurations obtained using E1 turned out to be those installed in the crest of the slope and especially those installed with the pile cap beam. These configurations were determined to be in the third group. The results indicate that installing the piles at the toe of the slope does not contribute to slope stabilization as much as the configurations in which the piles were placed in the middle or at the crest of the slope do.

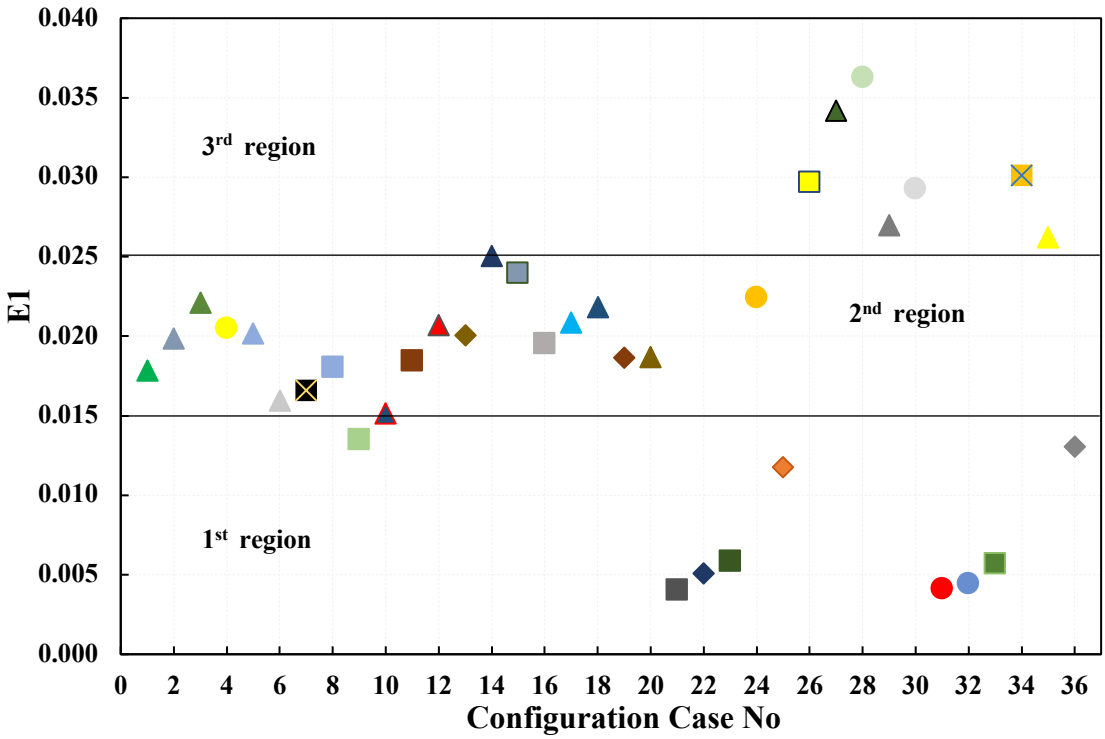


Figure 4.61. Pile configuration case number versus E1.

The displacement of the pile head is also crucial to optimize slope stabilization with piles, as it affects the load transfer, structural integrity, ease of operation and the design efficiency. Proper displacement control ensures effective load distribution, improves the interaction between piles and the soil and prevents local failures and structural damage. Minimizing displacement preserves the usability of the slope and its stability, and also ensures that the piles do not exceed their capacity, preventing structural failure. This contributes to the economic

efficiency by optimizing the number, length and diameter of piles, reducing the use of materials and overall project costs. Continuous monitoring and analysis of the pile head displacement allows potential problems to be identified in advance and facilitates the development of adaptive management strategies, ensuring timely maintenance and adjustment. To meet these needs, another efficiency coefficientfactor, E2 was defined to evaluate the stabilized slopes based on the number of piles used in this group and the pile head displacement (U_{PH}). This coefficient factor is referred to as E2 that. In it, the product of the number of piles and the maximum U_{PH} is divided by one, the formula of this coefficient can be expressed as

$$E2 = \frac{1}{Number\ of\ piles \times U_{PH}}. \tag{4.4}$$

Figure 4.62 shows the variation of E2, in which y coordinate represents E2, and the X coordinate represents the FS_{LPS}. Due to the nature of this efficiency formula, pile groups with a low number of piles and high displacement values have the highest coefficients. The graph was divied in to four regions, first region indicates the most efficient configuratiıns. The common features of the pile groups in this most efficient first region are that they are installed at the crest of the slope, and in all these groups, a pile cap was used.

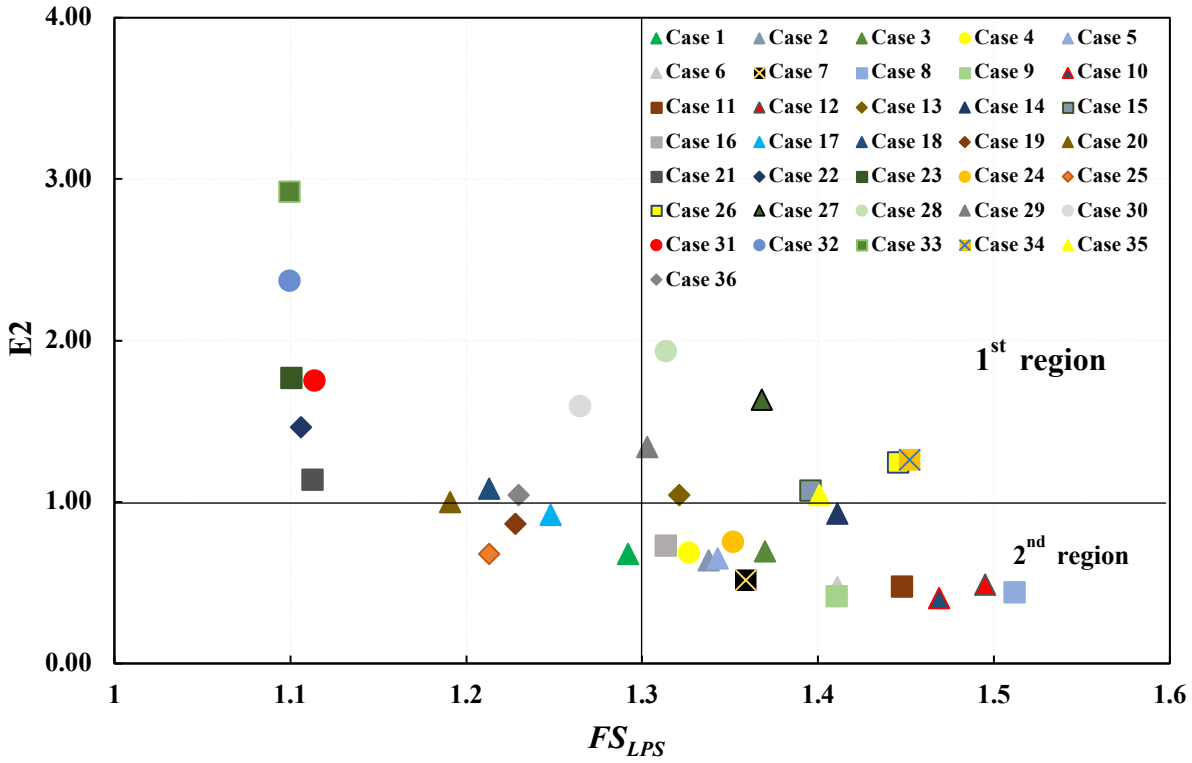


Figure 4.62. FS_{LPS} versus E2 coefficient.

The volume of piles (the number and length in the case of considering a fixed diameter) directly influences costs more than the number of piles as the total pile volume correlates with the material expenses in slope stabilization. Finding more efficient configurations to reduce the total volume used is crucial for minimizing costs while maintaining stability. All FS_{LPS} values were plot in Figure 4.63, in which the y-axis on the graph represents FS_{LPS} values, while the x-axis represents the total volume of concrete used for piles in each configuration. Figure 4.63 shows a relatively direct correlation between total volume of concrete used and FS_{LPS} values, where configurations with higher total volume of concrete, and hence those provide higher slope reinformement yield higher FS_{LPS} for most cases considered. at the exception to this is the pile configurations with pile groups placed at the toe of the slope (*i.e.*, Case 21, 22, 23, 31, 32, 33), they do not follow this trend, and provide lower FS_{LPS}. As discussed previously, this is because this pile positioning can not contribute to the stability regardless of the amount of reinforcing elements in the slope. Pile groups placed at the crest of the slope with constrained pile head

condition gave a higher FS_{LPS} values than configurations designed in double row with low S/D ratio (*i.e.*, Case 6, 9). Overall, Figure 4.63 shows the advantages of higher number of rows in pile group and pile cap beam placement on pile groups located at the crest and disadvangtage of placing piles at the toe of the slope. Plan view of Cases 21-23 and 31-33 is shown in Figure 4.64.

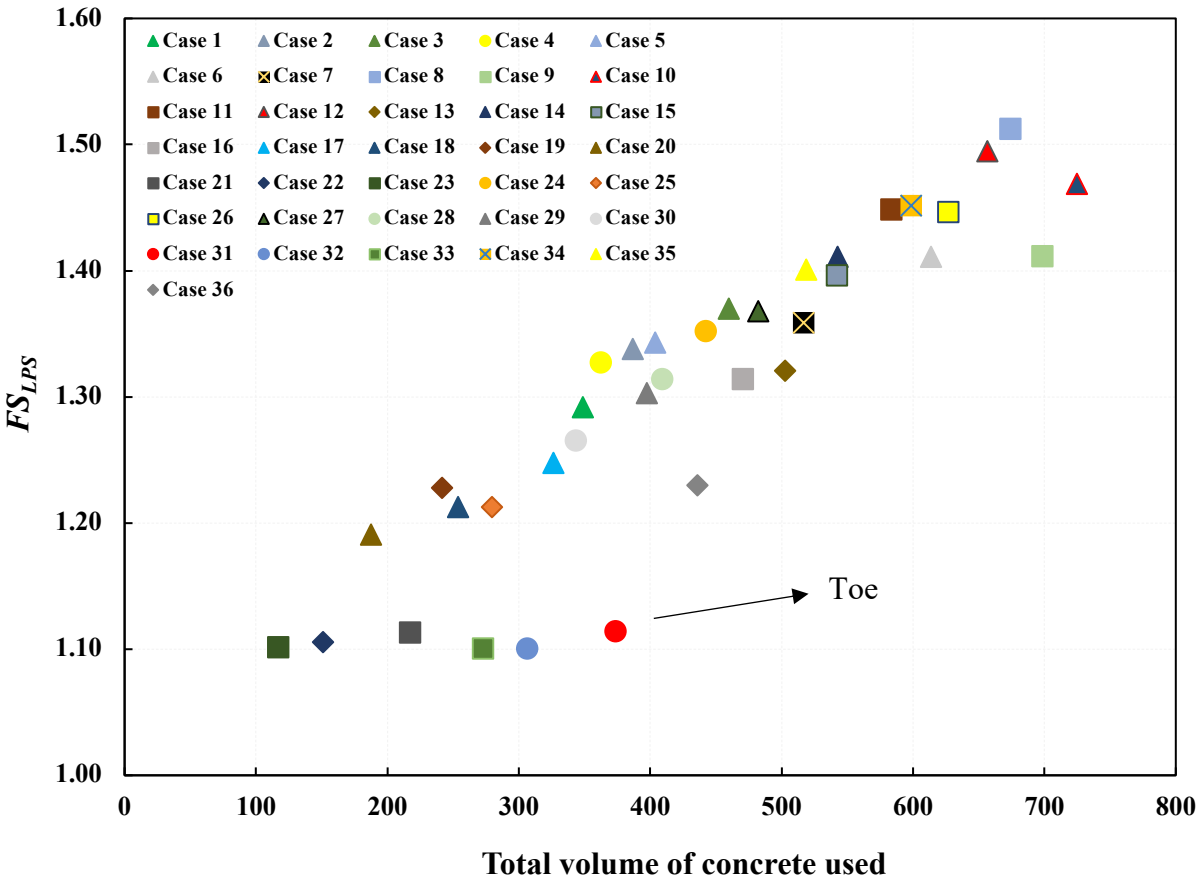
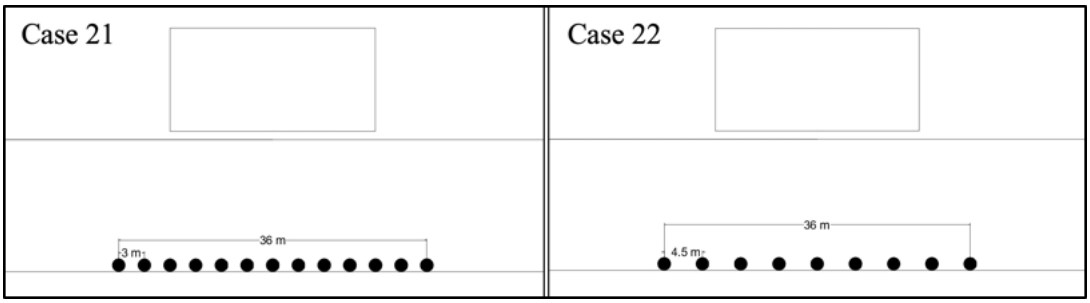
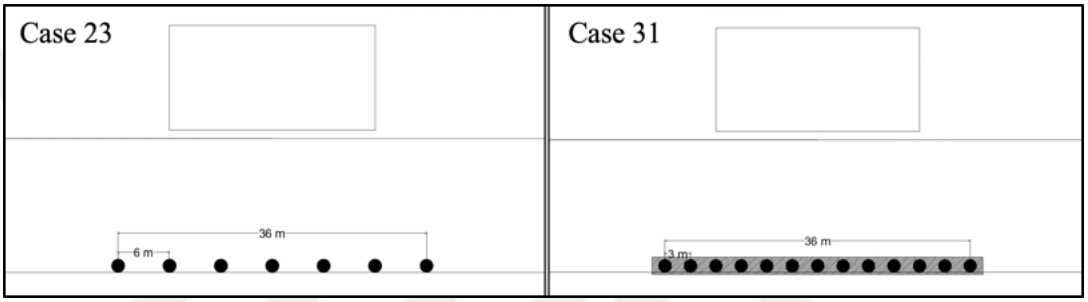


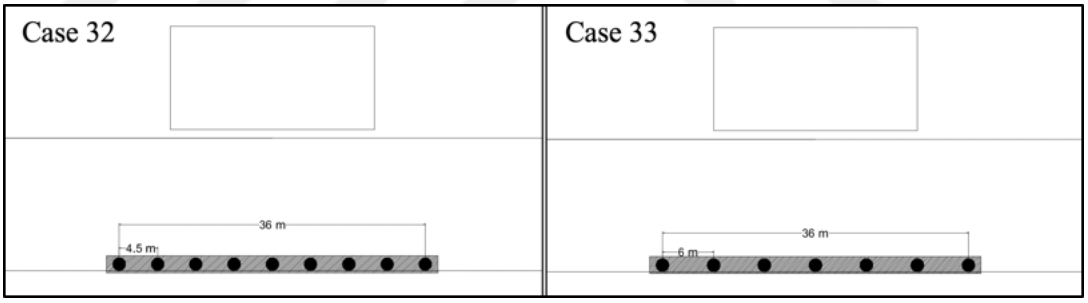
Figure 4.63. Total volume of concrete used versus FS_{LPS}.



(a)



(b)



(c)

Figure 4.64. Plan view of configurations: (a) Cases 21 and 22, (b) Cases 23 and 32, (c) Cases 32 and 33.

The third efficiency factor is E3, was developed to consider the total amount of concrete volume used. E3 represents the ratio of the *FS* increase (attained by the installation of the pile group with respect to the original *FS* of the locally loaded unstabilized slope) to standart volume of concrete (V_S) . The formula of V_S is written as

$$V_S = \frac{Total\ volume\ of\ concrete}{100}. \tag{4.5}$$

Formula of third efficiency factor E3 coefficient can be expressed as

$$E3 = \frac{(FS_{LPS} - FS)}{V_S}. \tag{4.6}$$

Figure 4.65 shows configuration case number versus values of E3. Figure 4.65 indicates that pile groups placed at the toe show low efficiency. Pile groups designed in single row and placed in the middle of the slope without pile cap beam shows relatively high efficiency compared to the piles placed at the crest without pile cap beam. This is an interesting finding that could be attained after defining E3, that seems to be a better representation of efficiency compared with E1 and E2. It is also important to note that when a pile cap beam is placed on them, the configurations with piles located at the crest of the slope outperform the cases placed in the middle of the slope in terms of efficiency. The results highlighthe the effectiveness of of placing pile cap beam especially when the pile groups are located at the crest of the slope.

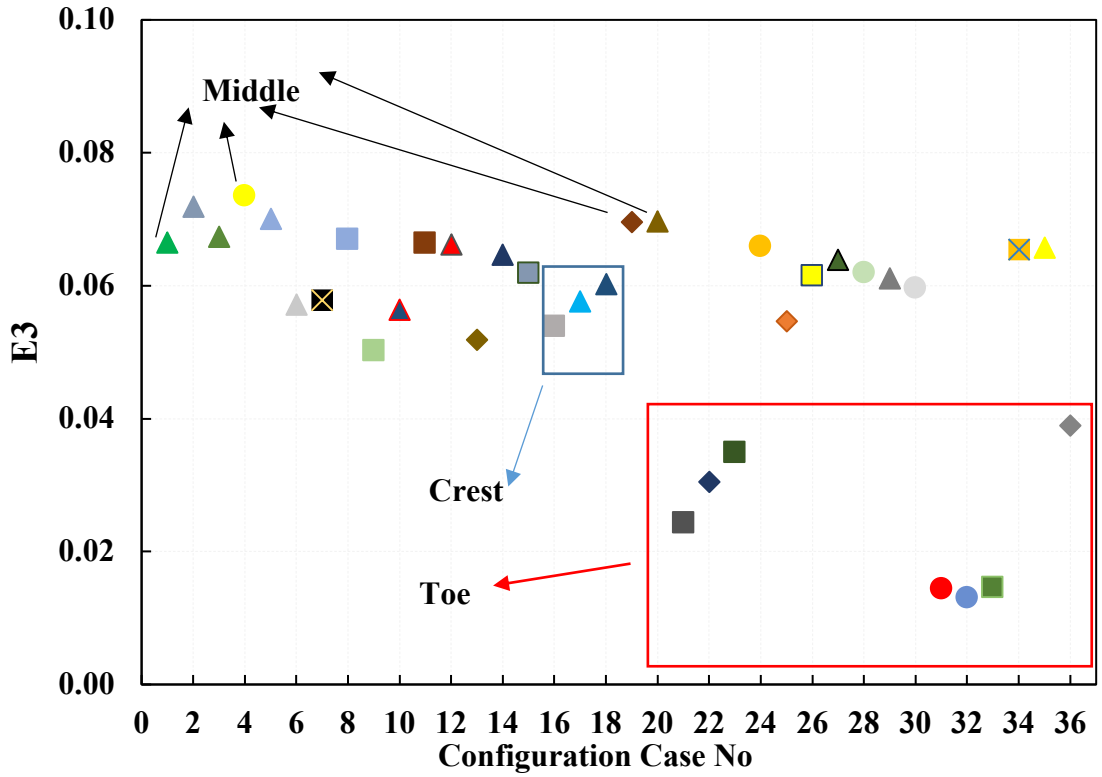


Figure 4.65. Pile configuration case number versus E3.

5. CONCLUSIONS

In this study, the influence of pile group configuration on the stability of the slope, pile internal forces, slope displacements, and pile head displacements was examined. The main goal and novelty of the study was to determine the most efficient pile group configurations. The study was limited to stabilization of clayey slopes underlain by a sand layer, as such the piles were socketed in this layer. Therefore, the effects of the pile spacing to pile diameter ratio (S/D= 1.33 to 4 range), the number of rows (n = 1, 2, and 3), the position of the pile group along the slope (crest, middle, toe), and the pile head conditions (free pile head and constrained pile head using a pile cap beam) were analyzed for natural (no surcharge), continuously loaded and locally loaded slopes. Based on the results from the 3D FEM analysis of pile-stabilized slopes using both slice and full models, the several conclusions were drawn.

- Reducing the S/D ratio has a positive impact on the stabilization of both natural (no surcharge) and loaded (locally and continuously) slopes. In natural pile- stabilized slopes as undrained shear strength (S_u) value decreases, the reduction of S/D ratio becomes a more important factor than the number of rows in the group. In other words, these results indicate that bringing the piles closer to each other offers a better solution for stabilizing natural slopes with relatively low S_u as it inhibits the soil flow between the piles.
- When the S/D ratio increases, the failure zone of the locally loaded pile-stabilized slope enlarges.
- The outermost pile head displacement (U_{PH}) values were almost equal for various S/D ratios in locally loaded pile-stabilized slope, the influence of the S/D ratio was only observed just beneath the surcharge load application zone. This implies that in the design of pile groups, to increase the factor of safety of the locally loaded slopes (FS_{LPS}) having lower S/D ratios just near the loading zone is sufficient.
- In locally lodaded slopes, as S/D ratio increases FS_{LPS} decreases almost linearly with a similar trend for the cases incorporating piles with free head conditions are placed at the crest and the middle of the slope.

- In locally lodaded slopes, the influence of the S/D ratio on FS_{LPS} is most significant for piles with constrained pile head conditions placed at the crest of a slope. This impact significantly decreases when the piles with constrained head are positioned in the middle of the slope.
- Regrardless of the pile head condition, the effect of S/D ratio is negligible when the piles are located at the toe of the slope.
- For all slope cases investigated (natural, continuously loaded and locally loaded), the number of rows in the pile group configuration is one of the main factors influencing the increase in factor of safety (*FS*) of the slope. For continuously loaded and locally loaded slopes, the number of rows becomes the most important parameter affecting the stabilization of the slope. Following from this fact, for stabilizing continuously loaded slopes increasing the number of rows in the configuration seems to be a more efficient solution.
- For locally loaded slopes, keeping the same number of piles, installing piles in a double row fashion provides greater FS_{LPS} than the one obtained by placing them in a single row as long as the reinforcement length of piles in the plan view cover the zone of influence of the local surcharge load.
- For natural pile-stabilized slopes, the position of the pile group along the slope (crest, middle and toe of the slope) affects the slope stabilization significantly. For all pile positions along the slope, improvements in FS_{0_PS} was observed.
- For continuously loaded and locally loaded pile-stabilized slopes, almost no changes were observed in FS_{CL_PS} and FS_{LPS} values indicating toe pile position should not be selected for the stabilization loaded clayey slopes underlain by sand.
- Placing piles at the crest of the slope yields the highest $FS_{0_PS,}$ FS_{CL_PS} and FS_{LPS} values for natural, continuously loaded and loaded slopes, indicating it is possible to achieve higher *FS* values only by changing the positioning of them along the slope, without changing the number piles.
- Installing piles at the crest of the slope restricts the failure zone of the locally loaded pile-stabilized slopes in the upper part of the slope, while placing piles at the middle or toe of the slope progressively enlarges this failure zone by making it deeper and wider.

- In the locally loaded slopes for groups installed at the toe of the slope provided the lowest FS_{LPS} values, reducing the S/D ratio and installing a pile cap beam on the pile group did not also affect the FS_{LPS}.
- The installation of a pile cap beam positively affects the stabilization of the locally loaded slope, while the number of piles remains unchanged. Installing the pile cap beam in configurations located at the crest of the slope provides a greater increase of FS_{LPS} compared to installing it on configurations placed in the middle of the slope.
- For locally loaded slopes, for all pile group positions along the slope (crest, middle, toe), installation of the pile cap beam made the U_{PH} distribution more even by mobilizing the outermost piles. The S/D ratio and the number of rows do not affect the overall trend /distribution of U_{PH} .
- For locally loaded slopes pile cap beam placement is more effectiveon increasing the FS_{LPS} in cases of pile groups with higher S/D ratios when they are placed in the middle of the slope. Conversely, for pile groups placed at the crest of the slope, the effect of pile cap beam placement is more pronounced for piles groups with lower S/D ratios.
- The overall distribution of bending moment along the pile does not significanyly change by S/D ratio and the number of rows. However, pile positioning and installing a pile cap beam changes this distribution along the pile. The most uniform bending moment distribution along the pile, was observed when the pile groups are installed closer to the load, in essence at the crest with a pile cap beam.
- An efficient solution in terms of minimizing the required number of piles for locally loaded slope is to install piles at the crest of the slope using a pile cap beam. This configuration can be implemented in either single or double row. However, when a higher FS_{LPS} is required for a given number of piles without the option of a pile cap beam, using multiple rows with higher S/D ratio could be preferred.
- The staggered configuration is the most efficient among all other double row and single row configurations used in locally loaded slopes and natural slopes. Staggered configuration provides relatively higher *FS* values by utilizing the same number of piles. *FS* can be further enchanced to reach a target value, by placement of a pile cap beam on this group configuration.

- Based on the volume of required concrete (for piles and pile cap beam), the most efficient pile group position for piles with free pile head condition is the middle of the slope, but in the case of constrained pile head condition placement of the pile group at the crest of the slope becomes more efficient compared to middle position for the locally loaded slopes.
- Pile configuration in the center zone aligned with the surcharge load significantly affects the *FS.* Outer piles near the edges (that are placed beyond the surcharge are), are required to cover the zone of influence of the surcharge load. However, configuration aspects of the outermost piles (number of rows, S/D ratio, pile position and row inclination) do not alter the FS_{LPS} .
- Circle shaped configuration, a configuration similar to colmuns placed at the middle of the slope, did not lead to a significantly higher FS_{LPS} value than the arch shaped and more conservative configuration approaches with with triple rows placed in the middle of the slope.

Future research on model tests in the laboratory that considers soil-structure interaction with varying soil properties can provide insights on effectiveness of stabilization and the validity of the numerical analysis. Case studies with long-term monitoring can reveal time-dependent behavior, and field tests will yield empirical data for practical guidelines. Additionally, future research can also focus on understanding the effects of dynamic loading conditions. These research areas will advance the understanding and application of pile group configurations, leading to more effective, sustainable, and economical slope stability solutions.

REFERENCES

Abdelaziz, A., D. Hafez, A. Hussein, 2017, "The Effect of Pile Parameters on the Factor of Safety of Piled Slopes Using 3D Numerical Analysis", *HBRC Journal,* Vol. 13, No. 3, pp. 277–285.

Abramson, L. W., T. S. Lee, S. Sharma, and G.M. Boyce, 1996, Slope Stability and Stabilization Methods, John Wiley and Sons, New Jersey, USA.

Aliah, S. Z., C.Y. Lee, 2016, "Simplified Analysis of Slope Stabilizing Piles", *International Journal of Civil and Structural Engineering Research*, Vol. 4, No. 1, pp: 286-290.

Ausilio, E., Conte, E., & Dente, G., 2000, "Seismic Stability Analysis of Reinforced Slopes", *Soil Dynamics and Earthquake Engineering*, Vol. 19, No. 3, pp. 159–172.

Ausilio, E., E. Conte, G. Dente, 2001, "Stability Analysis of Slopes Reinforced with Piles", *Computers and Geotechnics*, Vol. 28, pp. 591–611.

Benmebarek, M. A., S. Benmebarek, M. Rad, and R. Ray, 2021, "Pile Optimization in Slope Stabilization by 2D and 3D Numerical Analyses", *International Journal of Geotechnical Engineering*, Vol. 16, No. 2, pp. 211–224.

Brinkgreve, R. B. J., S. Kumarswamy, W. M. Swolfs, F. Fonseca, N. Ragi Manoj, L. Zampich, and N. Zalamea, 2021, PLAXIS 3D 2021 Manual. PLAXIS bv, Delft, Netherlands.

Cai, F., and K. Ugai, 2000, "Numerical Analysis of the Stability of a Slope Reinforced with Piles", *Soils and Foundations*, Vol. 40, No. 1, pp. 73–84.

Chae, K.S., K. Ugai, and A. Wakai, 2004, "Lateral Resistance of Short Single Piles and Pile Groups Located Near Slopes", *International Journal of Geomechanics*, Vol. 4, No. 2, pp. 73–84.

Chandrasekaran, S. S., & A. Boominathan, a. G., 2010, "Group Interaction Effects on Laterally Loaded Piles in Clay", *Journal of Geotechnical and Geoenvironmental Engineering*, Vol. 136, No. 4, pp. 573-582.

Dai, X., A. Fa-you, Zhang, P., and Yan, S., 2022, "A Comparative Study between Polyline and Straight Line Arrangements of Antislide Piles Based on Soil Arching Effect", *Advances in Civil Engineering*, Vol. 2022, No. 1.

Duncan, J.M., 1996, "State of the Art: Limit Equilibrium and Finite-Element Analysis of Slopes" , *Journal of Geotechnical Engineering*, Vol. 122, pp. 577-596.

Ellis, E.A., I. K. Durrani, D. J. Reddish, 2010, "Numerical Modelling of Discrete Pile Rows for Slope Stability and Generic Guidance for Design", *Géotechnique*, Vol. 60, No. 3, pp. 185–195.

El Sawwaf, M., 2008, "Lateral Behavior of Vertical Pile group Embedded in Stabilized Earth Slope", *Journal of Geotechnical and Geoenvironmental Engineering*, Vol. 134, No. 7, pp. 1015-1020.

Gao, Y., M. Ye, and F. Zhang, 2015, "Three-dimensional Analysis of Slopes Reinforced with Piles", *J. Cent. South Univ.,* Vol. 22, No. 6, pp. 2322–2327.

Gerolymos, N., O. Papakyriakopoulos, and R. B. J. Brinkgreve, 2014, "Macroelement Modeling of Piles in Cohesive Soil Subjected to Combined Lateral and Axial Loading", Proceedings of the 8th European Conference on Numerical Methods in Geotechnical Engineering, Delft, Netherlands, pp. 373–378.

Griffiths, D. V., and P. Lane, 1999, "Slope Stability Analysis by Finite Elements", *Geotechnique*, Vol. 49, No. 3, pp. 387–403.

Herda et al., 2023, "Behavior of Stabilizing Piles to Increase Stability of Residual Soil Slope", *International Journal of Applied Engineering and Technology*, Vol. 5, No. 3, pp. 185-191.

Ho, I-Hsuan, 2017, "Three-dimensional Finite Element Analysis for Soil Slopes Stabilisation Using Piles", *Geomechanics and Geoengineering*, Vol. 12, No. 4, pp. 234–249.

Hu, X., Liu, D., Niu, L., Liu, C., Wang, X., & Fu, R., 2021, "Development of Soil–pile Interactions and Failure Mechanisms in a Pile-reinforced Landslide", *Engineering Geology*, Vol. 294, No. 8.

Hu G, Y. Xia, X. Ruan, M. Zheng, 2022, "Working Mechanism and Method for Theoretical Calculation of Arch–chord Coupled Anti-sliding Structure", *Engineering Reports*, Vol. 4, No. 2.

Ito, T., T. Matsui, and W. Hong, 1982, "Extended Design Method for Multi-Row Stabilizing Piles against Landslide", *Soils and Foundations*, Vol. 22, No. 1, pp. 1–13.

Jesmani, M., A. Kasrania, M. Kamalzare, et al., 2015, "Undrained Vertical Bearing Capacity of Pile Located Near Soft Clay Slope", *Journal of Engineering Research*, Vol. 3, No. 3, pp. 21-38.

Kahyaoğlu, M. R., O. Onal, G. Imançlı, G. Ozden, & A. Ş. Kayalar, 2012, "Soil Arching and Load Transfer Mechanism for Slope Stabilized with Piles", *Journal of Civil Engineering and Management*, Vol. 18, No. 5, pp. 701–708.

Kanagasabai, S., J. A. Smethurst, and W. Powrie, 2011, "Three-dimensional Numerical Modelling of Discrete Piles Used to Stabilize Landslides", *Canadian Geotechnical Journal*, Vol. 48, No. 9, pp. 1393-1411.

Kourkoulis, R., F. Gelagoti, I. Anastasopoulos, and G. Gazetas, 2011, "Slope Stabilizing Piles and Pile-Groups: Parametric Study and Design Insights", *Journal of Geotechnical and Geoenvironmental Engineering*, Vol. 137, No. 7, pp. 663–677.

Lai, H., Zheng, J., Zhang, R., & Cui, M., 2018, "Classification and Characteristics of Soil Arching Structures in Pile-supported Embankments", *Computers and Geotechnics*, Vol. 98, pp. 153–171.

Lei, H., X. Liu, Y. Song, et al., 2021, "Stability Analysis of Slope Reinforced by Double-row Stabilizing Piles with Different Locations", *Natural Hazards*, Vol. 106, pp. 19–42.

Li, C., J. Wu, H. Tang, J. Wang, F. Chen, D. Liang, 2015, "A Novel Optimal Plane Arrangement of Stabilizing Piles Based on Soil Arching Effect and Stability Limit for 3D Colluvial Landslides", *Engineering Geology*, Vol. 195, pp. 236-247.

Li, C., W. Chen, Y. Song, et al., 2020, "Optimal Location of Piles in Stabilizing Slopes Based on a Simplified Double-row Piles Model", *KSCE Journal of Civil Engineering*, Vol. 24, pp. 377–389.

Li, H., H. Wang, G. Yue, F. Zhao, W. Li, 2021, "Arch Antislide Pile-wall Structure System: Model and Optimization", *Mathematical Problems in Engineering*, Vol. 2021, pp. 1-16.

Li, X., X. Pei, M. Gutierrez, et al., 2021, "Optimal Location of Piles in Slope Stabilization by Limit Analysis", *Acta Geotechnica*, Vol. 7, pp. 253–259.

Li, X., S. He, Y. Luo, and Y. Wu, 2011, "Numerical Studies of the Position of Piles in Slope Stabilization", *Geomechanics and Geoengineering: An International Journal*, Vol. 6, No. 3, pp. 209-215.

Liang, R. Y., and M. Yamin, 2010, "Three-dimensional Finite Behavior in Slope/drilled Shafts System", *International Journal for Numerical and Analytical Methods in Geomechanics*, Vol. 34, No. 11, pp. 1157–1168.

Mezazigh, S., and D. Levacher, 1998, "Laterally Loaded Piles in Sand: Slope Effect on P–Y Reaction Curves", *Canadian Geotechnical Journal*, Vol. 35, No. 3, pp. 433–441.

Pan, J. Q., Z.Y. Wang, T.X. Dong, B. Liang, 2017, "Analysis on the Best Position and the Pile Distance of Anti-slide Pile of Reinforced Soil Slope", In: 3rd International Conference on Energy Materials and Environment Engineering, Bangkok,Thailand, Vol. 61 , No. 1.

Rabie, M., 2014, "Comparison Study Between Traditional and Finite Element Methods for Slopes under Heavy Rainfall", *HBRC Journal/HBRC Journal*, Vol. 10, No.2, pp. 160–168.

Smethurst, J. A., & Powrie, W., 2007, "Monitoring and Analysis of the Bending Behaviour of Discrete Piles Used to Stabilise a Railway Embankment", *Géotechnique/Geotechnique*, Vol. 57 , No.8 , pp. 663–677.

Tekdemir, E., "Three-Dimensional Short-Term Stability Analysis of Clayey Slopes Stabilized with Piles" , MSc. Thesis, Bogazici University, 2023.

Ter-Martirosyan, A., Sidorov, V., & Almakaeva, A., 2019, "Determining the Interfaces Parameters for Geotechnical Modelling", *E3S Web of Conferences*, Tashkent, Uzbekistan, Vol. 97, No. 3.

Terzaghi, K., 1950, “Mechanism of Landslides”, *Application of Geology to Engineering Practice*, pp. 83–123.

Obrzud, R. and A. Truty, 2010, *The Hardening Soil Model – A Practical Guidebook, Z_Soil.PC*, Zace Services Ltd., Préverenges, Switzerland.

Potyondy, J. G.,1961, “Skin Friction between Various Soils and Construction Materials”, *Geotechnique*, Vol. 11, No. 4, pp. 339–353.

Yang, S., Ren, X., & Zhang, J., 2011, “Study on Embedded Length of Piles for Slope Reinforced with One Row of Piles”, *Journal of Rock Mechanics and Geotechnical Engineering/Journal of Rock Mechanics and Geotechnical Engineering*, Vol. 3, No. 2, pp. 167–178.